Paleo-environment of the Northern Jordan Rift region based on speleothems from Zalmon Cave, Israel

Thesis for the Degree of Master of Science

Submitted by:

Jonathan Keinan

Under the supervision of:

Prof. Amotz Agnon

Prof. Amos Frumkin

Dr. Miryam Bar-Matthews

December 2016

Department of Geology

Institute of Earth Sciences

Faculty of Mathematics and Natural Sciences

The Hebrew University of Jerusalem

Abstract

Speleothems have long been used to decipher paleoclimate, and numerous cave locations in the Eastern Mediterranean have been studied; however the Eastern Galilee has until recently featured no accessible speleothem caves. The newly discovered Zalmon Cave offers an opportunity to study the Eastern Mediterranean paleoclimate in the northern Jordan Rift. The cave is located in the Dead Sea catchment approximately 8 km west of the Sea of Galilee. The study of Zalmon Cave speleothems, based on accurate dating and isotopic records, is giving additional insight into the late Quaternary paleoclimate of the Levant. Speleothems from Zalmon Cave grew during glacial and interglacial intervals, in contrast to Ma'ale Efrayim Cave and Dead Sea Escarpment caves located further south along the Jordan – Dead Sea Rift, in which speleothems deposited mostly during glacial intervals. Comparison of the isotopic records of Zalmon Cave to published isotopic records of speleothems from the Northern Galilee and central Israel shows that the carbon isotopic composition ($\delta^{13}C$) is similar for most of the time interval suggesting similar vegetation types, in agreement with present-day conditions. In contrast, the oxygen isotopic profiles ($\delta^{18}O$) are similar only during interglacial intervals. During the last glacial period, the $\delta^{18}O$ values of Zalmon Cave speleothems are lower than Peqi'in Cave and Ma'ale Efrayim Cave by ~0.5-1‰ and lower than Soreq Cave by ~1-2‰. This suggests warmer temperatures and/or more rainfall in the Eastern Galilee compared to central Israel. Addressing the prominent ^{18}O depletion eastward and northward during glacial periods, the possible influence of lower sea level and different synoptic system on the rainfall pattern during these times are investigated. Comparison of the $\delta^{18}O$ records from Eastern Mediterranean speleothem caves to planktonic Foraminifera *G. Ruber* in marine cores located off the Israeli coast ($\Delta\delta^{18}O_{sea\text{-}land}$) highlights three behavior patterns during the last glacial period: 1) $\Delta\delta^{18}O_{sea\text{-}land}$ is greater for Zalmon Cave speleothems compared to Soreq Cave speleothems located in central Israel. 2) There is greater similarity of land records to the marine core located in the southern Eastern Mediterranean Sea, rather than the northern part. 3) The highest $\Delta\delta^{18}O_{sea\text{-}Zalmon}$ correlate remarkably well with reconstructions of Lake Lisan levels. All three observations support the southern shift of the rainfall track and increasing amount of rainfall in the northern part of the Jordan Rift during the last glacial.

Acknowledgments

I would like to express my gratitude first and foremost to my supervisors, Amotz Agnon, Amos Frumkin and Miryam Bar-Matthews for the interest and enthusiasm they showed in my work, their guidance and their willingness to help at any giving moment. I have learned a lot from them and profoundly benefitted from their knowledge and experience. This work would not have been possible without the tremendous help and support of Dr. Avner Ayalon. His advice and encouragement were always important guiding lights towards my personal and professional development. I would also like to thank Dr. Anton Vaks for very useful discussions which were valuable for the thinking process.

A special thanks to the wonderful staff from the Geochemistry Department at the Geological Survey of Israel (GSI) for showing me the ropes: Natalya Tapliakov for teaching me the laboratory work with extreme patience, Yevgeni Zakon for his help every time something went wrong, Tami Zilberman for her endless help with the stable isotope measurements and to Iyad Swaed for his assistance with petrographic slides.

To our group in Neev Centre: Yaniv Darvasi, Osnat Barnea and Inga Boianju. I always knew I had someone to turn to whenever I needed advice. Their help and support meant a lot to me.

Many thanks to Bat-Sheva Cohen, Nili Almog and Channa Nezer-Cohen for help with graphics and publications.

I am indebted to the superb students from the GSI: Tamir Shay and Eldar Buzaglo, for their endless help with laboratory work.

I would also like to thank my friends from the geology department who shared my happiness, understood what I was going through and lifted me up when needed.

To my parents, Ehud and Hannah, I wish to thank for standing by me and for their pride in any achievement I had, no matter how small it was. To my beloved family and friends, thank you for always being there for me, listening and advising.

A special thanks is also in order for everyone who took the time to help me with field work: Yuval Burstein, Yael Braun, Noam Arnon, Tamir Shay, Yaniv Darvasi, Sari Roded and Inga Boianjo. I could not have done it without you guys.

And last but not least, to Natalie. Every now and then I'm still trying to figure out what a girl like her is doing with a guy like me…

Table of contents

List of figures

List of tables

1 Background

1.1 General Introduction

During October 2013, while expanding route 65 in the eastern part of the Lower Galilee, a cavity was opened in the roadcut. This turned out to lead to a newly discovered speleothem-rich cave, Zalmon Cave, located in the Dead Sea catchment approximately 8 km west of the Sea of Galilee (Figures 1 and 2) within the karstic Turonian B'ina Formation (Arkin et al., 1965; Bogoch and Sneh, 2008). The entrance to the cave is 23 meters above sea level and is roughly 35 kilometers east of the Mediterranean Sea. The climate in the region is Mediterranean, with average annual precipitation of ~550 mm (IMS - Israel Meteorological Service, 2011) and an annual temperature average of 21°C. The cave is an isolated chamber cave (Frumkin and Fischhendler, 2005) which had been disconnected from the surface until its exposure as a result of the road construction. The cave was mapped shortly after its discovery by the Cave Research Center (see appendix for cave map and cross sections).

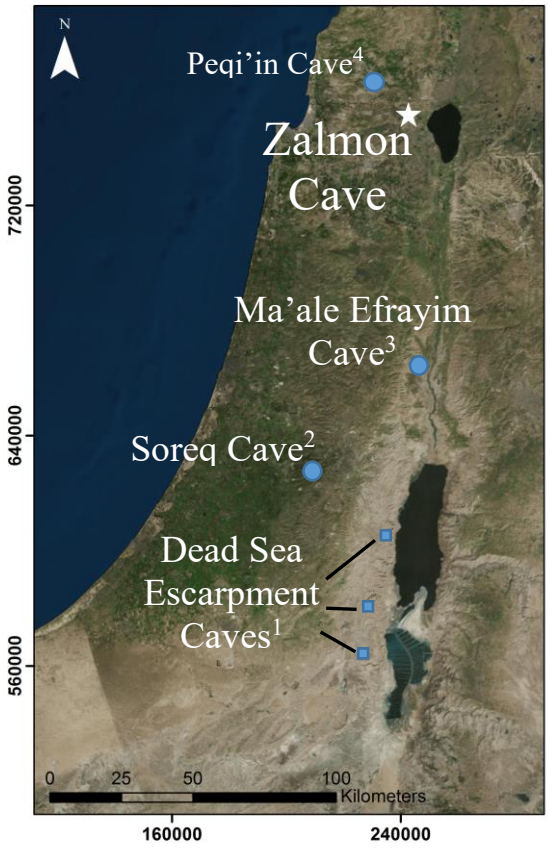

Figure 1: Zalmon Cave Location alongside previous research sites on orthorectified satellite image (ITM grid).

1) **Lisker et al. 2010**
2) **Bar-Matthews et al. 1999**
3) **Vaks et al. 2003**
4) **Bar-Matthews et al. 2003.**

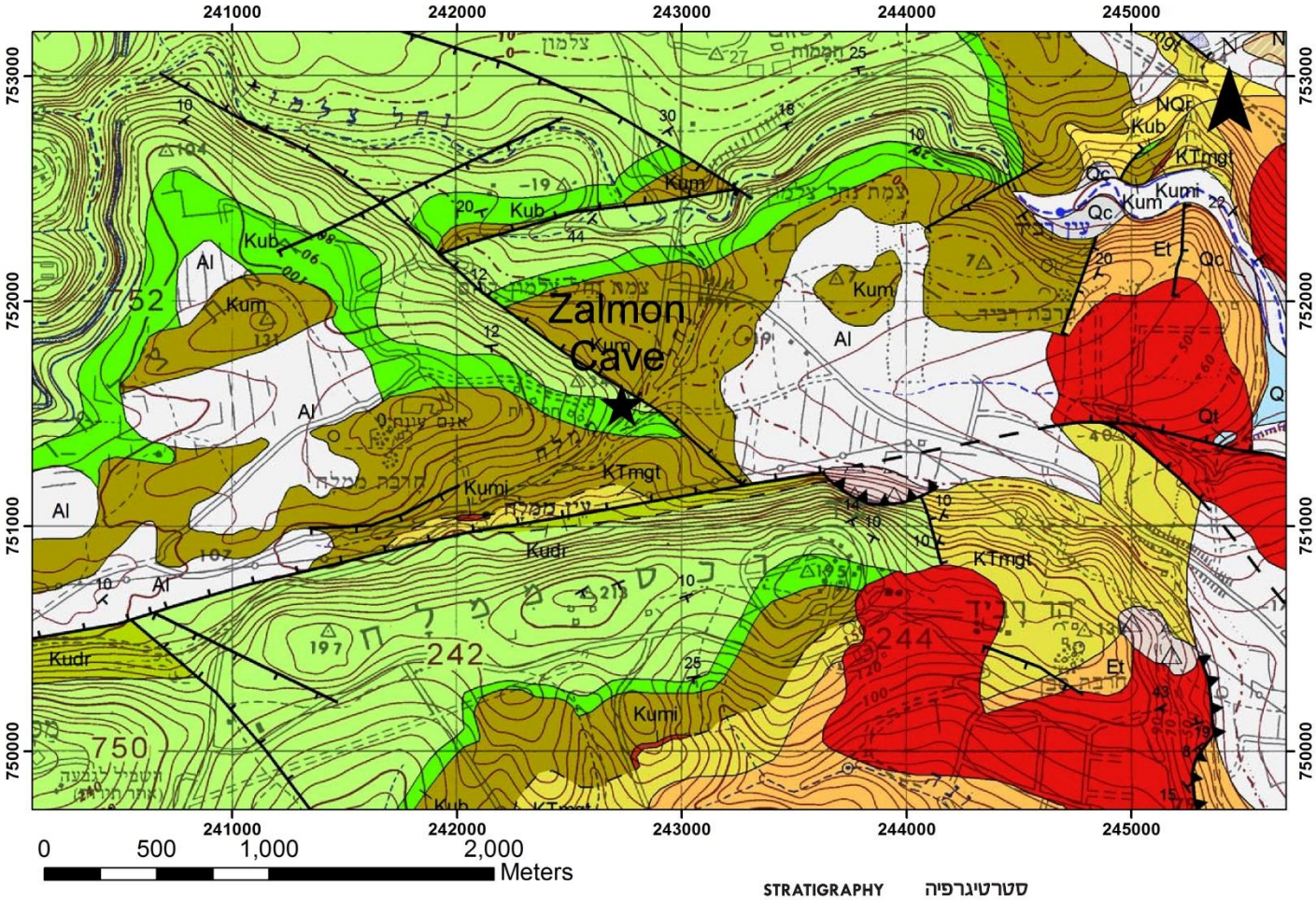

Figure 2: Location of Zalmon on a 1:50000 geological map (Bogoch and Sneh, 2008) and the geological units.

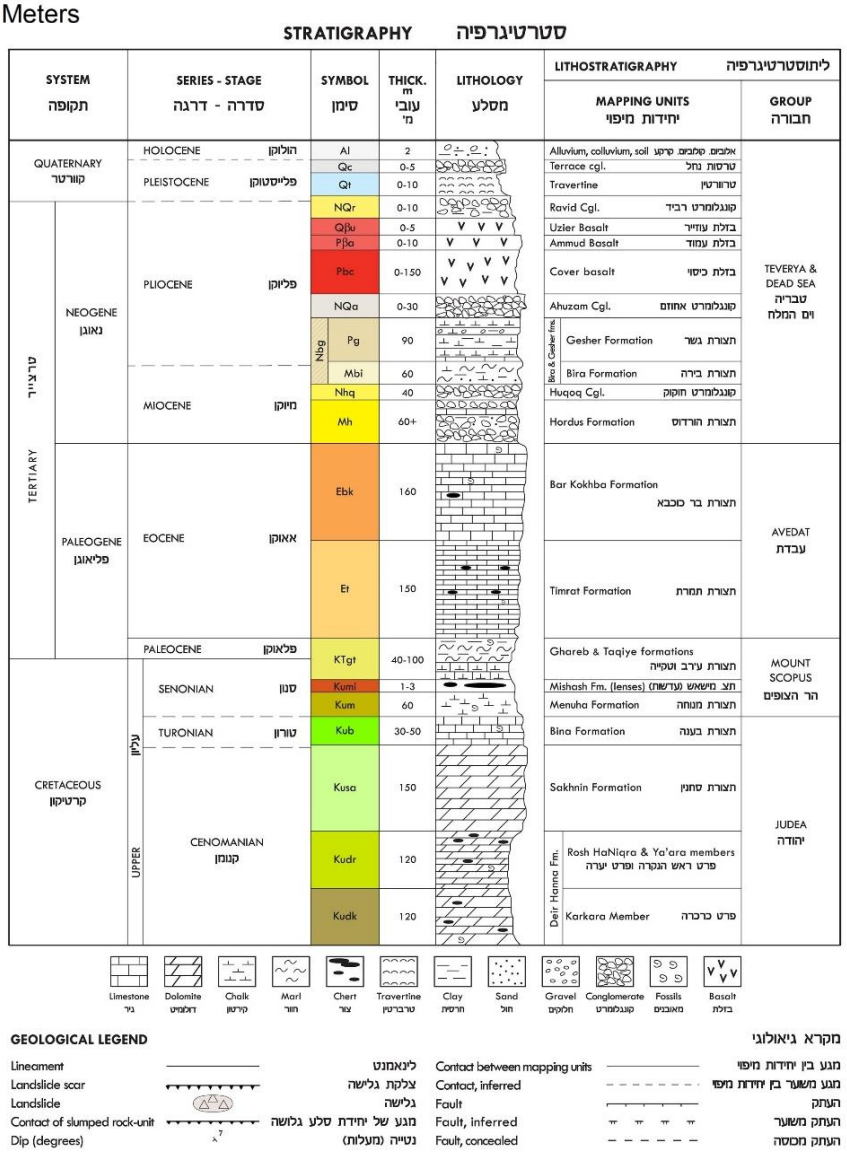

1.2 Eastern Galilee: Geological setting

The Galilee is subdivided based on morphologic and structural characteristics into the Upper Galilee and Lower Galilee, both exhibiting several notable tectonic systems:

- The Syrian Arch fold system (Picard, 1943) which is active since the Senonian. It is comprised of a series of anticlines and synclines stretching from northern Sinai to Syria with roughly N-S direction in Galilee (Flexer et al., 1970).
- Conjugate fault systems trending SE-NW and SW-NE with mostly lateral displacement. Zalmon Cave developed in close proximity to these faults (Figure 2). These systems were active mostly during the Miocene and their topographical expression has been mostly eroded. Another fault system of mostly E-W exhibits usually normal displacement, which developed since the Miocene, prior and alongside the development of the Dead Sea Transform system. This structure forms a series of elongated tectonic blocks which dominate much of the Galilee (Freund, 1970; Ron et al., 1984). Active normal faulting has been established for a fault in this system ~15km NW of the cave (Mitchell et al., 2001).
- Pleistocene tectonism arched the Galilee by 200 meters over a wavelength of 40-60 kilometers, from the Mediterranean coastal plane to the Dead Sea Transform. This arch is considered to be related to the development of the Dead Sea Transform (Matmon et al., 1999).

1.2.1 The Dead Sea Transform

The Dead Sea Transform (DST), over 1000 km long, has been active since the Miocene (Garfunkel et al., 1981), trending from the spreading center in the Red Sea to the Maras/Hatay Triple Junction in the north (Chorowicz et al., 1994; Mahmoud et al., 2013). Since the beginning of its activity 18 Ma, the DST has a total left-lateral offset of approximately 105 km (Freund et al., 1968). Pre-instrumental earthquakes of the DST, both historic and prehistoric have been studied extensively by use of archeological evidence, lake seismites and seismites in cave speleothems as summarized by Agnon (2014). Slip rates calculated by archeological and geological markers at various segments of the DST yield varying rates of 2-10 mm/y (Freund et al., 1968; Garfunkel, 1981; Ginat et al., 1998; Klinger et al., 2000; Niemi et al., 2001; Marco et al., 2005; Le Beon et al.,

2008; Masson et al., 2015). Zalmon cave is located in the northern part of the Dead Sea Catchment (~43000 km^2) which formed along the DST (Garfunkel, 1981).

1.2.2 Quaternary Paleo-lakes and their climatic implications

The Dead Sea Catchment (DSC) covers climatic regimes ranging from moist Mediterranean to extremely arid (IMS - Israel Meteorological Service, 2011). Most of the basin is located in the 'rain shadow' of Israel (Vaks et al., 2003). During the Pleistocene and Holocene, various terminal lakes developed in the depression along the DSC which have deposited evaporate, carbonate and clastic sediments. The mid to late Quaternary lakes that occupied the DSC were:

- Lake Amora occupied the basin following the disconnection of Sedom Lagoon (Zak, 1967) from the open sea. According to Torfstein et al. (2009), Lake Amora had spanned seven glacial-interglacial cycles from ~740 to 70 ka.
- Lake Samra occupied the Dead Sea Basin during the last interglacial (~140-75 ka). Samra Formation is correlative to the uppermost part of Amora Formation (Waldmann et al., 2007).
- Lake Lisan, the precursor of the Dead Sea, existed from ~70 to 15 ka. Its levels were greatly influenced by regional climate conditions of the Eastern Mediterranean (Enzel et al., 2008). The lake level varied between ~330 and ~180 meters below sea level peaking at ~27-23 ka; thereafter the lake continuously shrank until its almost complete desiccation at ~11-12 ka (Bartov et al., 2002).
- The Holocene Dead Sea has been occupying the depression since ~10 ka. During most of the Holocene the Dead Sea level had been approximately -400m with ~±30m oscillations, mostly during the early Holocene (Enzel et al., 2003).

These lakes can be considered as 'amplifier lakes' since their levels and sedimentary facies are sensitive to rapid change in climatic conditions (Stein, 2001). The lake levels are a gauge to the balance of water in the catchment area so they are occasionally used as paleo-climate indicators (Machlus et al., 2000; Bartov et al., 2002; Prasad et al., 2004; Lisker et al., 2009). The cyclic nature of these levels and of the lake sediments reflects the regional climate. Water levels have fluctuated greatly between glacial and interglacial intervals, reaching their peak during glacial periods. These variations have been well recorded in paleo-lake levels, stratigraphic sequences (Bartov et al., 2002; Migowski et al., 2006;

Waldmann et al., 2009; Neugebauer et al., 2016) and isotopic compositions of lacustrine sediments (Kolodny et al., 2005; Torfstein et al., 2015).

1.3 Speleothems

1.3.1 Speleothem formation

Speleothems usually form in caves within carbonate host rocks as a result of chemical reactions between rain water, soil and host rock (Figure 3). Biological activity in the soil causes the CO_2 pressure of porewater to be much higher than in the atmosphere (Hendy, 1971; Dreybrodt, 1999). Hence, rainwater infiltrating the soil is enriched in CO_2 which in turn causes the formation of carbonic acid:

$$(1)\, CO_{2(g)} \leftrightarrow CO_{2(aq)}$$
$$(2)\, H_2O_{(l)} + CO_{2(aq)} \leftrightarrow H_2CO_{3(aq)}$$

The weakly acidic water (pH=~5-6) flows through the carbonate host rock, dissolving it and incorporating trace elements such as uranium, mostly as UO_2^{2+}, the highly soluble uranyl ion (Richards and Dorale, 2003). The solution becomes saturated with respect to calcium-carbonate:

$$(3)\, H_2CO_{3(aq)} + CaCO_{3(s)} \leftrightarrow Ca^{2+}{}_{(aq)} + 2HCO^-_{3\,(aq)}$$

Calcite or aragonite precipitates when the water reaches the cave and becomes supersaturated with respect to calcium-carbonate: The CO_2 pressure in the cave atmosphere is lower than in the infiltrating water, causing degassing of CO_2 and hence a rise in pH. (Dreybrodt, 1999; Frisia and Borsato, 2010):

$$(4)\, Ca^{2+}{}_{(aq)} + 2HCO^-_{3\,(aq)} \leftrightarrow CaCO_{3(s)} + CO_{2(g)} + H_2O_{(l)}$$

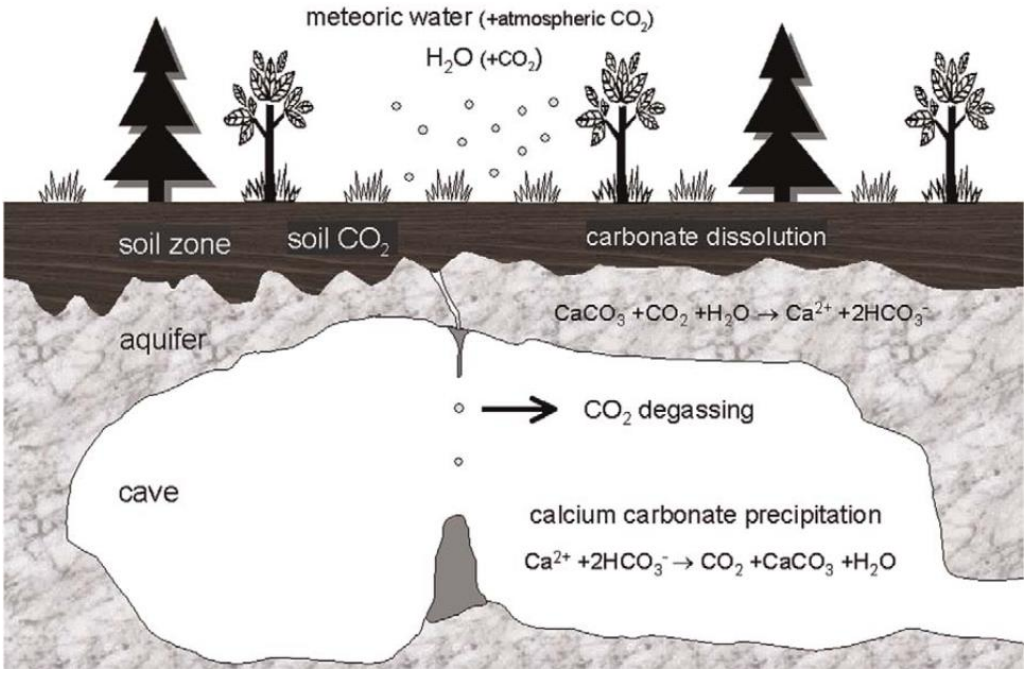

Figure 3: Speleothem formation mechanism (Frisia and Borsato, 2010)

1.3.2 U-series dating

The decay chain of Uranium 238 called the "Uranium series" offers the most reliable and precise dating method of carbonate speleothems. It is based on the radioactive decay series of ^{238}U to ^{206}Pb. In any naturally occurring material, a state of secular equilibrium will be reached after several million years, since the half-life of the parent isotopes ($t_{1/2}{}^{238}U=4.468\cdot10^9y$) is much larger than the half-life of the intermediate daughters in the decay chains ($t_{1/2}{}^{234}U=2.455\cdot10^5y$) (Jaffey et al., 1971) making the U-Th dating method useful only for deposits younger than ~500 ka. For this reason secular equilibrium of host rock carbonates can usually be assumed. Equilibrium can be disrupted due to chemical fractionation between U and Th in aqueous environments. The extent to which the uranium-series decay chain in a deposit have returned to secular equilibrium in a closed system from an initial state of disequilibrium can be expressed as a function of time, using the decay constants involved if the following conditions are satisfied:

- No gain or loss of parent nuclide or daughter products occurred since the time of formation.
- Intermediate and daughter decay products at the time of formation were absent or, if present, can be corrected for (Richards and Dorale, 2003).

The average abundances of U and Th in the earth's crust are 1.7 and 8.5 ppm respectively (Wedepohl, 1995), while their relative abundances in the hydrosphere vary due to their differing solubility in surface and near surface environments (Richards and Dorale, 2003). Thorium is very insoluble due to its high ionic charge (+4) and is quickly adsorbed to surfaces of clay minerals. In contrast, uranium is easily dissolved in the form of uranyl ions (UO_2^{2+}). During precipitation of speleothems the uranyl ion can easily replace calcium in the crystal lattice and is therefore commonly incorporated in speleothems.

Thorium content at time of formation can often be considered to be negligible in the pure authigenic phase of calcite or aragonite speleothems, however, this component is often accompanied by allochthonous material likely adsorbed to clay minerals with a significant amount of Thorium. Various methods are available to account for the presence of inherited daughter isotopes but the uncertainty of the final estimate is greater than would be expected for pure material.

In an open system any initial ^{230}Th is always accompanied by a much larger amount of ^{232}Th where detrital Thorium has been incorporated into the system because the $^{232}Th/^{230}Th$ atomic ratio in most crustal materials is $2 \cdot 10^5$ (Hellstrom, 2006). For this and because of its extremely long half-life of $1.401 \cdot 10^{10}$y, the presence of ^{232}Th can be used to indicate the degree of contamination. It is accepted that where ^{232}Th contamination is sufficiently low the effect of using incorrect initial $^{232}Th/^{230}Th$ will be negligible (Richards and Dorale, 2003) (see section 3.4.1 for further details).

1.3.3 Stable isotopes of speleothems

The isotopic composition of speleothems may vary considerably depending on the temperature and the isotopic composition of the source water and CO_2 from which the $CaCO_3$ precipitated.

1.3.3.1 Stable isotopes – Oxygen

The isotopic composition of oxygen during the formation of speleothems (under equilibrium conditions) depends on the composition of the water from which the $CaCO_3$ precipitated. It is inversely proportional to the formation temperature by the following equation (Friedman and O'Neil, 1977):

$$1000 \ln \alpha_{(calcite-water)} = \delta^{18}O_{(calcite)} - \delta^{18}O_{(water)} = 2.78 \cdot 10^6 T^{-2} - 2.89$$

where T is the temperature in ^{o}K. The temperature of a cave with no natural opening is usually the same as the average annual temperature of its region and is not affected by seasonal variations (Schwarcz, 1986). The composition of the water percolating into the cave is dictated by the isotopic composition of the meteoric water and by isotopic variations taking place in the unsaturated zone (epikarst).

The isotopic composition of oxygen and hydrogen of meteoric water depends on various factors:

Source effect

The composition of the rain is directly linked to the source of the water. The striking similarity between the $\delta^{18}O$ from northern and central Israel caves and the Eastern Mediterranean $\delta^{18}O_{G.ruber}$ record indicates that the source effect dominates the major fluctuations of speleothem $\delta^{18}O$ (Frumkin et al., 1999; Bar-Matthews et al., 2000; Bar-Matthews et al., 2003; Kolodny et al., 2005; Almogi-Labin et al., 2009). The isotopic composition of the source waters (oceans) is inversely correlated to coeval ice-sheets mainly due to ice volume effect. Ice volume has varied greatly between glacial and interglacial intervals changing the isotopic composition of the oceans. This is because of isotopic fractionation during formation of vapor at the source and because of Rayleigh fractionation as the moisture travels to high latitudes from equatorial regions (Dansgaard, 1964).

Amount effect

The amount of rain correlates with its isotopic composition. During the condensation of cloud droplets from vapour, the first molecules that change into the liquid form are the heavier ones (containing ^{18}O and D). The initial composition of rain would be enriched by ^{18}O and D and as more rain precipitates the cloud is gradually depleted of these isotopes. For this reason a larger amount of rain is characterized by lighter isotopic values. Ayalon et al. (2004) and Orland et al. (2014) showed a negative linear relationship between the amount of annual rainfall in Soreq Cave and its $\delta^{18}O$.

Continentality/Rainout effect

As a cloud moves farther away from its source the isotopic composition of the rain becomes more negative since the water composed of heavier isotopes is removed in the initial phases. For this reason the water remaining in the cloud becomes more depleted as the cloud moves away from its source which in turn causes the composition of water in

inland regions to be lighter than coastal ones (Dansgaard, 1964). This has also been demonstrated in Israel (Ayalon et al., 2004)

Elevation effect

As a weather system passes a topographical barrier such as a mountain the air expands and cools adiabatically. This causes the rate of condensation to rise and therefore a larger amount of precipitation. ^{18}O and D are preferentially removed first from the cloud leaving the water left in the cloud depleted of heavy isotopes. As a result, precipitation on the other side of a topographical barrier is low in $\delta^{18}O$ and δD (Dansgaard, 1964).

Evaporation effect

Raindrops passing through dry and warm air undergo partial evaporation. This causes kinetic fractionation in which the isotopic composition of oxygen undergoes a larger change than that of hydrogen. The evaporation effect is less dominant during massive rain events (>15 mm) due to the high humidity. Rainfall events of more than 10-15mm generally follow the Eastern Mediterranean Meteoric Water Line (MMWL) while rainfall events with less than 15mm exhibit an anomalously low D-excess of <20‰. This is attributed to evaporation effects beneath the clouds causing higher rainwater $\delta^{18}O$ values and the slope of δD-$\delta^{18}O$ to be slightly more moderate than that of the MMWL (Ayalon et al., 1998; Ayalon et al., 2004).

1.3.3.2 Stable isotopes – Carbon

The $\delta^{13}C$ values of cave waters reflect the contribution of the host rock and of soil CO_2, CO_2 degassing and carbonate precipitation (Bar-Matthews et al., 1996; Frumkin et al., 2000). Soil CO_2 is a major source of carbon to the speleothems, and $\delta^{13}C$ of soil CO_2 gas mostly depends on the type of vegetation's photosynthesis pathway. Hence, $\delta^{13}C$ fluctuations shown in speleothems may reflect changes in the vegetation type in the cave area. There are two major photosynthetic pathways: C3 and C4. The C3 pathway is usually used by trees, shrubs and humid climate herbs. The C4 pathway is used by grasses and herbs more adapted to warmer climate. Average $\delta^{13}C$ value of C3 vegetation is ~-27‰, and of C4 is ~-12‰ (VPDB). The expected $\delta^{13}C$ range of speleothems in regions dominated by C3 plants is between ~-14 to -6‰ whereas for those dominated by C4 plants is ~-6 to +2‰ (McDermott, 2004).

Speleothem $\delta^{13}C$ and $\delta^{18}O$ records may also be influenced by kinetic isotope effects so that temperature controlled equilibrium fractionation models alone cannot adequately

explain the significance of the records. For instance rapid calcite precipitation can lower the $\delta^{13}C$ by lowering the C isotope fractionation between calcite and dissolved inorganic carbon (Mickler et al., 2004). Proper interpretation of records may require that the non-equilibrium isotope effects, causing $\delta^{13}C$ and $\delta^{18}O$ covariations in speleothems, be calibrated to physical conditions in the cave, such as temperature, cave CO_2 pressure, drip rates, calcite precipitation rates, stalactite geometry, and drip water chemistry (Mickler et al., 2006).

1.3.4 Speleothem petrography as an indicator of deposition conditions

The microscopic textures observed in speleothems is an indication of deposition conditions, hiatuses, rate of water flow, CO_2 degassing rate and post depositional phenomena such as erosion of speleothems. For example, by observing changes in columnar calcite types, high-frequency variability of $\delta^{13}C$ values in stalagmites could be explained as related to changes in drip rate and degassing (Boch et al., 2011).

Experiments have demonstrated that crystal morphology and growth mechanisms yield much information on the physicochemical state of the parent fluid. Crystals form when the solution departs from equilibrium, which, for sparingly soluble salts (such as calcium carbonate), is the degree of supersaturation. As supersaturation increases, crystal habits are expected to change from prismatic to spherulitic (Frisia et al., 2000). Isotope fractionation in calcite violates equilibrium when crystals grow at high supersaturation (Kim and O'Neil, 1997). Departure from equilibrium growth, therefore, may influence both the form (habit) and the chemical properties of calcite crystals (Frisia et al., 2000).

1.3.5 Speleothems as indicators of Eastern Mediterranean paleoclimate

Paleoclimate reconstruction in the Eastern Mediterranean has been based primarily on research of speleothems and lacustrine records. Speleothems have been used as archives of environmental changes, using their isotopic and chemical composition, with accurate U-series age control. Once the speleothem age model is determined, a detailed climatic reconstruction can be made, using their $\delta^{18}O$ and $\delta^{13}C$ values. Speleothems may grow continuously if the supersaturated solution is available (Dreybrodt, 1999), however hiatuses are common due to changes in the hydrological system, climate change (McDermott, 2004) and/or tectonic activity (Kagan et al., 2005; Braun et al., 2009). The

unique environment in caves protects against erosion and degradation. Calcite cave deposits therefore preserve a very detailed record of events, both tectonic and climatic.

The present-day climate conditions in the southern Levant range from the sub-humid Mediterranean (mean annual rainfall >800 mm/yr) in the north, to extremely dry in the southern Negev (<50 mm/yr). The steep precipitation gradient over less than 300 km, combined with a primarily carbonate rock terrain, makes an ideal area for speleothem-based paleoclimate studies. Paleoclimate research has been conducted in numerous different caves in Israel (Figure 4) covering diverse climatic regimes such as Jerusalem Cave (Frumkin et al., 1999), Soreq (Bar-Matthews et al., 1997), Ma'ale Efrayim (Vaks et al., 2003), Manot (Hershkovitz et al., 2015), Peqi'in (Bar-Matthews et al., 2003), Mizpe Shelagim (Ayalon et al., 2013), Ma'ale Deragot and Tzavoa in the Northern Negev (Vaks et al., 2006), Ashalim Cave, Even-Sid and Ktura (Vaks et al., 2010; Vaks et al., 2013), Izzim (Vaks et al., 2010), Central and southern Negev Desert caves (Vaks et al., 2007) and along the Dead Sea escarpment (Lisker et al., 2009).

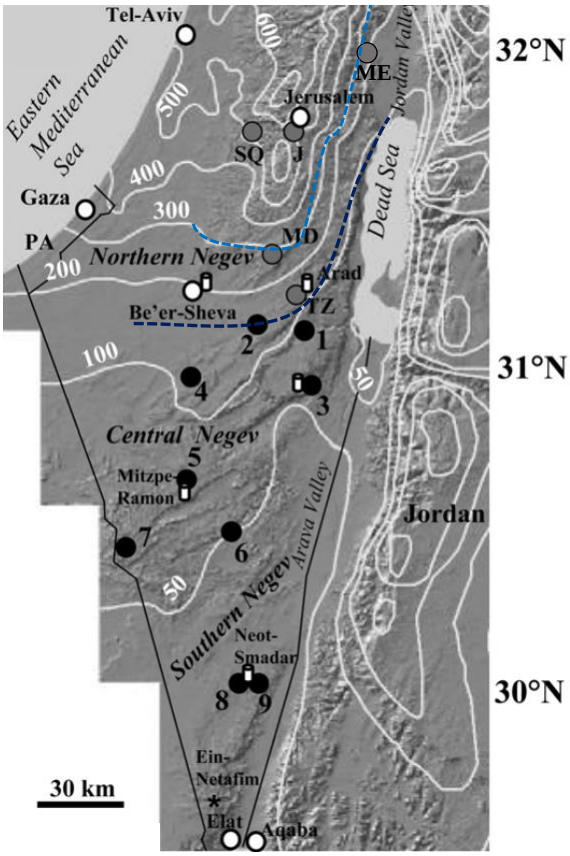

Figure 4: Map showing precipitation and location of the studied caves modified after Vaks et al. (2010). Light Blue line - boundary of continuous speleothem deposition. Dark blue line - limit of intensive glacial deposition. Isohyets are marked by white lines and studied caves by black circles and numbers as following: 1 - Hol-Zakh Cave, 2 - Izzim Cave, 3 - Makhtesh-ha-Qatan Cave, 4 - Ashalim Cave, 5 - Even-Sid mini-caves, 6 - Ma'ale-ha-Meyshar Cave, 7 - Wadi-Lotz Cave, 8 - Shizafon mini-caves and 9 - Ktora Cracks (Vaks et al., 2010). Caves from northern and central Israel are marked by grey circles and abbreviations as follows: ME – Ma'ale Efrayim (Vaks et al., 2003), SQ - Soreq Cave (Bar-Matthews et al., 1997; Bar-Matthews et al., 2003), J - Jerusalem Cave (Frumkin et al., 1999), MD - Ma'ale-Dragot Caves, TZ - Tzavoa Cave (Vaks et al., 2006). Rain sampling stations at Be'er-Sheva, Arad, Makhtech-ha-Qatan, Mitzpe-Ramon and Neot Smadar, are indicated by white cylinders. Ein-Netafim spring near Elat is shown by a star.

In the Eastern Mediterranean the assumed minimal amount of annual precipitation required for speleothem deposition is 300-350 mm during interglacial periods and 200-275 mm during glacial periods (Vaks et al., 2006; Vaks et al., 2010). For this reason

and because of lower glacial temperatures, speleothems in the rain shadow semi-desert region of the Jordan Valley as observed in Ma'ale Efrayim Cave (ME) deposited mostly during glacial periods and moderately so during peak interglacials (Vaks et al., 2003). Observed also in the Dead Sea Escarpment caves (Lisker et al., 2010), this indicates a more positive water balance during glacials allowing more water to enter the unsaturated zone.

Negev humid periods (NHP) are defined by Vaks et al. (2010) as time intervals with a high ratio of precipitation to evaporation. They are characterized by extensive speleothem deposition and low $\delta^{18}O$ values. NHPs are observed in the northern Negev Desert both during glacial and interglacial periods (Vaks et al., 2010). Tzavoa Cave in the northern Negev exhibits similar depositional intervals during glacials as ME cave indicating that during cooler and wetter glacial intervals the desert boundary migrated ~30-50 km southward and eastward compared to its present-day position (Figure 4). This resulted in a more humid climate in the higher altitude parts of the Jordan Valley and the northern Negev. In contrary, central and southern Negev NHPs occurred mostly during interglacial periods. The frequency of depositional episodes and thickness of individual laminae decreases southwards, implying a general decrease in rainfall from north to south (Vaks et al., 2010), similar to the present-day precipitation trend.

Within caves located in the Mediterranean climate area (northern and central Israel), speleothems have been continuously growing during glacial and interglacial periods (Frumkin et al., 1999; Bar-Matthews et al., 2000; Bar-Matthews et al., 2003) for at least 240 ka, indicating that the area has never experienced extreme aridity (water was always available in the unsaturated zone). The isotopic composition of these speleothems reflects climate changes in the Eastern Mediterranean climatic belt. Under present day conditions, rainwater collected from Ma'ale Efrayim (ME) Cave site is ^{18}O enriched relative to that of the Soreq Cave site implying increased evaporation by higher temperatures on the eastern side of the mountain ridge (Vaks et al., 2003; Ayalon et al., 2004). In contrast to modern day conditions, the glacial isotopic profiles of Soreq Cave and ME Cave located at different sides of the central mountain ridge show a high correlation, implying a similar source of rain for both regions during this time. This is also inferred from similar $\delta^{13}C$ values indicating similar vegetation types. The similar profiles indicate that, during the lower glacial temperatures, the amount of rainfall in the Jordan Valley was larger and/or

the rain shadow effect was significantly weaker. The transition from the cold glacial conditions to the warmer interglacial in the ME region was characterized by an increase in temperatures and aridity of the Jordan Valley.

Mount Hermon in northern Israel is in the southernmost point of the Alpine-type karst extending from Turkey to Syria and Lebanon. This region receives most of its precipitation as snowfall. Speleothem deposition in Mizpe Shelagim Cave located at Mount Hermon was continuous during interglacials and restricted to short warming episodes during the last glacial period (Ayalon et al., 2013). Based on fluid inclusion studies, speleothem growth is restricted to temperatures above 3 ^{o}C (Ayalon et al., 2013). These speleothem-based studies cover different climatic zones and their wide use and findings clearly demonstrate that speleothem isotopic compositions capture global climatic diversity, changes, and teleconnection processes from far regions. The comparison and correlations between various studies are crucial to understanding the spatial and chronological changes of the climate. The differences in the isotopic composition of speleothems deposited during the same time interval and the periods of growth non-growth of speleothems from various parts of Israel demonstrate clearly that regional differences are climatically driven.

2 Research objectives

The purpose of this study is to reconstruct late Quaternary paleoclimate in the region by dating speleothems from Zalmon cave. This is achieved by creating a high resolution, well-dated isotopic profile of $\delta^{18}O$ and $\delta^{13}C$ and by determining whether deposition in the cave was continuous or limited to specific time intervals. The location of the cave (Figure 1) invites comparison with Dead Sea lacustrine records (Stein, 2001; Lisker et al., 2009) and speleothem records from central, northern and the Dead Sea regions of Israel. This unique location offers an unprecedented opportunity to assess the local climate in a region, previously unreachable for this type of research.

The study of Zalmon cave is significant for three main reasons:

- With reconstruction available for the paleoclimate of the south and central Dead Sea region (Vaks et al., 2007; Lisker et al., 2010; Torfstein et al., 2015) this study will constrain the paleoclimate gradients from the northern part of the Dead Sea farther south.
- Zalmon cave is located in the northern catchment of Lake Lisan and its precursors (Kaufman, 1971), offering a possible insight into the hydrological conditions during its high glacial stands (Bartov et al., 2002; Torfstein et al., 2015).
- Paleoclimate changes, often correlate with the migration of historic and prehistoric civilizations (Vaks et al., 2007; Bar-Matthews and Ayalon, 2011; Frumkin et al., 2011; Bar-Matthews, 2014; Hershkovitz et al., 2015). The region has numerous evidence of human settlements in caves (e.g. Schwarcz et al., 1988; Hovers et al., 1995; Mcbrearty and Brooks, 2000; Frumkin et al., 2007; Hershkovitz et al., 2015), associated with the "Out of Africa" dispersal. Exploring the paleoclimate in the region can shed light on why hominins occupied the region and the environmental impacts on Neolithization (Goring-Morris and Belfer-Cohen, 2011).

3 Methodology

3.1 Speleothem sampling

During the study various speleothems from within the cave that are reasonably preserved were sampled. They were mapped, photographed and removed in as complete a state as possible. The speleothems were sectioned at The Geological Survey of Israel (GSI) using a diamond saw and polished in order to expose their internal structure. Suitable speleothems were dated and their oxygen and carbon isotopic composition as well as their petrography was studied.

3.2 Petrography

Speleothems were cut and polished in order to make thin sections. Their petrography and mineralogy was studied using an Olympus BX50 polarizing microscope at the GSI, in order to check for impurities, locate hiatuses and identify crystal habitat.

3.3 U-Th dating

Samples for dating were acquired at the GSI using a diamond drill in order to excavate 0.2-0.3 grams of sampling material (Figure 6-13). Each sampled material was dissolved in 7M HNO_3 and a $^{229}Th/^{236}U$ spike was added. These solutions were evaporated to dryness, and the residue re-dissolved in 4 ml of 7M HNO_3, then loaded onto mini-columns that contained 2 ml of Bio-Rad AG 1X8 200-400 mesh resin. Uranium was eluted with 1M HBr, and Thorium with 6M HCl into teflon beakers. These were placed on a hot plate set at 215ºC, to evaporate the solutions to complete dryness. Residues were dissolved in 2 ml and 5 ml of 0.1M HNO_3 respectively (Grant et al., 2012).

U-Th dating was determined using a Nu Instruments Ltd (UK) Multi-Collector-Inductively-Coupled-Plasma-Mass-Spectrometer (MC-ICP-MS) equipped with 12 Faraday cups and 3 ion counters. Each sample was introduced to the MC-ICP-MS through an Aridus® micro-concentric desolvating nebulizer sample introduction system. The instrumental mass bias was corrected (using an exponential equation) by measuring the $^{235}U/^{238}U$ ratio and correcting with the natural $^{235}U/^{238}U$ ratio. Ion counters were calibrated relative to Faraday cups using several cycles of measurement with a different collector configuration in each particular analysis (Vaks et al., 2006; Grant et al., 2012).

3.4 Age calculation and correction procedures

Ages of speleothems were based on the following equation (Kaufman et al., 1998):

$$\left(\frac{^{230}Th}{^{234}U}\right)=\left(\frac{^{238}U}{^{234}U}\right)\cdot(1-e^{-\lambda_{230}t})+\left(1-\left[\frac{^{238}U}{^{234}U}\right]\right)\cdot\left(\frac{\lambda_{230}}{\lambda_{230}-\lambda_{234}}\right)\cdot\left[1-e^{(-\lambda_{230}-\lambda_{234})t}\right]$$

Where t is the age, λ_{230} and λ_{234} are the decay constants of ^{230}Th and ^{234}U, respectively, and all ratios represent activity ratios. The ages were calculated using an EXCEL™ macro developed for that purpose based on Newton-Raphson iteration, which gives the final age and the analytical error as ±2σ (two standard errors of the mean). Initial calculations were based on the assumption that no initial ^{230}Th was present in the sample.

3.4.1 Age corrections

Kaufman et al. (1998) argued that ages obtained from a sample with ^{230}Th/^{232}Th<30 required correction. Above this ratio the correction becomes negligible compared to the analytical uncertainty of the measurement. Richards and Dorale (2003) and Li et al. (1989) argued for thresholds of between 100 to 300 for the case of mass spectrometer dating. Most of the samples from Zalmon Cave have a ^{230}Th/^{232}Th>100 so a correction was not necessary. For samples with a ^{230}Th/^{232}Th<100 the same correction factor of 1.8, which was obtained for Soreq Cave (Grant et al., 2012) and Manot Cave (Hershkovitz et al., 2015), was used.

3.4.2 Wiggle-matching

A second method applied to correction factor determination is the wiggle-matching technique (Kagan et al., 2005). δ^{18}O and δ^{13}C profiles from Zalmon Cave were compared and fitted (wiggle-matched) to the well dated δ^{18}O and δ^{13}C profiles of Soreq Cave, Judea Mountains, Israel. This procedure is justified by the fact that speleothems from northern and central Israel show very similar isotopic values and trends (Bar-Matthews et al., 2003; Hershkovitz et al., 2015). After dating the top, bottom, and several laminae at the middle of the speleothem, an age model for the speleothem is established assuming the measured age represents the center of the drilled area and that there is a constant growth rate between two measured laminae. Both caves show significant fluctuations in their stable isotopic profiles, which enable wiggle-matching of the Zalmon peaks to the accurately dated Soreq profile (Grant et al., 2012).

3.5 Checking for deposition in isotopic equilibrium

Isotopic composition of speleothems is the result of the mode of formation. Hendy (1971) distinguishes between three main processes:

a. "Equilibrium fractionated deposition" – the loss of CO_2 from the solution is slow enough to enable isotopic equilibrium between the precipitated calcite and the water, so variations in $^{18}O/^{16}O$ depend solely on climate changes.

b. "Kinetically fractionated deposition" – rapid loss of CO_2 results in kinetic fractionation between HCO_3^- and $CO_{2\,(aq)}$. In this case the CO_2 lost from the solution will be depleted in ^{13}C and ^{18}O therefore the calcite precipitated will show a simultaneous enrichment in both ^{13}C and ^{18}O.

c. Evaporation of water – the solution becomes supersaturated with respect to calcite, causing the precipitated calcite to be enriched in ^{18}O. Evaporation of water is usually negligible since the relative humidity in isolated caves is usually very high and the airflow very low.

Speleothems deposited under b or c conditions are usually not suitable for paleoclimate reconstruction as the solution from which the calcite was deposited is enriched with heavy isotopes and hence invalidating carbonate paleotemperature equations. The calcite precipitated will cease to be in isotopic equilibrium with the water and climatically induced fluctuations of $\delta^{18}O$ would be swamped by a much stronger kinetically induced signal.

For this reason Hendy's (1971) criteria is used in order to identify whether or not precipitation of calcite occurred under equilibrium conditions. If various samples from the same laminae appear to show a correlation between enrichment in ^{18}O and ^{13}C this would suggest disequilibrium due to loss of CO_2. If the isotopic composition of the oxygen does not remain constant (i.e. maximum difference of less than 1‰ between two measured samples) throughout the lamina, it suggests disequilibrium due to evaporation of water while water flows down the speleothem. If a laminae fails one of these tests it is likely caused by kinetic isotopic fractionation, and the speleothem cannot be used as a paleothermometer.

Dorale and Liu (2009) claimed the Hendy test is insufficient in most cases and proposed a "replication test": the comparison between two growth laminae of the same age (i.e. two

different speleothems), to see if they give similar isotopic profiles (Bar-Matthews et al., 1997; Dorale and Liu, 2009).

To verify that speleothems were deposited in isotopic equilibrium 5 laminae were measured according to Hendy's (1971) criteria. In addition several speleothems covering similar time intervals were studied concomitantly in order to determine if the isotopic record is replicated (Bar-Matthews et al., 1997; Dorale, 1998).

3.6 Isotopic composition of speleothems

For the purpose of constructing oxygen ($\delta^{18}O$) and carbon ($\delta^{13}C$) isotopic profiles laminae were sampled using a 0.8mm diamond drill along the stalagmite growth axis, between 13 to 17 drill holes per cm (Figure 6-11). 350 μg from each sampled drill hole was placed at the bottom of a clean vacuum vessel and a few drops of 100% phosphoric acid (H_3PO_4) were placed at the top. The vessel was then positioned horizontally and flushed with pure Helium for 10 minutes in order to remove atmospheric air (Figure 5). After flushing, the sample and acid interact, releasing CO_2 into the sealed vessel. Oxygen and carbon isotopes were measured using a Finnigan Gas Bench II extraction system attached to a ThermoFinnigan Delta PLUS XP continuous flow mass spectrometer. A standard was measured every 8 samples. All $\delta^{18}O$ and $\delta^{13}C$ values obtained were calibrated against Carrara marble and the international standard NBS-19, and reported in per-mil (‰) relative to the VPDB standard.

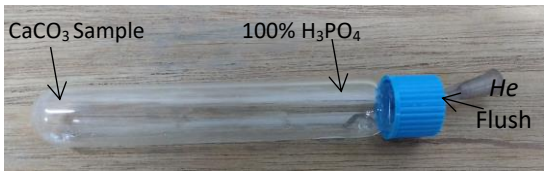

Figure 5: Preparation for helium flush: Horizontally placed vessel with sample at the bottom and acid at the top. Acid and sample are not in contact.

4 Results

A total of fifteen speleothems were collected from Zalmon Cave. Eight of them were found potentially suitable for paleoclimate reconstruction and were dated. Six of these were sampled for isotopic profiles. ZAL1, 2, 3, 4 were found broken and their original location in the cave is not known. ZAL5, 6, 7 and 11 were removed in-situ by a sledgehammer (Figure 34 in the appendix).

4.1 U-Th Dating

A total of 102 samples were dated. Seven have a $^{230}Th/^{232}Th$ ratio of less than 30 and another 23 have a $^{230}Th/^{232}Th$ ratio between 30 and 100.

4.1.1 ZAL1

ZAL1 is a stalagmite approximately 18 cm long and 8 cm wide (Figure 6). It is a porous stalagmite and portions of it broke while drilling. Laminae are very thin and the calcite is lightly colored. Twenty laminae were dated yielding consecutive growth from ~159 to 126 ka and from ~80 to 52 ka (Table 1). A hiatus exists between ZAL1-D and ZAL1-O, evident as a thin dark lamina (blue arrow in Figure 6). Three dates located below a very porous portion of the stalagmite are out of stratigraphic order (ZAL1-B, ZAL1-Q and ZAL1-F). This stalagmite appears to have undergone post sedimentary alteration causing disturbance in the ages.

4.1.2 ZAL2

ZAL2 is a stalagmite 18 cm long and 8 cm wide (Figure 7). It is comprised of alternating layers varying from dark to light calcite laminae. Seventeen laminae were dated yielding growth from ~64.5 to 5.1 ka with two hiatuses evident as a thin white lamina between ~48.6 and 38.6 ka and between ~20 ka and 6.9 ka (Table 2, blue arrows in Figure 7). Another two thin white laminae exist at sampling points ZAL2-20 and ZAL2-72. Apart from one date (ZAL2-R) all ages are in stratigraphic order. The top five dates have a high ratio of detrital component indicated by a $^{230}Th/^{232}Th$ ratio of less than 30 resulting in an age correction of more than 10% (Table 2).

4.1.3 ZAL3

ZAL3 is a stalagmite 18 cm long and 10 cm wide (Figure 8) comprised of ~3mm alternating layers of dark and light calcite laminae. No post sedimentation alterations are

visible. Thirteen laminae were dated yielding growth from ~64 to 42.5 ka with no observable periods of hiatus (Table 3). At the top of the stalagmite a younger speleothem appears (ZAL3-D) dated to ~38 ka. One dated lamina (ZAL3-G) shows a slight age reversal. All other ages are in stratigraphic order. There is a partial overlap in growth periods between ZAL3 and ZAL2.

4.1.4 ZAL4

ZAL4 is a small stalagmite 13 cm long and 7 cm wide. The central part of it appears porous with diagenetic alteration (Figure 9). The top 4 cm of this stalagmite have a darker, more laminar composition. Twelve laminae were dated yielding growth from ~121 to 96 ka (Table 4). Samples are in stratigraphic order with three major exceptions: ZAL4-I, dated to 36.5 ka, is too young. ZAL4-J and ZAL4-K dated to 136 ka and 232 ka respectively are too old.

4.1.5 ZAL5

ZAL5 is a large stalagmite, 27 cm long and 23 cm wide (Figure 10) deposited between ~145 and 47 ka (Table 5) with a long hiatus between ~116 and 47 ka. All dates are in stratigraphic order within the error of measurement. It is the fastest grown speleothem sampled in this research. The laminae are very thin with a shift in the location of the growth axis following the deposition of lamina ZAL5-D, however dating shows hiatus periods. There is a white >2cm long homogenous layer between lamina ZAL5-H and ZAL5-I. The outer ~1.5cm is a much darker laminated calcite. The top of it is dated to 47.2 ka. There is a partial overlap in growth periods between ZAL5 and ZAL1.

4.1.6 ZAL6

ZAL6 is a small stalagmite 8 cm long and 7 cm wide (Figure 11, top right). The top 3 cm were deposited between ~24.5 to 6.9 ka (Table 6) with a hiatus between ~18.9 to 12.8 ka (between dating samples ZAL6-E and ZAL6-D) evident as a thin lightly colored lamina. This is also visible in the petrographic thin section (Figure 11, bottom right) indicated by micrite fabric (Frisia, 2015). The laminae appear translucent, homogeneous, >2mm thick indicating slow continuous growth. An unconformity exists between the top and bottom section which was deposited between ~91.3 and 58 ka. This speleothem had the lowest dating errors.

4.1.7 ZAL7

ZAL7 is a relatively large stalagmite over 35 cm in length. It shows no observable hiatuses, seismites or post depositional alterations (Figure 12). Seven samples were dated yielding growth from ~302 ka to at least ~237 ka (Table 7). It is the oldest and largest speleothem collected in this study. The age of sample (ZAL7-B) is out of stratigraphic order.

4.1.8 ZAL11

ZAL11 is a stalagmite that had begun to grow on a broken and rewelded stalagmite. The bottommost date, ZAL11-A, is either exceptionally old or has been diagenetically altered after its break. The following 2 dates are out of stratigraphic order. ZAL11-B and ZAL11-C are overturned. All dates following are in stratigraphic order. Samples ZAL11D-H show deposition from ~140 to 81 ka (Table 8), however growth was not continuous. A hiatus is visible as a change of growth axis (broken line, Figure 13) and as a very sharp variation in color and texture between sample ZAL11-F (130 ka) and ZAL11-E (96.4 ka). The section preceding the break is a very lightly colored 30cm long section, possibly with diagenetic alterations, on which another 6 cm segment was deposited (Figure 13). This top section is composed of interchanging thin layers of dark and light material.

Figures 6-13: Sections of the studied stalagmites with rulers for scale. Numbers represent sampling points for stable isotopes. Capital letters represent sampling points for dating. Calculated ages displayed in ka with 2σ error. For samples with $^{230}Th/^{232}Th<100$, corrected ages are displayed. Overturned ages in red. Hiatuses displayed as blue arrows.

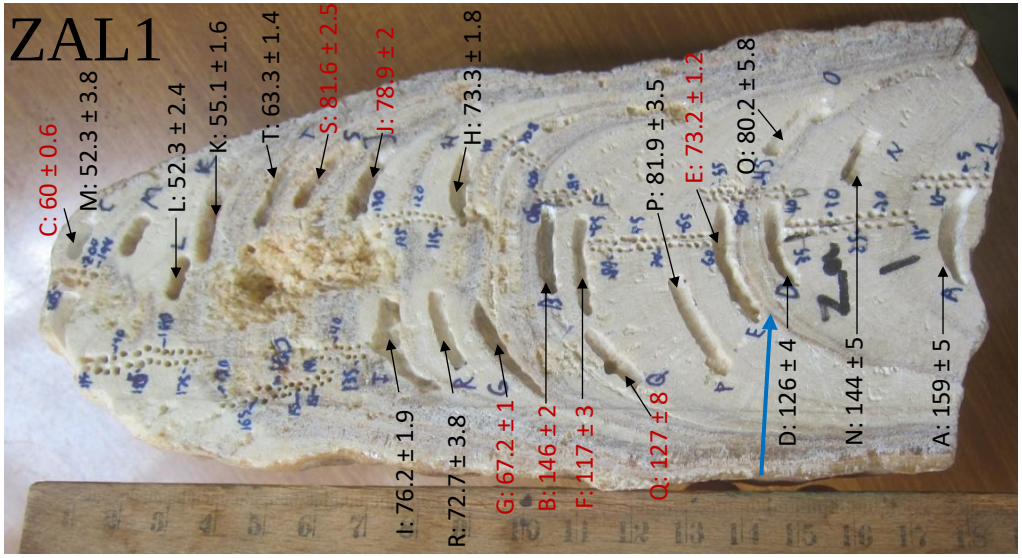

Figure 6: Photograph of ZAL1. Laminae are very thin and the calcite is lightly colored. It is a porous stalagmite in its middle-upper part. A hiatus exists between ZAL1-D and ZAL1-O, evident as a thin dark lamina (blue arrow). Several ages are out stratigraphic order, mostly in close proximity to porous areas of the stalgmite.

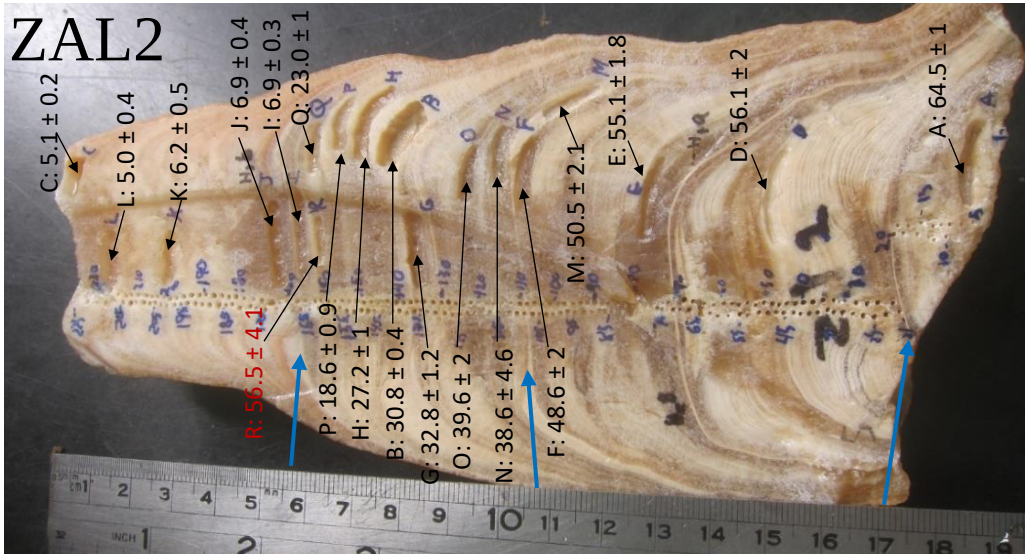

Figure 7: Photograph of ZAL2. It is comprised of alternating layers varying from dark to light calcite laminae. Two hiatuses, marked with blue arrows, are evident as a thin white lamina between ~48.6 and 38.6 ka and between ~20 ka and 6.9 ka. Another thin white lamina at sampling points ZAL2-20 was identified as a hiatus by a sharp change in isotopic composition. Apart from one date (ZAL2-R) all ages are in stratigraphic order.

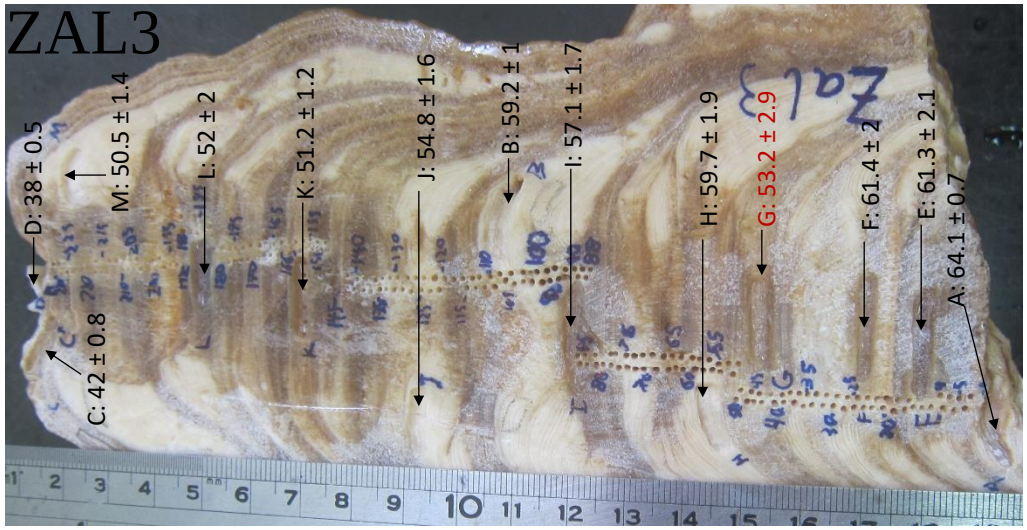

Figure 8: Photograph of ZAL3. comprised of ~3mm alternating layers of dark and light calcite laminae. No post sedimentation alterations are visible and no observable periods of hiatus. At the top of the stalagmite a younger speleothem appears (ZAL3-D). ZAL3-G is slightly overturned. All other ages are in stratigraphic order.

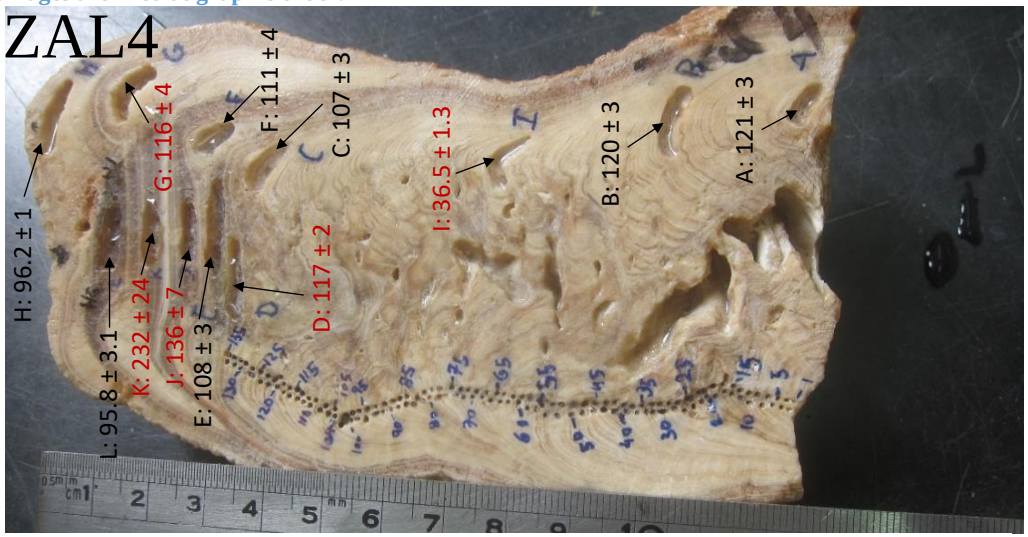

Figure 9: Photograph of ZAL4. The central part of it appears porous with possible diagenetic alterations. Sample ZAL4-I, dated to 36.5 ka, is exceptionaly young possibly due to close proximity to these alterations. The top 4 cm have a darker, more laminar composition. Due to apparent age reversals this section was not sampled for stable isotopes.

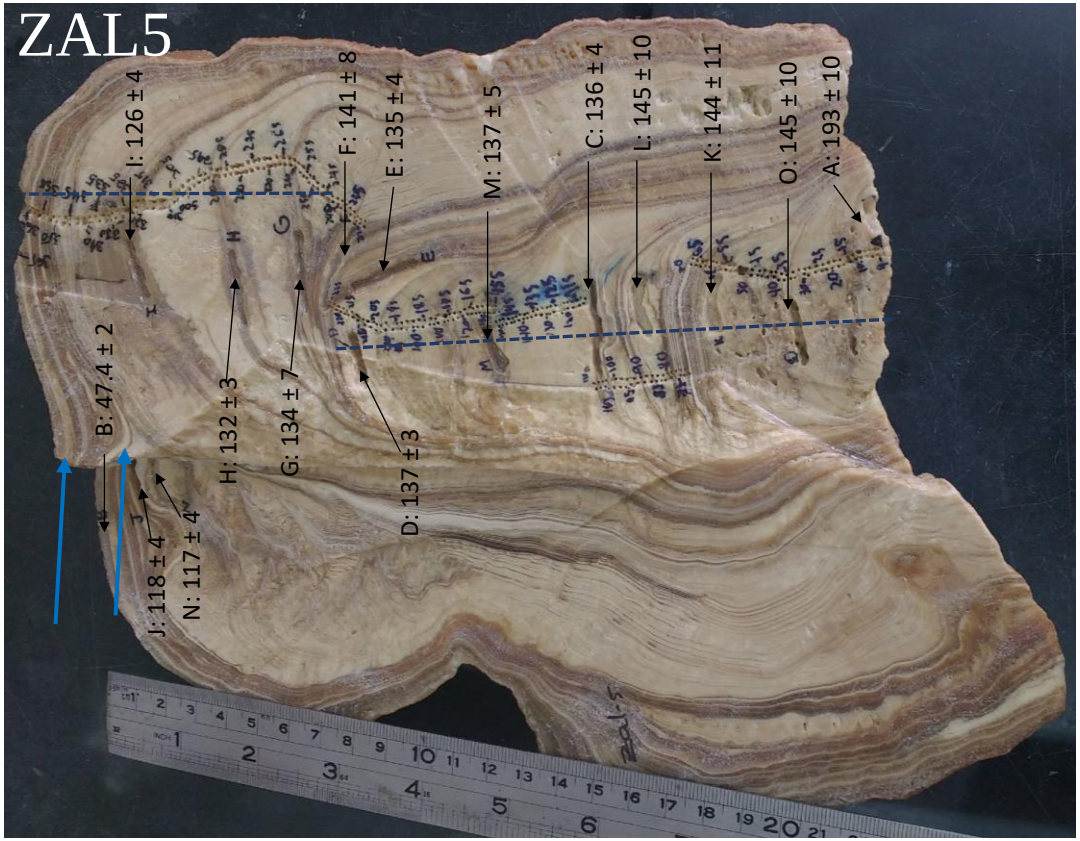

Figure 10: Photograph of ZAL5. The laminae are very thin with a shift in the location of the growth axis (broken line) following the deposition of lamina ZAL5-D. Dating shows no hiatus periods. The outer ~1.5 cm is composed of darker laminated calcite. The thin white laminae below ZAL5-B and ZAL5-N were identified as hiatuses by changes in petrography and isotopic composition (blue arrows).

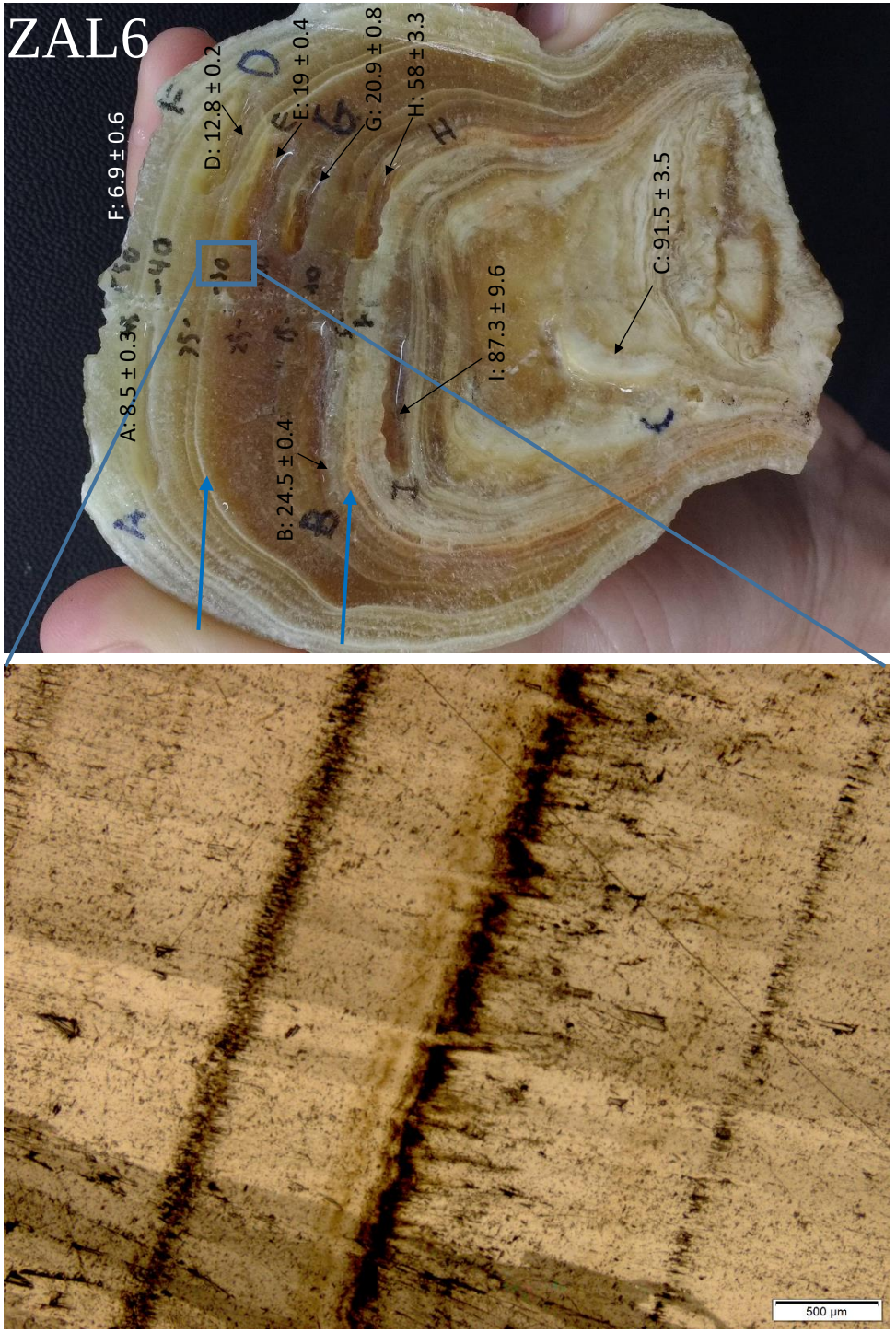

Figure 11: Top right - photograph of ZAL6. The laminae appear translucent homogeneous, >2mm thick indicating slow continuous growth. An unconformity exists between the top and bottom section. The top 3 cm were deposited between ~24.5 to ~6.9 ka with a hiatus between ZAL6-E (~18.9 ka) to ZAL6-D (~12.8 ka) evident as a thin lightly colored lamina (blue arrow). The bottom section was not sampled for stable isotopes. Bottom right – polarized petrographic thin section of the hiatus between ZAL6-D and ZAL6-E indicated by black micrite fabric.

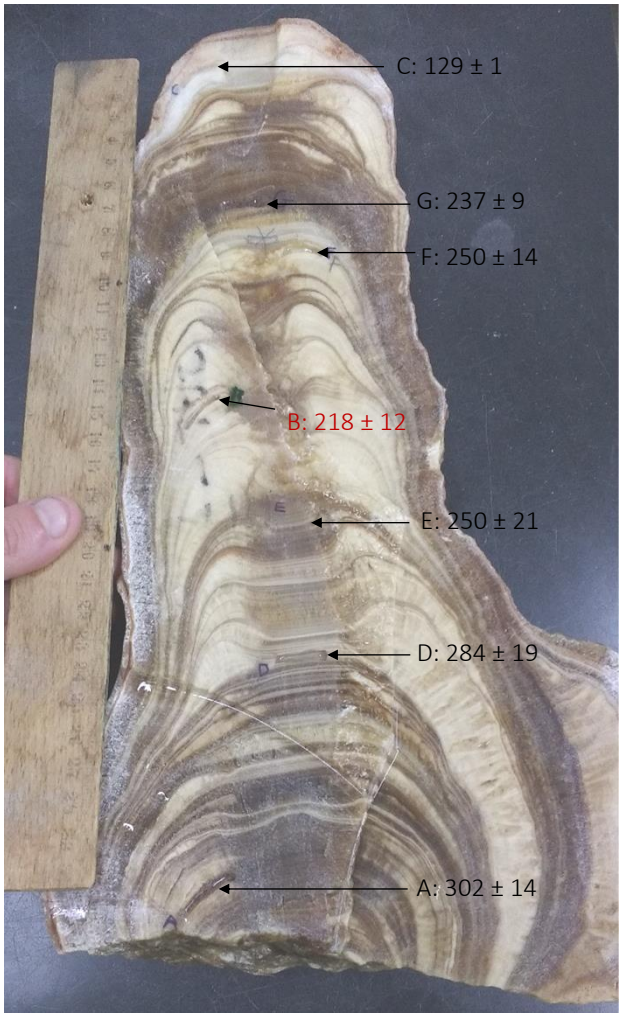

Figure 12: Photograph of ZAL7. No hiatuses or post depositional alterations are visible. 7 samples were dated yielding growth from ~302 ka to at least ~237 ka. It is the oldest and largest speleothem collected in this study. The age of sample (ZAL7-B) is out of stratigraphic order. This stalagmite was not sampled for stable isotopes.

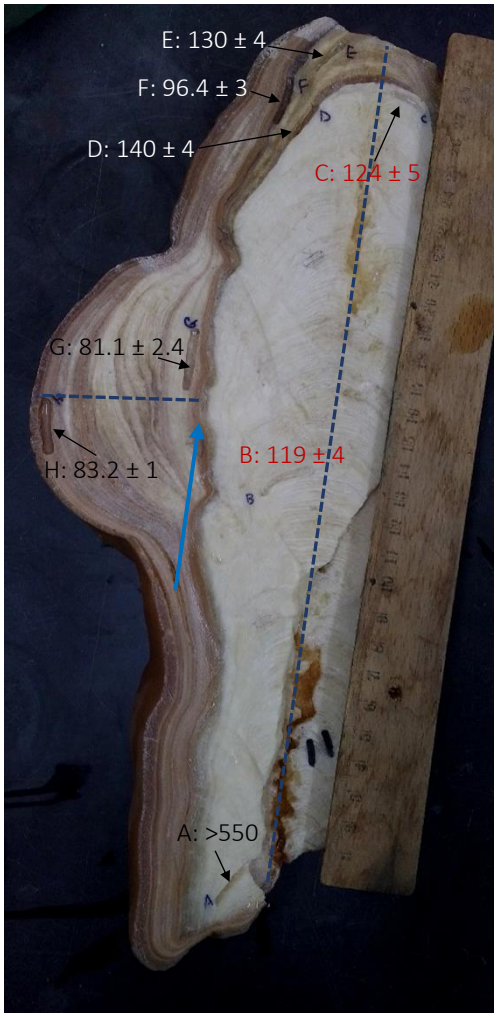

Figure 13: Photograph of ZAL11. A change of growth axis (broken line) and as a very sharp variation in color and texture exists between sample ZAL11-F (130 ka) and ZAL11-E (96.4 ka). ZAL11-B and ZAL11-C are overturned. This laminae in this part of the stalagmite are lightly colored, faded and likely diagentically altered. All dates following the internal calcite core are in stratigraphic order.

4.2 *Verification of Isotopic equilibrium*

Five laminae from four different stalagmites were sampled in various locations to determine if the speleothems were formed in isotopic equilibrium according to Hendy's (1971) criteria (Figure 14). In every lamina changes of $\delta^{13}C$ do not correlate with changes of $\delta^{18}O$. $\delta^{18}O$ change throughout the lamina, shows maximum difference of 0.35‰.

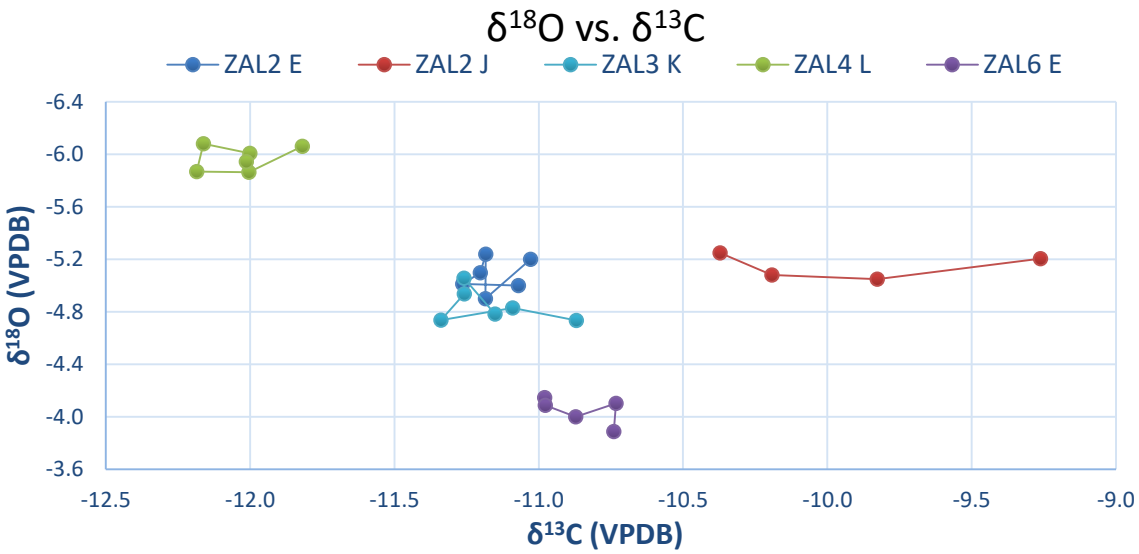

Figure 14: $\delta^{18}O$ vs $\delta^{13}C$ along 5 representative laminae from samples ZAL2, ZAL3, ZAL4 and ZAL6. $\delta^{18}O$ change throughout the laminae, shows maximum variation of 0.35‰. Changes of $\delta^{13}C$ do not correlate with changes of $\delta^{18}O$.

4.3 *Age models*

ZAL6: The top segment of this stalagmite was deposited from 24.5 to 7 ka yielding an average deposition rate of 1.5 mm/ka and varying rates between 1.1 to 3.7 mm/ka. The age model is constrained by 6 ages which are less than 0.8 cm apart and linear growth was assumed between dates. The bottom segment was not sampled for stable isotopes and is not shown in the age model. Dating errors are less than 0.8 ka and no age correction was needed (Figure 15). A hiatus was identified by petrographic and isotopic variations between 19 and 12.8 ka.

ZAL2: The age model is divided into 3 segments of deposition identified by dating results and petrographic variations. Large age gaps are apparent before and after these hiatuses (Figure 16). The bottom segment is 9 cm long and constrained by 5 dates between 64.5 and 48 ka. Growth rates for this segment vary between 5.3 and 9.1 mm/ka. The middle section was deposited between ~42 and 19 ka and is constrained by 7 dates with varying growth rates between 1.2 to 2.9 mm/ka. The date of ZAL2-R is out of stratigraphic order

and was discarded. There is a slight age reversal between laminae ZAL2-Q and ZAL2-P which could not be corrected within the dating error, therefore the average of these two dates was used for the age model. The top segment grew between 13 and 7 ka and is the fastest grown section with growth rates varying between 11.3 and 95 mm/ka and an average deposition rate of ~30 mm/ka. It is constrained by 5 dates with dating errors of less than 0.5 ka.

ZAL3: The age model for ZAL3 is a single continuous segment with varying growth rates between 4.4 to 30.7 mm/ka and an average growth rate of 11.6 mm/ka. Slight age reversals were corrected within the dating error. The date of ZAL3-G (53.2 ka) is slightly out of stratigraphic order and was discarded from the age model. ZAL3-D, the topmost date is a small speleothem formed at least 4 ka after ZAL3 stopped growing and is not part of the age model. Lamina ZAL3-C, (42±0.8 ka), was assumed to have been drilled too close to the edge of the stalagmite and was discarded from the age model as well. This is also justified by the fact that this lamina has a much lower $^{230}Th/^{232}Th$ than the rest of the speleothem suggesting possible introduction of detrital matter (Table 3). All other ages needed a correction within the measurement error to match the profile constructed from the bottom segment of ZAL2 (Figure 17).

ZAL1: The bottom segment of this stalagmite was deposited at a rate of ~1 mm/ka and the age model is constrained by 3 dates. An age gap of more than 40 ka is apparent between the top and bottom segments. Numerous age reversals make it impossible to create a reliable age model for the top segment. Linear growth was assumed between lamina ZAL1-O (dated to 80.2 ka) and lamina ZAL5-M (52.3ka) and is marked as a broken line (Figure 18) with an average deposition rate of 4.1 mm/ka.

ZAL4: The bottom 10 cm of this stalagmite are constrained by 3 dates. The age of 36.5 ka acquired from lamina ZAL4-I was discarded since it is extraordinarily reversed and a constant growth rate of 8.2 mm/ka was assumed from ZAL4-A to ZAL4-C. This assumption changes the age of ZAL4 B from 120.1 ka to 118.1, which is within the measurement error. The top 3 cm show numerous overturns and an age was not constructed from this segment and it was not sampled for stable isotopes. ZAL4-I and ZAL4-K are beyond the scale of the graph (Figure 19).

ZAL5: Aside from the top 1.5 cm this sample was deposited continuously. ZAL5-C, dated to 136±4 ka, is slightly overturned but within the dating error. It was corrected to

138 ka. Constant growth rate of 9.6 mm/ka was assumed from the bottom of the stalagmite to ZAL5-C and then, a faster growth rate of 21.7 mm/ka from ZAL5-C to ZAL5-H (132 ka) (Figure 20). The exceptionally old lamina ZAL5-A, dated to 193ka, was assumed incorrect or possibly contaminated and discarded.

Further age corrections based on isotopic compositions are elaborated in the next section.

Figures 15-20: Age models for ZAL1-6 presented in chronological order from young to old. Uncorrected ages displayed as black dots with error bars. For samples with $^{230}Th/^{232}Th<100$, corrected ages are displayed. Linear growth was assumed between dated laminae. Age model as a blue line. Right vertical axis is the depth (cm) from the top of the stalagmite. Left vertical axis is the corresponding stable isotope sample. Considerations for age corrections are elaborated in the text.

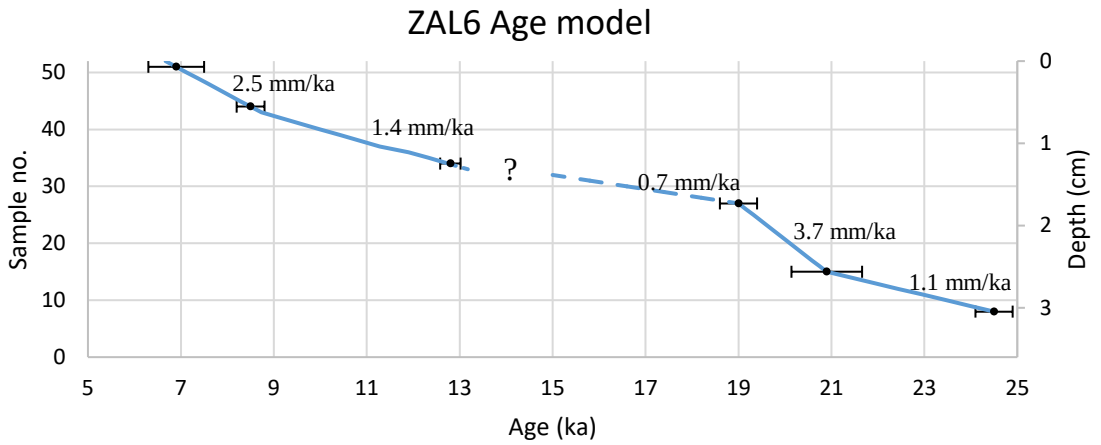

Figure 15: ZAL6 age model. No ages were corrected. The duration of the hiatus between 19 and 12.8 ka was estimated to be from 15 to 13.2 ka according to the best fit of ZAL6 $\delta^{18}O$ to Soreq Cave speleothems $\delta^{18}O$ profile.

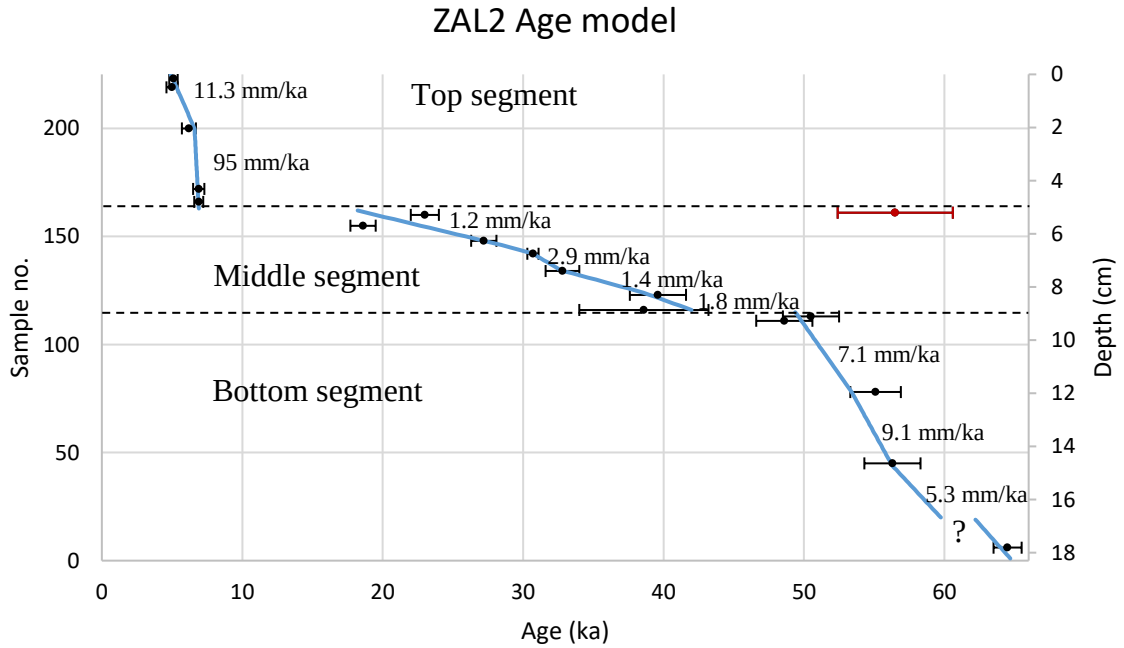

Figure 16: ZAL2 age model. The date of 56.5 ka is outstandingly of stratigraphic order and was discarded. There is a slight age reversal between laminae ZAL2-Q (23 ka) and ZAL2-P (18.6 ka), therefore the average of these two dates was used for the age model.

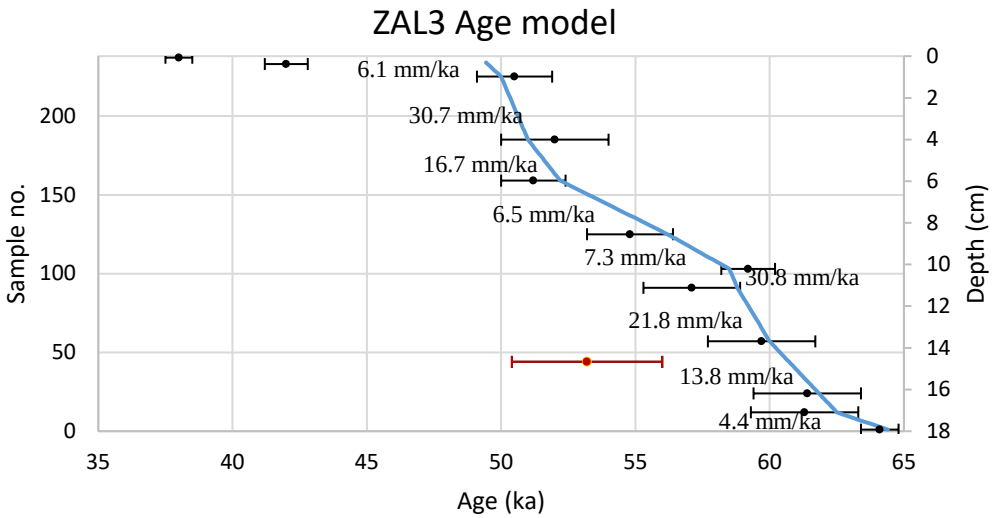

Figure 17: ZAL3 age model. The date of ZAL3-G (53.2 ka) is slightly out of stratigraphic order and was discarded from the age model. Lamina ZAL3-C, dated to 42±0.8 ka, was assumed to have been drilled too close to the edge of the stalagmite and was discarded from the age model

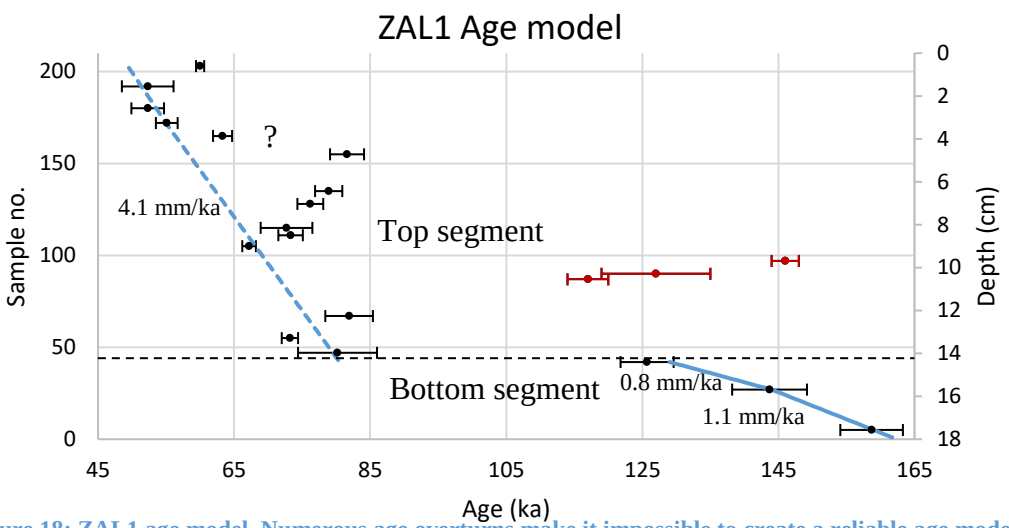

Figure 18: ZAL1 age model. Numerous age overturns make it impossible to create a reliable age model. Linear growth was assumed between lamina ZAL1-O (80.2 ka) and lamina ZAL5-M (52.3 ka) and is marked as a broken line.

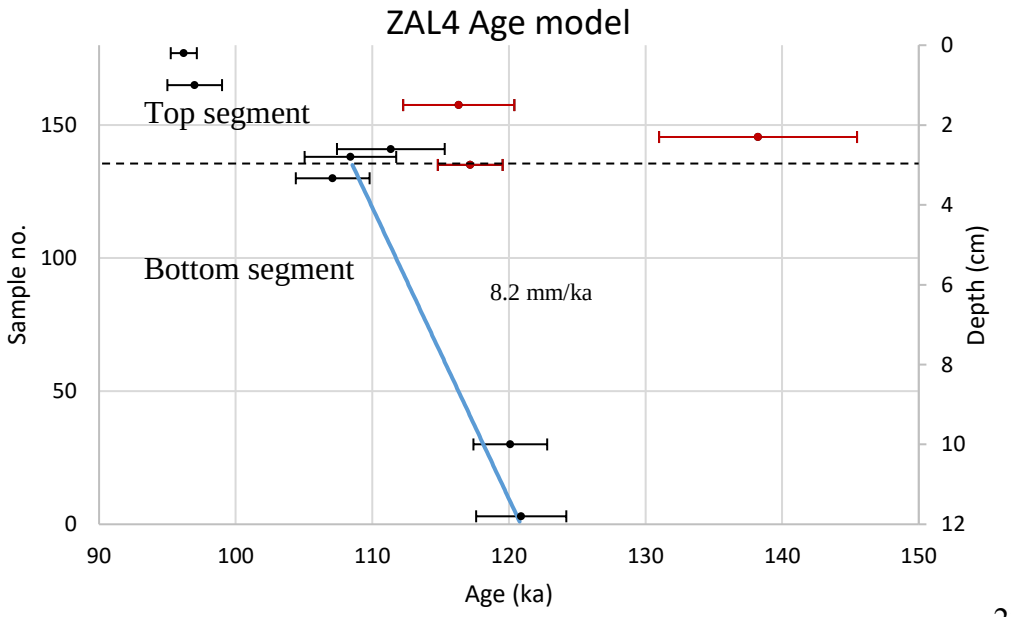

Figure 19: ZAL4 age model. Due to numerous age overturns the top section was not sampled for stable isotopes.

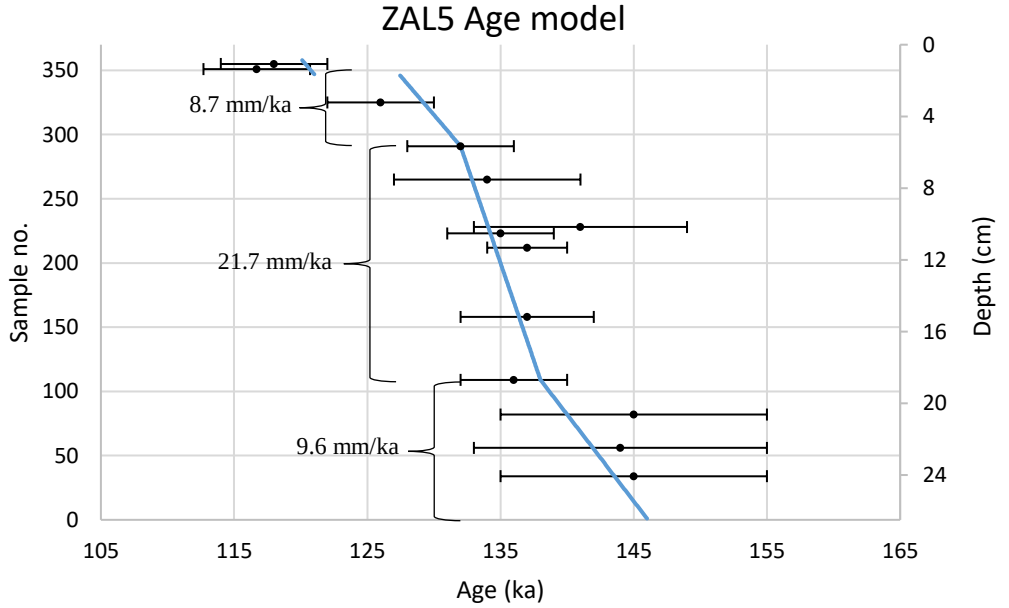

Figure 20: ZAL5 age model. ZAL5-C (136±4 ka) is slightly overturned but within the measurement error. It was corrected to 138 ka and constant growth was assumed from the bottom of the stalagmite to lamina ZAL5-C and then, at a faster growth rate, from ZAL5-C to ZAL5-H (132 ka). Further corrections and identification of hiatuses by isotopic compositions are elaborated in the text.

4.4 Isotopic profiles

A total of 1216 samples from six different stalagmites were drilled for stable isotope measurements. Single points that deviated were discarded. Hiatuses not indicated by dating were identified by change in petrography and sharp variations in the isotopic composition. All profiles are displayed with the y axis in reverse order. Ages of significant peaks or trends in the $\delta^{18}O$ were corrected (within the dating measurement error) to fit the well-dated profiles of Soreq Cave (Grant et al., 2012). For the full isotopic data and wiggle matched ages see Table 9 in the appendix. Isotopic profiles are divided into periods of continuous growth. For discussion purposes 71-14 ka is referred to as the last glacial period. 130-71 ka is referred to as the last interglacial period. The definitions of the Marine Isotope Stages (MIS) are as published by Lisiecki and Raymo (2005).

4.4.1 Age interval 1: 14 – 5 ka

The top portion of ZAL2 which has uncorrected ages of ~7.5 to ~6 ka and corrected ages of ~6.9 to ~5.1 ka was fitted to match the $\delta^{18}O$ profiles of ZAL6 and Soreq Cave speleothems (Figure 21). Wiggle-matched ages based on $\delta^{18}O$ deviate from corrected ages by less than 0.3 ka, well within the measurement error. $\delta^{18}O$ gradually decreases from ~-4‰ at ~13 ka to -6.1‰ at 9.5-8.5 ka and remains almost constant with minor fluctuations between -6.4‰ to -5.2‰ until 5 ka. $\delta^{18}O$ of ZAL6 correlates with the gradual decrease of Soreq Cave speleothems from ~13 to 8 ka. From 8 to 7 ka ZAL6 $\delta^{18}O$ is ~1.5‰ higher than Soreq Cave speleothems. $\delta^{13}C$ varies between -13.2‰ and -11.5‰ from 13 to 9 ka, gradually rises to -9‰ at 6 ka and then decreases again to -11‰ at 5ka. The exceptionally high $\delta^{13}C$ of Soreq from ~9.5 to 7 ka is not observed in Zalmon Cave speleothems. Between ~6.5 and 5.5 ka $\delta^{13}C$ of ZAL2 is ~2‰ higher than Soreq Cave speleothems. Apart from these time intervals, there is a good correlation between the isotopic profiles of ZAL2, ZAL6 and Soreq Cave speleothems.

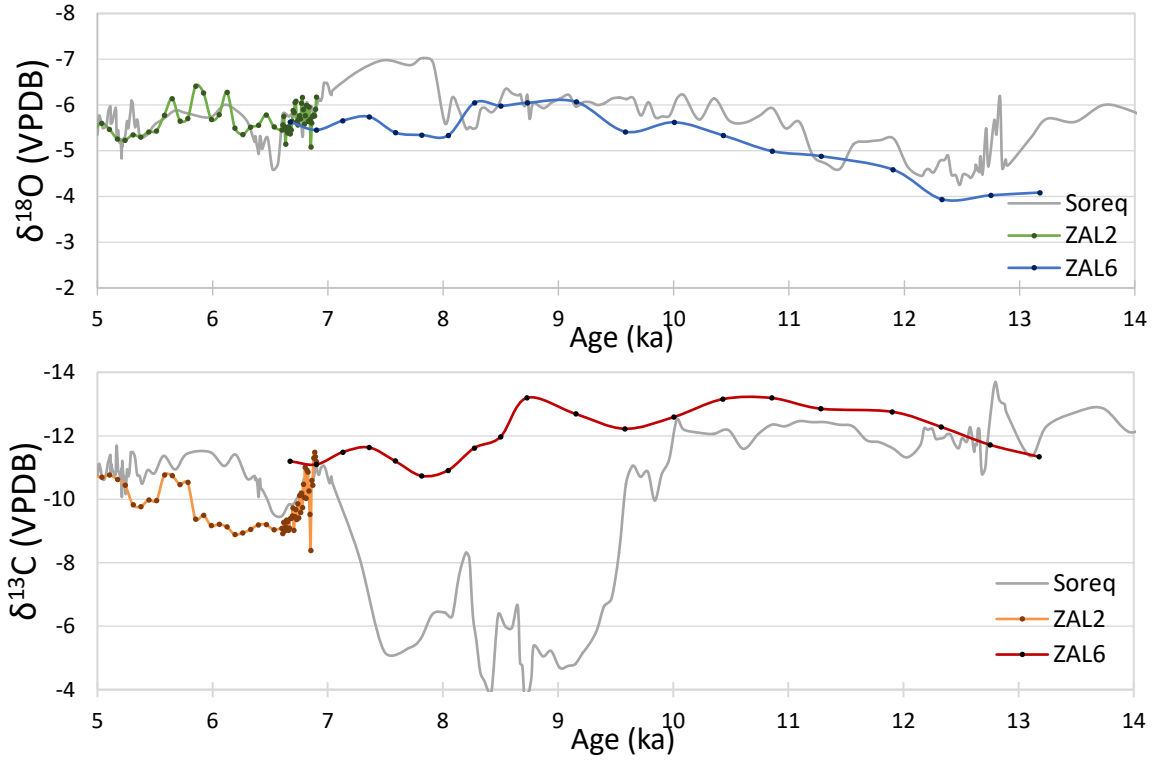

Figure 21: Isotopic profiles of age interval 1. There is a similar trend between the oxygen profile of ZAL2, ZAL6 and Soreq Cave speleothems. The exceptionally high $\delta^{13}C$ of Soreq Cave speleothems between 9.5 and 7 ka is not observed in Zalmon Cave.

4.4.2 Age interval 2: 42-15 ka

The central part of ZAL2 was wiggle-matched, within the dating errors of the corrected ages, to fit the $\delta^{18}O$ profile of ZAL6 (Figure 22). The duration of the hiatus between ZAL6-E (~19 ka) and ZAL6-D (~12.8 ka) was estimated to be from 15 to 13.2 ka according to the best fit of ZAL6 $\delta^{18}O$ to Soreq $\delta^{18}O$ profile.

$\delta^{18}O$ during this period varies between -5.5‰ and -3.7‰ and is consistently lower than that of Soreq Cave speleothems by ~0.5-2‰. $\delta^{13}C$ varies between -12.5‰ and -9.5‰ and is almost consistently lower than that of Soreq Cave speleothems by ~0.5-1.5‰. The sampling resolution for this time period is low due to slow growth rate. At ~16 ka the profiles of Soreq and Zalmon reach similar values (Figure 22).

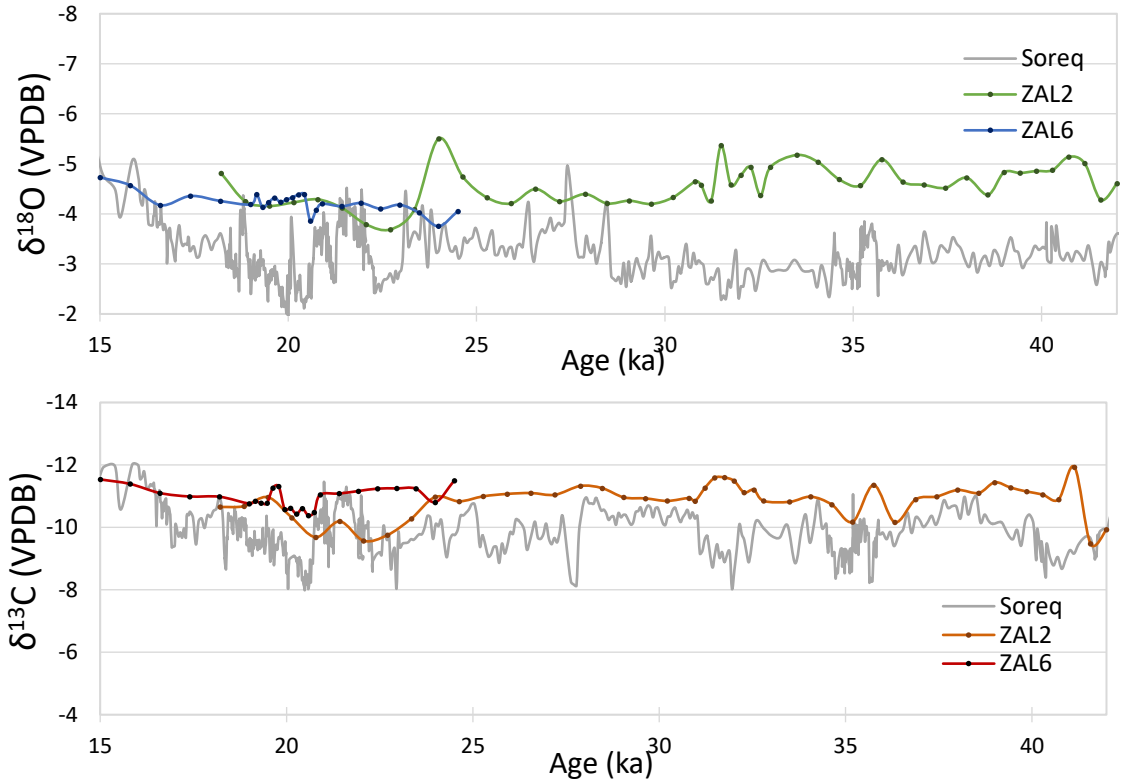

Figure 22: Isotopic profiles of age interval 2. Zalmon cave $\delta^{18}O$ is consistently lower than that of Soreq Cave speleothems by ~0.5-2‰. Zalmon Cave $\delta^{13}C$ is lower than that of Soreq Cave speleothems by ~0.5-1.5‰

4.4.3 Age interval 3: 65-49 ka

ZAL3 is a sample with very high resolution for the period of ~64 to 49 ka and correlates well with the bottom section of ZAL2, which has the same age range (Figure 23). The ages of ZAL2 were corrected within their dating error to correlate with the profile of ZAL3. A hiatus was located based on a major variation of more than 4‰ $\delta^{13}C$ and 4‰ $\delta^{18}O$ between sampling point ZAL2-19 and ZAL2-20 (Table 9). The duration and time of this hiatus was estimated by the best correlation with ZAL3, from 62.2 to 59.6ka. The thin white lamina between ZAL2-71 and ZAL2-72 show no significant variations of isotopic composition and was assumed to be continuous growth.

$\delta^{18}O$ during this time period varies between -7.5‰ and -3.8‰. Fluctuations are much larger than during the mid-late stages, possibly due to the higher sampling resolution. Zalmon Cave $\delta^{18}O$ is consistently lower than that of Soreq Cave speleothems by ~0.5-2‰, with the exception of 55 to 54 ka when Zalmon Cave and Soreq Cave speleothems exhibit similar $\delta^{18}O$ values. $\delta^{13}C$ varies between -12.2‰ and -7‰ and is similar to that of Soreq Cave speleothems with the exception of 55 to 54 ka when Zalmon

Cave $\delta^{13}C$ is ~2‰ higher than Soreq Cave $\delta^{13}C$. Both the oxygen and carbon isotopic compositions of ZAL2 and ZAL3 are in good agreement (Figure 23).

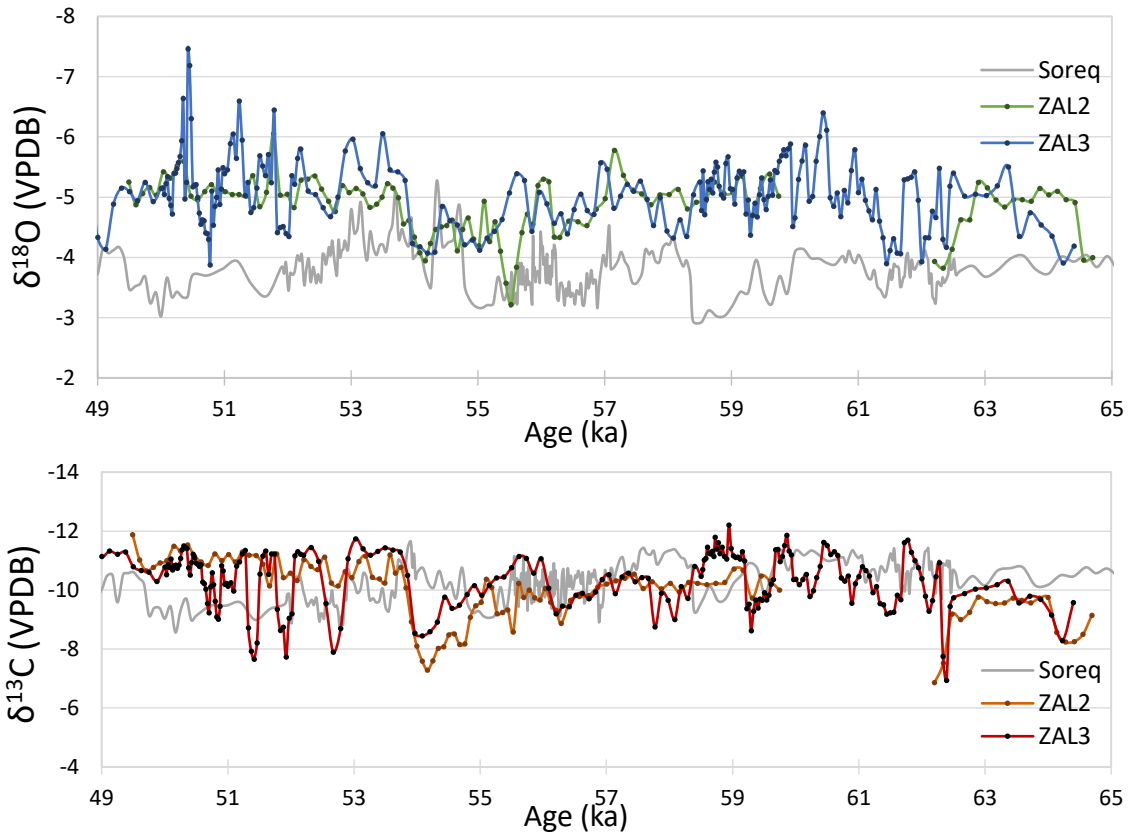

Figure 23: Isotopic profiles of age interval 3. ZAL2 and ZAL3 exhibit similar isotopic values and trends. Zalmon Cave $\delta^{18}O$ is consistently lower than that of Soreq Cave speleothems by ~0.5-2‰. $\delta^{13}C$ of Zalmon and Soreq Cave speleothems show similar values.

4.4.4 Age interval 4: 80-60ka

The previous interval is extended based on the dates and isotopic profiles of the top segment of ZAL1. This record should only be viewed as a general trend since roughly half its ages are not in stratigraphic order. From ~80 to ~71 ka Zalmon Cave speleothems and Soreq Cave speleothems exhibit similar $\delta^{18}O$ values. During this time period Zalmon Cave $\delta^{13}C$ is higher than Soreq Cave speleothems by 1-2‰.

From ~71 to ~60 ka Zalmon Cave $\delta^{18}O$ is lower than Soreq Cave speleothems by 1-2‰. During this time period Zalmon Cave speleothems and Soreq Cave speleothems exhibit similar $\delta^{13}C$ values.

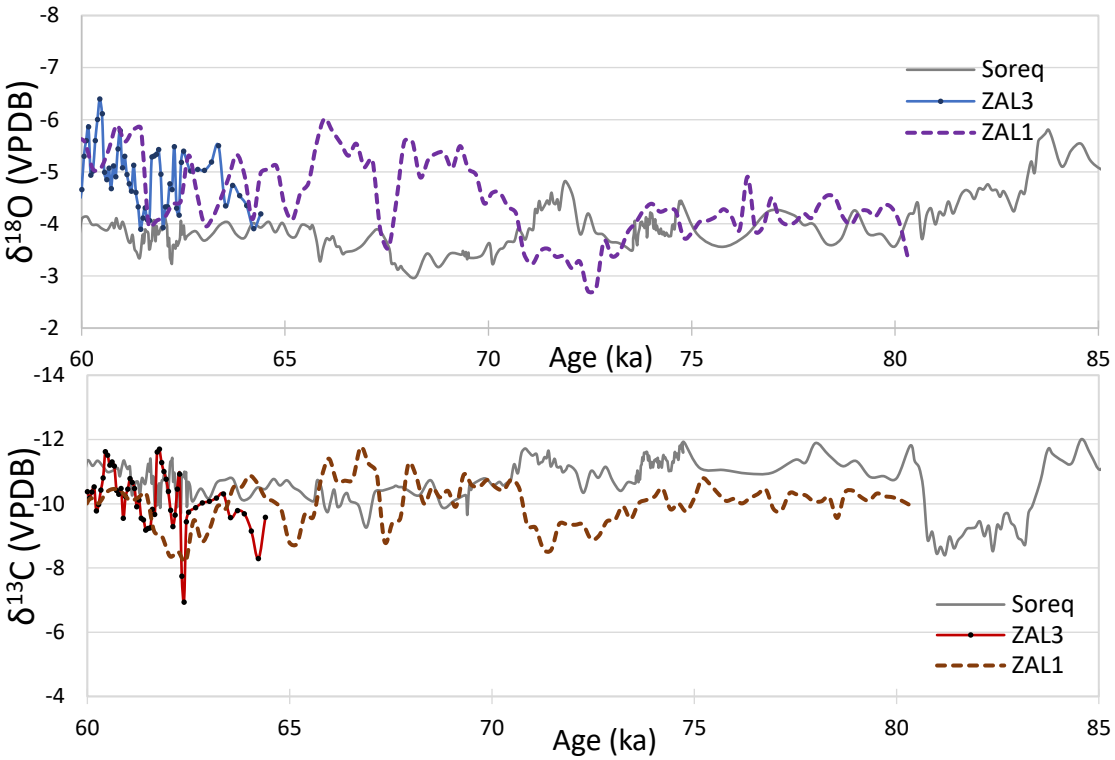

Figure 24: Isotopic profiles of age interval 4 - extension of the glacial isotopic profile into MIS5 based on ZAL1. From 80 to 71 ka ZAL1 has similar $\delta^{18}O$ values and higher $\delta^{13}C$ than Soreq Cave speleothems. From 71 to 60 ka ZAL1 has lower $\delta^{18}O$ and similar $\delta^{13}C$ values than Soreq Cave speleothems.

4.4.5 Age interval 5: 121-107 ka

The isotopic profiles of ZAL4 correlate well with the profile of Soreq (Figure 25). Both Soreq and Zalmon Caves' isotopic profiles for this time period show little fluctuations so wiggle matching was not needed. The top portion of ZAL4 was not used for isotopic profile construction due to its age reversals. $\delta^{18}O$ varies between -5.9‰ and -4.1‰ and is in good agreement with that of Soreq Cave speleothems. $\delta^{13}C$ varies between -12.2‰ and -9.9‰ with very minor fluctuations. The $\delta^{13}C$ profile of Zalmon Cave speleothems is slightly higher than that of Soreq Cave speleothems by roughly 1-2‰.

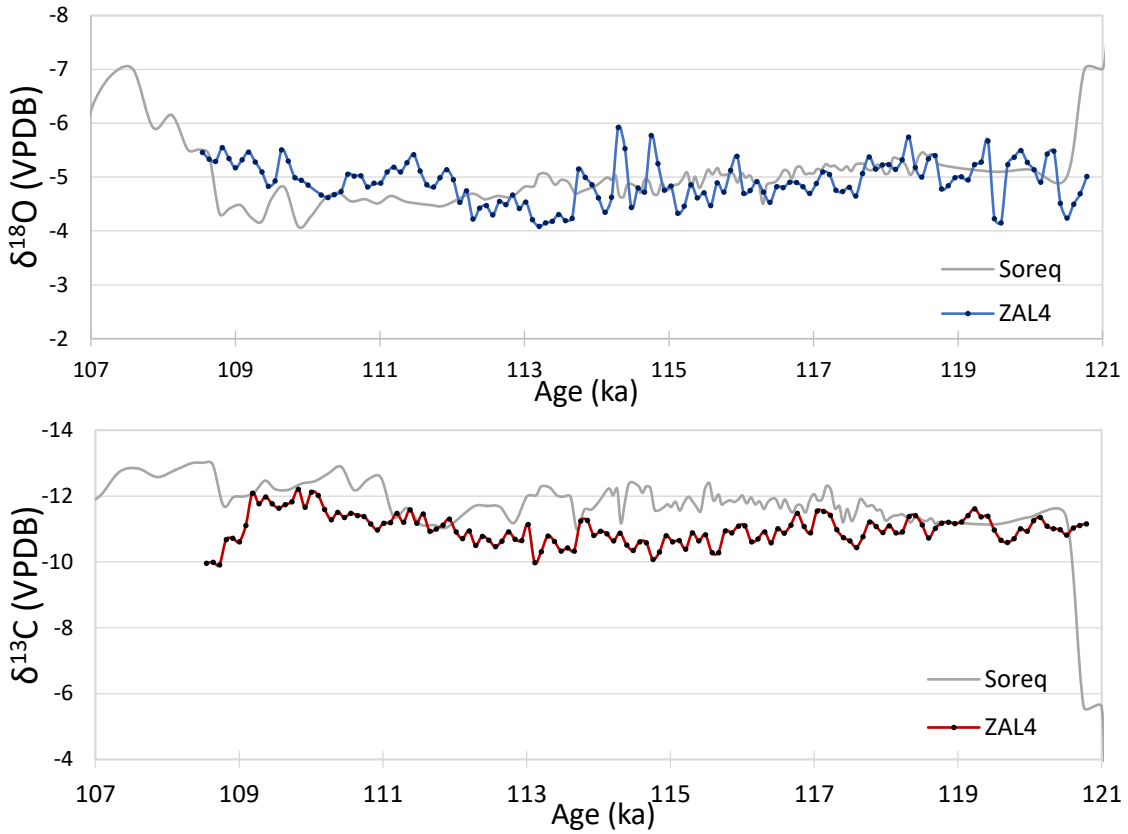

Figure 25: Isotopic profiles of age interval 5. ZAL4 $\delta^{18}O$ is in good agreement with that of Soreq Cave speleothems. ZAL4 $\delta^{13}C$ is ~1-2‰ higher than Soreq Cave speleothems. Both profiles show very minor oscilations.

4.4.6 Age interval 6: 160-115ka

The profile for this time interval is constructed using speleothems ZAL5 and ZAL1. The major variation in $\delta^{13}C$ and, to a lesser extent in $\delta^{18}O$, between ZAL5-345 and ZAL5-348 was attributed the exceptionally high $\delta^{13}C$ observed in Soreq at 128ka. This point was given an age of 128 ka and was assumed to precede a hiatus. Under these assumptions all ages used are within the dating error of the laminae's calculated ages (Table 9, Figure 16). ZAL5-347 to ZAL5-358 were wiggle matched in accordance with the sharp descending $\delta^{13}C$ profile of Soreq Cave speleothems at ~121 ka. The $\delta^{18}O$ was matched in accordance with ZAL4 and displayed as a broken line (Figure 26). The ages assigned to these laminae are within the dating errors of ZAL5-N and ZAL5-J (Table 9, Figure 16). The isotopic profile created from this portion of ZAL5 is displayed as a broken line (Figure 26). The top of the stalagmite is dated to 47.2 ka and a hiatus was identified ~5 mm below as a thin

white lamina (sampling point ZAL5-359, Figure 10) also indicated by a sharp variation of 2.5‰ $\delta^{13}C$ and 0.8‰ $\delta^{18}O$ between sample ZAL5-358 and ZAL5-359 (Table 9).

The bottom portion of ZAL1 has low sampling resolution due to slow growth rate. Its isotopic profile roughly correlates with ZAL5 from ~146 ka to 135 ka (Figure 26). Since the very high $\delta^{13}C$ values are not observed in this portion of ZAL1 it was assumed not to be younger than 128ka. The sampling resolution of ZAL5 is ~5-10 times higher than Soreq during this time period. From ~146 to 135 ka $\delta^{18}O$ of ZAL5 varies between -5.3‰ and -3.6‰ and then gradually becomes lower, with notable oscillations, from -3.6‰ at 135ka to -7.2‰ at 128. $\delta^{18}O$ of ZAL5 is ~1‰ lower than Soreq from 146 to 140 ka. From 140 to 128 ka ZAL5 $\delta^{18}O$ is in good agreement with that of Soreq Cave speleothems. ZAL5 $\delta^{13}C$ varies between -12.2‰ and -9.9‰ with very minor fluctuations from 146 to 130 ka, then gradually decreases to -13.3‰ before experiencing a very sharp increase to values of ~0‰ at ~128ka. ZAL1, ZAL5 and Soreq Cave $\delta^{13}C$ values are in good agreement through this time period.

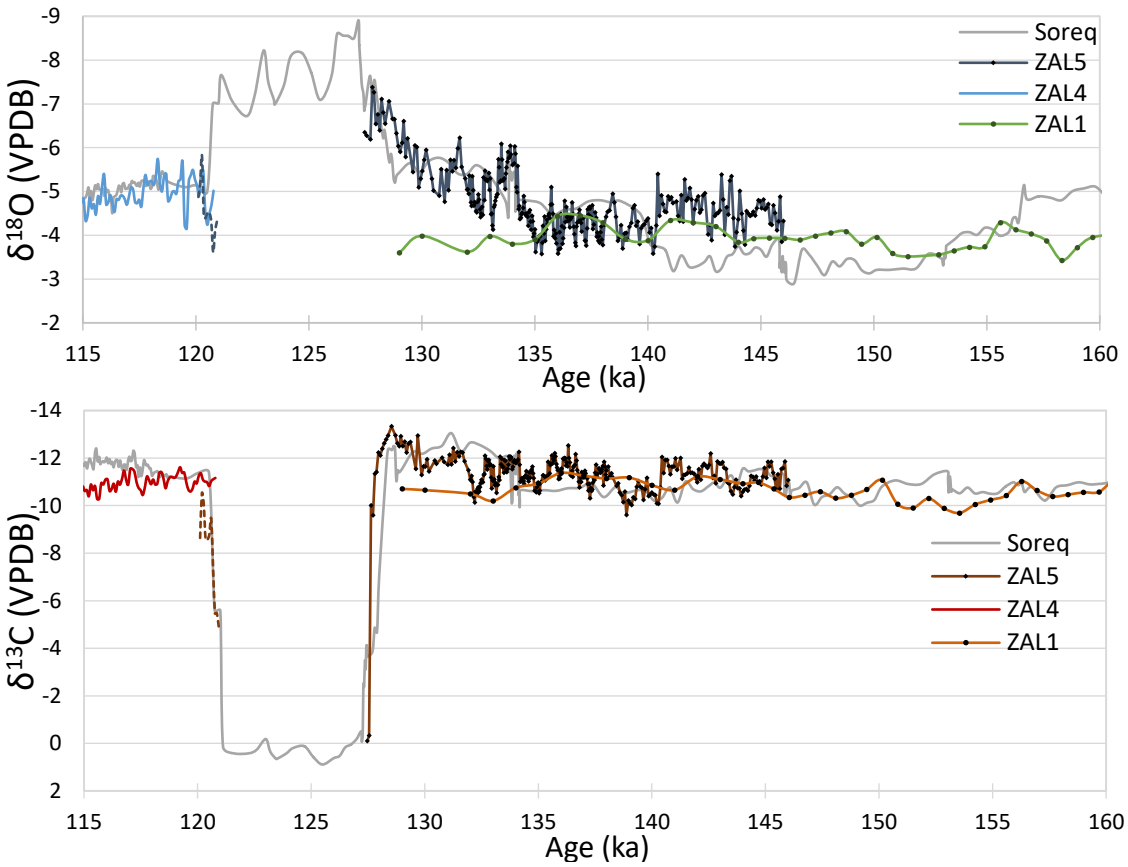

Figure 26: Isotopic profiles of age interval 6. ZAL5 has a much higher sampling resolution than Soreq. ZAL5 $\delta^{18}O$ is ~1‰ lower than Soreq Cave speleothems from 146 to 140 ka. From 140 to 128 ka ZAL5 $\delta^{18}O$ is in good agreement with that of Soreq Cave speleothems. A hiatus is apparent for most of the high $\delta^{13}C$ period occurring in Soreq Cave from ~128.5 to 120.5 ka.

5 Discussion

5.1 Deposition in isotopic equilibrium

Zalmon Cave speleothems were deposited in isotopic equilibrium based on Hendy's (1971) criteria (Figure 14). Moreover, isotopic composition of speleothems that were deposited during the same time interval show striking similarities (Figure 23) satisfying the "replication test" (Bar-Matthews et al., 1997; Dorale and Liu, 2009). This suggests that kinetic fractionation effects are negligible and that the speleothems from Zalmon Cave are suitable for paleoclimate reconstruction.

5.2 Growth Periods

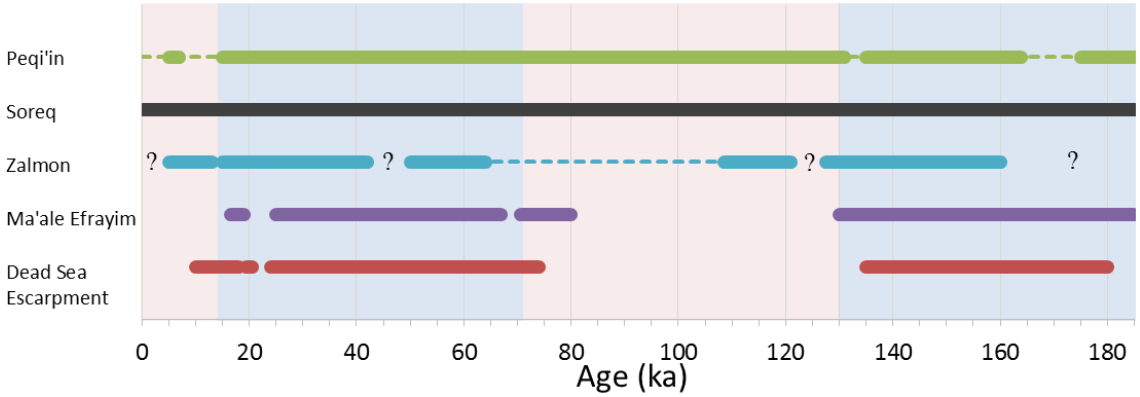

Figure 27: Periods of speleothem deposition from various caves in Israel. Light blue fields represent glacial periods, light red fields represent interglacial periods. For Zalmon cave, broken line represents depositional periods requiring further study.

Deposition in Zalmon cave was mostly continuous both during glacial and interglacial periods (Figure 27). No samples were dated between 50-42 ka, 15-13 ka and 5-0 ka. From 107 to 65 ka current ages require further study. Lack of deposition can reflect either lack of sampling, as is assumed for Peqi'in Cave (Bar-Matthews et al., 2003), or depositional hiatuses. Deposition of speleothems during interglacial periods suggests that Eastern Galilee received an average annual rainfall of at least 300mm as was suggested for the Negev Desert (Vaks et al., 2006), central and northern Israel (Bar-Matthews et al., 2003). Within caves located in the Dead Sea Escarpment speleothem deposition was slow as indicated by very thin sequences and was limited primarily to glacial periods (Lisker et al., 2010). Similar patterns of deposition are also observed in Ma'ale Efrayim with slightly higher deposition rates evident from the thicker sequences (Vaks et al., 2003).

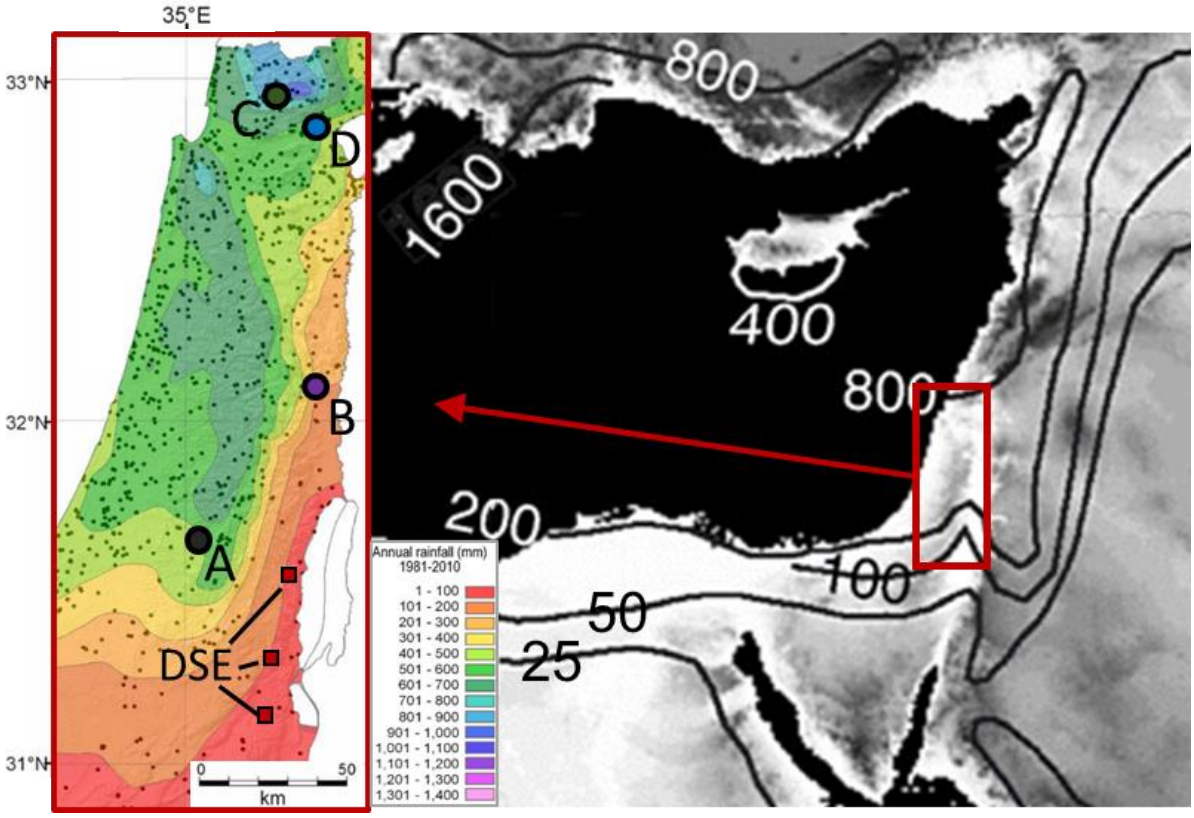

Figure 28: Annual isohyet maps. Right panel: Eastern Mediterranean modified after Enzel et al. (2008). Left panel: Average 1981-2010 annual rainfall (mm) modified after Ziv et al. (2014). Rain sampling stations as black dots. Location of caves as colored circles: A – Soreq Cave, B - Ma'ale Efrayim Cave (Vaks et al., 2003), C - Peqi'in Cave (Bar-Matthews et al., 2003), D - Zalmon Cave (present study). DSE - Dead Sea escarpment caves (Lisker et al., 2010)

Regardless whether absence of speleothem dates, corresponding to interglacials, in Zalmon Cave represents a lack of sampling or hiatuses, it is clear that the growth pattern gradually changes from south to north along the Jordan Rift. The southern rift exhibits very minimal growth limited only to glacial periods. The central rift exhibits higher glacial deposition rates with limited interglacial deposition. The northern rift exhibits continuous growth for longer time intervals through most of the interglacial and glacial periods. This suggests more rainfall in the northern part of the DST compared to its southern extension, similar to present-day conditions (Figure 28).

It is most probable that the main source of precipitation of Zalmon cave, located in the northern part of the rift is associated with a moisture source from the Eastern Mediterranean Sea, similar to central and Northern Israel (Bar-Matthews et al., 2003). This is also the contributor of 90% of the rainfall today (Saaroni et al., 2010).

5.3 Isotopic composition of speleothems from Zalmon Cave and their paleoclimate significance

$\delta^{18}O$ values of Zalmon Cave speleothems vary between -6 and -3.5‰ while $\delta^{18}O$ values of Soreq Cave speleothems vary between -8.5 to -2‰ during the same time intervals exhibiting a much greater variation between glacial and interglacial periods (Figure 29). Comparison of the isotopic compositions clearly shows that maximum glacial values in Zalmon Cave are ~1-1.5‰ lower than caves in central Israel (Frumkin et al., 2000; Bar-Matthews et al., 2003; Grant et al., 2012) during the same time interval. Here we explore the reasons why Zalmon cave speleothems are more depleted in ^{18}O during glacial periods, in contrast to interglacial times where their isotopic composition becomes similar to those of central Israel. This depletion trend is also observed, to a lesser extent, when comparing the isotopic records with those of Ma'ale Efrayim Cave speleothems (Vaks et al., 2003) and Peqi'in Cave speleothems (Bar-Matthews et al., 2003) indicating a general ^{18}O depletion trend from central Israel eastward and northward (Figure 29).

The offset between Zalmon Cave and Soreq Cave during MIS6 is less pronounced. $\delta^{18}O$ of Zalmon Cave speleothems is ~1‰ lower than Soreq Cave speleothems between ~155 and 140 ka, and almost not offset between ~140 and 128 ka. The climate in the central part of the eastern Mediterranean during MIS6, although cold, was most likely more humid and probably not as severe as the last glacial (Ayalon et al., 2002).

In order to examine the causes for the glacial differences between speleothem $\delta^{18}O$ records from Zalmon Cave and Soreq Cave, present day conditions are discussed. Based on neighboring Israel Meteorological Service stations the average annual temperature and precipitation in Zalmon Cave area is 21±0.5°C and 550 mm/y respectively, similar to Soreq Cave area which is 20.5°C and 500mm/y respectively. $\delta^{13}C$ values of Zalmon Cave speleothems vary between -9.5 to -12‰ for most of the glacial and interglacial depositional periods presented in this study demonstrating the dominance of C3 type vegetation. The ~2.5‰ variations in Zalmon Cave speleothems indicate mostly vegetation response to changes in soil productivity and cannot be attributed to a large scale change in vegetation. During glacial periods $\delta^{13}C$ remains low, ranging between ~-10 to -11‰ indicating that throughout the glacials, C3 vegetation dominated the cave's region implying relatively humid conditions.

Can a temperature difference alone, during the last glacial period, explain the $\delta^{18}O$ offset between Zalmon and Soreq cave speleothems? A change of 1‰ in $\delta^{18}O$ for carbonate precipitated in equilibrium would correspond to a change of about 4°C (Kim and O'Neil, 1997) meaning the difference in temperature between Zalmon Cave and Soreq Cave would have been 4-8°C higher during the last glacial. Clumped isotope thermometry, fluid inclusion studies and marine core temperatures (McGarry et al., 2004; Affek et al., 2008; Almogi-Labin et al., 2009) suggest that the temperature in Soreq Cave was 6-10°C colder during the LGM (when the $\delta^{18}O$ offset is 1.5‰) and 3°C colder at 56 ka (when the $\delta^{18}O$ offset is ~1‰). If temperatures in Zalmon Cave region were indeed 4-8°C higher it applies that during the last glacial period the temperature in Zalmon Cave area was similar to present-day which is highly coincidental and therefore improbable. Thus a temperature difference alone cannot explain this offset.

Another possible scenario which can explain the lower $\delta^{18}O$ of Zalmon Cave speleothems is increased rainfall in the region of Zalmon Cave compared to central Israel during the last glacial. Ayalon et al. (2004) show a present day linear relationship of 225 mm rain per 1‰ of $\delta^{18}O$ for Soreq Cave rainwater infiltrating the unsaturated zone. Orland et al. (2014) demonstrated an annual relationship of ~275 mm rain per 1‰ for a modern day

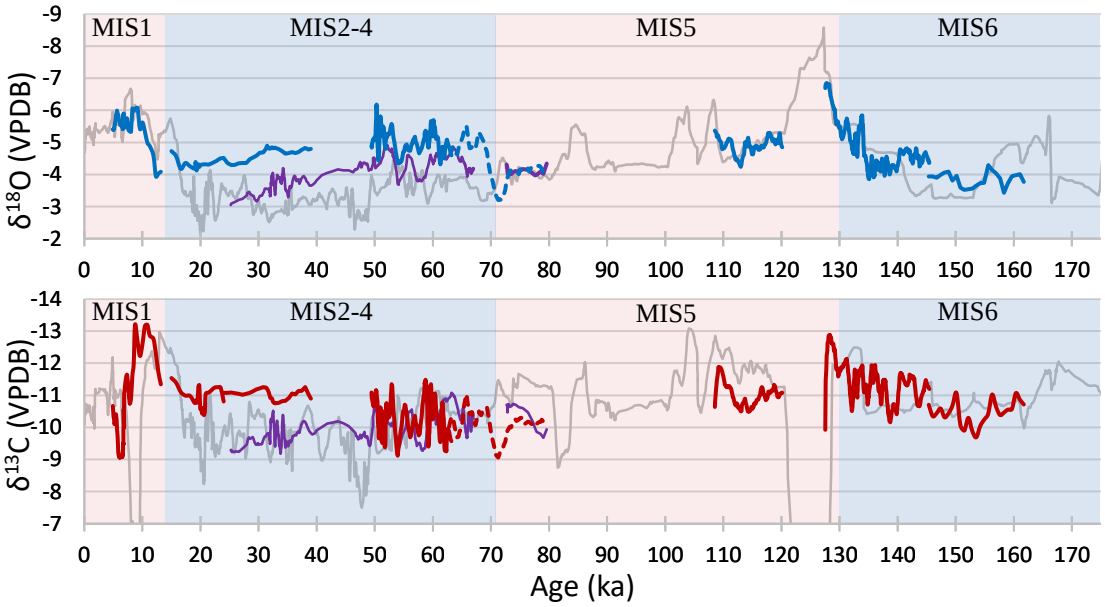

Figure 29: Comparison of isotopic profiles represented as a running average (further detail in Section 7.3). Zalmon Cave $\delta^{18}O$ and $\delta^{13}C$ as blue and red lines respectively. Ma'ale Efrayim in purple (Vaks et al., 2003). Soreq in light grey (Grant et al., 2012). $\delta^{18}O$ of Zalmon Cave speleothems varies between -6 and -3.5‰. $\delta^{18}O$ of Soreq Cave speleothems varies between -9 to -2‰ exhibiting a much greater variation between glacial to interglacial periods. Zalmon Cave $\delta^{18}O$ is ~1-1.5‰ lower than Soreq Cave speleothems during the last glacial periods but show similar values during interglacial periods. Likewise to a lesser extent, the profiles of Ma'ale Efrayim and Soreq are similarly offset. During MIS6 $\delta^{18}O$ of Zalmon Cave speleothems is ~1‰ lower than Soreq Cave speleothems from ~155 to 140ka and the offset almost vanishes from ~140 to 128ka. Offsets of less than 2‰ between the $\delta^{13}C$ profiles are observed for these time intervals.

Soreq Cave stalagmite. Goldsmith et al. (2016) published an exponential fit for Mediterranean sites: $\delta^{18}O = -1.625\ln(x) + 4.5$ where x is the rainfall (mm/year), however these relationships were not necessarily similar during the last glacial. Nevertheless, it is quite probable that a higher input from rainfall in Zalmon Cave region is one of the major factors causing the lower $\delta^{18}O$ values.

To explain this enhanced rainfall scenario a different moisture trajectory for the last glacial period is examined (Enzel et al., 2008; Goldsmith et al., 2016). Presently, the main contributors of rainfall in Israel, imparting 90% of the annual amount, are cyclones called Cyprus lows (storms passing, intensifying or even developing over Cyprus). These storms transport cool air originating from Eastern Europe over the warmer Mediterranean where it becomes moist and unstable (Saaroni et al., 2010). Enzel et al. (2008) proposed that during the last glacial the Eastern Mediterranean cyclones migrated southwards (Figure 30) as a result of snow covered Europe and Turkey as well as lowered sea level leading

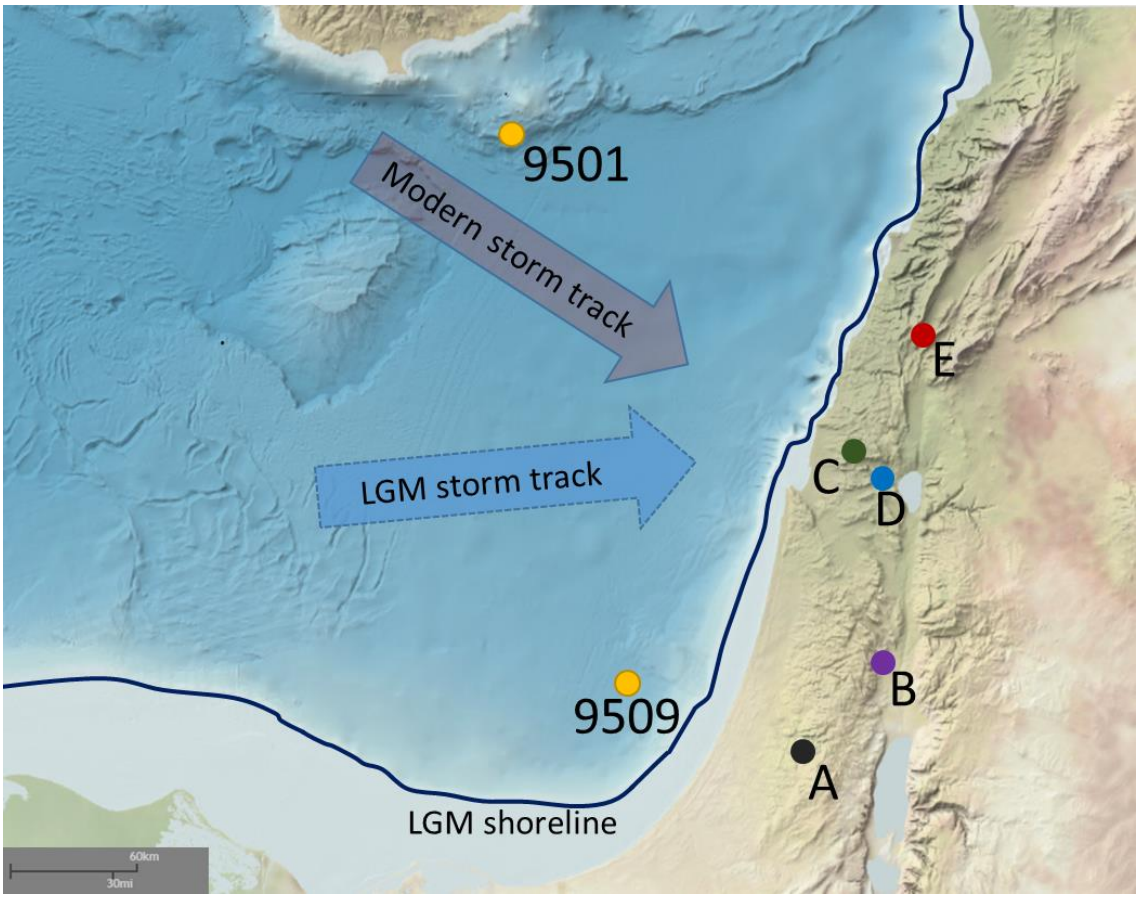

Figure 30: Bathymetric map of the Eastern Mediterranean Sea ("NOAA – National Oceanic and Atmospheric Administartion") with estimated last glacial maximum (LGM) shoreline as a blue line. Modern day wind directions as a red arrow. Proposed last glacial period wind direction as a blue arrow (Enzel et al., 2008). Cave locations represented by capital letters: A - Soreq, B - Ma'ale Efrayim, C – Peqi'in, D - Zalmon. E – Mizpe Shelagim Cave. Marine Core 9501 and 9509 locations as yellow circles (Almogi-Labin et al., 2009).

the storms to be funneled along the Mediterranean directly eastward to the Levant. Their lower pressure would have enhanced rainfall in the northern Levant while central Israel would have received roughly the same amounts. Examination of the bathymetry of the Eastern Mediterranean shows that during the LGM the regression near south and central Israel was ~20km larger than that of northern Israel and Lebanon (Hall et al., 1994) (Figure 30). Under present day synoptic systems, the larger distance from the source waters should cause lower $\delta^{18}O$ in Soreq Cave speleothems rather than Zalmon Cave. This implies that the storm track travelled a longer distance to the cave location, supporting the southern shift in the synoptic system.

Interestingly the largest offset towards lower $\delta^{18}O$ and $\delta^{13}C$ values in Zalmon Cave speleothems occurred during last glacial and coincide with the highest stand of Lake Lisan (Figure 31, F). There are several arguments for such high lake levels. Lake Lisan high stands are associated with high precipitation/evaporation ratios which possibly resulted from lower temperatures during the last glacial and more effective infiltration (Bar-Matthews et al., 1997; Bar-Matthews et al., 2003; Vaks et al., 2003; Vaks et al., 2006). Stein et al. (1997) claimed the high stands occurred at periods of relatively increased moisture and increased fresh water input in the lake catchment area. Enzel et al. (2008) suggested that the lake levels were directly influenced by regional climate in the Eastern Mediterranean during the late Pleistocene. Torfstein et al. (2013) claimed that evaporation rates during the glacial period were likely as high as or possibly higher than present day which emphasizes the requirement for significant freshwater input as the source of lake level high stands. They concluded that lake level fluctuations are overwhelmingly controlled by the precipitation component of the regional hydrological cycle.

To conclude, the low Zalmon Cave $\delta^{18}O$ values observed during the last glacial period most likely imply that the cave's region was more humid. This assumption is further supported by the slightly lower $\delta^{13}C$ values implying the dominance of C3 type vegetation ratio which adapted to humid climate. A probable explanation for the offset between Soreq and Zalmon caves can be explained by a combination of a temperature difference of 1-2°C and a larger amount of rainfall associated with a different synoptic system. The smaller offset during MIS6 probably indicates that the southern shift in storm was less dominant during this time.

5.4 The source effect variations

$\delta^{18}O$ values of cave drips reflect the $\delta^{18}O$ of rainwater from which speleothems were deposited, thus speleothems' $\delta^{18}O$ reflects mainly changes in sea surface source (Frumkin et al., 1999) of atmospheric vapor that leads to cloud formation. $\Delta\delta^{18}O$, defined as the difference between the marine sea surface source and rainfall, results from a complex combination of evaporation processes above the sea, distance traveled by the clouds over land, cooling effects due to increased elevation, and the "amount effect". Bar-Matthews et al. (2003) showed that the average $\Delta\delta^{18}O_{sea-land}$ values, as evident from the difference between speleothems $\delta^{18}O$ and the planktonic foraminifera *Globigerinoides ruber* $\delta^{18}O$ values, was relatively constant at 5.6±0.7‰ during the last 185 ka. $\Delta\delta^{18}O$ oscillations were interpreted to largely reflect the amount effect of decreasing $\delta^{18}O$ of rainfall with increasing amount. Kolodny et al. (2005) interpreted this relative constancy across the last glacial–present interglacial transition to indicate that the EM speleothems $\delta^{18}O$ record primarily reflects sea surface $\delta^{18}O$ changes. If, indeed, the source effect is the main control on speleothem $\delta^{18}O$, why is it reduced in Zalmon Cave speleothems, mainly during the last glacial?

The isotopic records of Zalmon cave as well as speleothem records from Soreq, Peqi'in and Ma'ale Efrayim caves (Bar-Matthews et al., 2003; Vaks et al., 2003; Grant et al., 2012) were compared to the $\delta^{18}O$ values of the planktonic foraminifera *G. ruber* from marine cores 9501 and 9509 as was done by Bar-Matthews et al. (2003) and Almogi-Labin et al. (2009). The differences are presented as a 3 point moving average (Figure 31A-D). For the time interval of ~50 to 42 ka for which there are no dated speleothems Zalmon Cave $\delta^{18}O$ was estimated to vary linearly and is presented as a broken line. For further information regarding this figure refer 7.4 in the appendix. During the last glacial period Zalmon Cave's $\Delta\delta^{18}O$ varies between 5 and 9‰ (Figure 31D) and is consistently higher than that of Soreq (Figure 31A) indicating Zalmon Cave speleothems' $\delta^{18}O$ deviates from the "source effect" much more than Soreq Cave speleothems. Peqi'in Cave $\Delta\delta^{18}O$ values (Figure 31C), although not as high as Zalmon Cave, are slightly higher than Soreq Cave as well implying there is a local system overriding the "source effect". Why the "source effect" in Zalmon Cave is less pronounced compared to central Israel? Can the southern shift of the glacial storm tracks explain this deviation?

Southward shifting of the storm direction during the last glacial period, in accordance with the proposed wind directions (Figure 30), implies a larger travel distance of the moisture over the land, perhaps ~10-30 km. This may have resulted in larger Rayleigh distillation of rainfall before reaching Zalmon Cave. This can explain the higher $\Delta\delta^{18}O_{sea\text{-}Zalmon}$ values. Furthermore, the $\Delta\delta^{18}O_{9509\text{-}cave}$ (the southern core) values for all 4 caves are lower than $\Delta\delta^{18}O_{9501\text{-}cave}$ (the northern core) and the differences are much larger during the late last glacial period i.e. ~32 to 15 ka (Figure 31 A-D and Figure 32). This is consistent with the southward direction of the synoptic system, as proposed, during the late glacial.

The highest deviation between $\Delta\delta^{18}O_{9509\text{-}Zalmon}$ and $\Delta\delta^{18}O_{9501\text{-}Zalmon}$ is observed during the peak levels of Lake Lisan stand (Figure 31F). While $\Delta\delta^{18}O_{sea(9501\ \&\ 9509)\text{-}Soreq}$ (Figure 32) remains similar between the MIS1 and the last glacial period, $\Delta\delta^{18}O_{sea\text{-}Zalmon}$ are ~1.5‰ higher during the last glacial period suggesting that these are periods of enhanced rainfall and that the amount effect is the most dominant factor responsible for these high differences. The periods with the lowest differences between $\Delta\delta^{18}O_{9501\text{-}Zalmon}$ and $\Delta\delta^{18}O_{9509\text{-}Zalmon}$ coincide with warm periods, evident from speleothem deposition periods in Mizpe Shelagim Cave (Ayalon et al., 2013) (Figure 30, Figure 31E). During interglacial and warmer glacial periods the synoptic system was most likely similar to present day (Figure 30).

Three significant observations from Figure 31:

1) Peak $\Delta\delta^{18}O_{sea\text{-}Zalmon}$ values correlate with peak Lake Lisan levels. The difference between $\Delta\delta^{18}O_{9509\text{-}Zalmon}$ and $\Delta\delta^{18}O_{9501\text{-}Zalmon}$ is the highest during these times.
2) During periods of deposition in Mizpe Shelagim Cave $\Delta\delta^{18}O$ of all four caves' values are slightly lower. In addition both cores' values become similar.
3) $\Delta\delta^{18}O_{sea\text{-}Soreq}$ do not vary between the last glacial and MIS1. $\Delta\delta^{18}O_{sea\text{-}Peqi'in}$ and $\Delta\delta^{18}O_{sea\text{-}Zalmon}$ exhibit higher values during the last glacial (Figure 32).

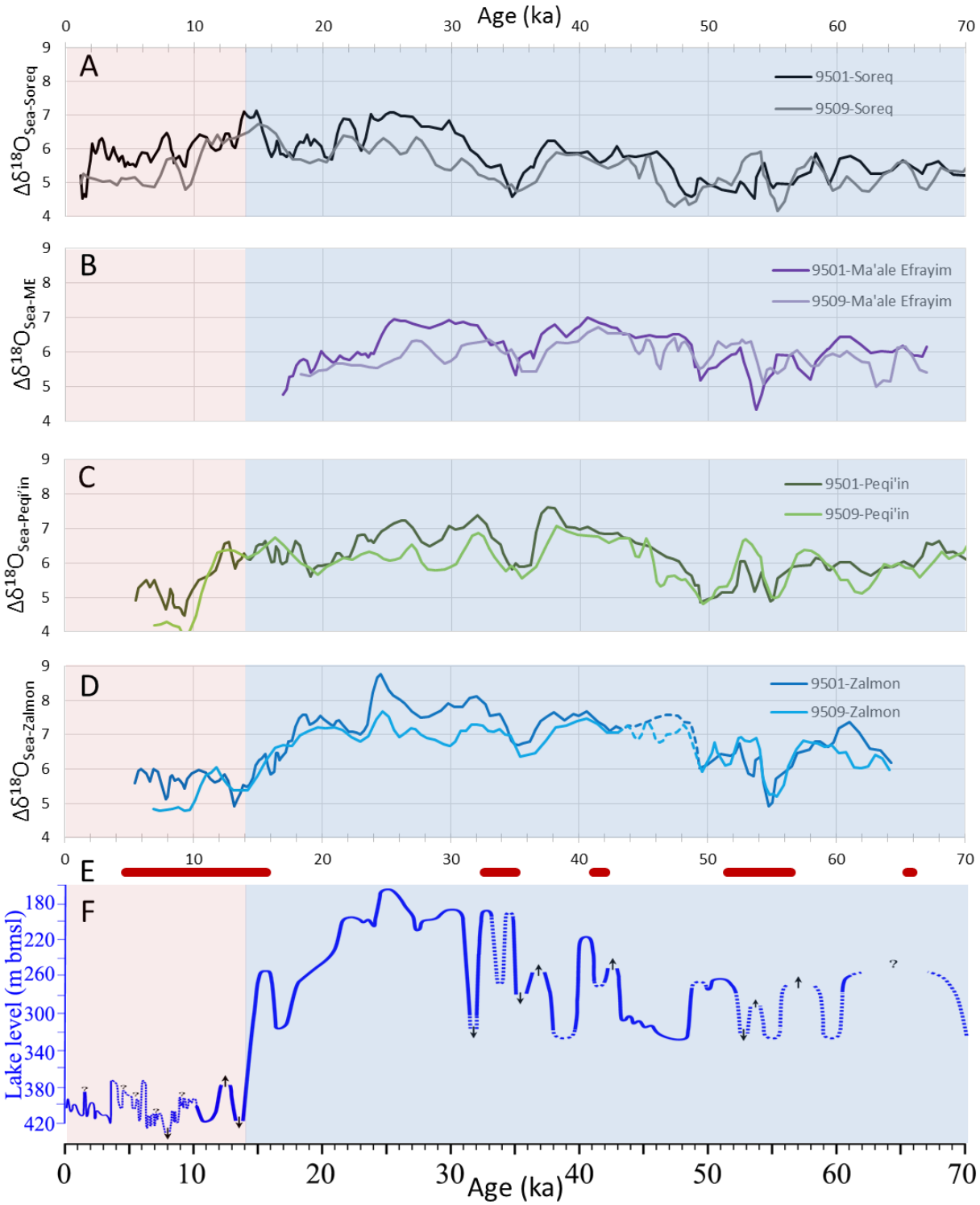

Figure 31: A-D Comparisons between $\delta^{18}O_{G.ruber}$ (Almogi-Labin et al., 2009) and $\delta^{18}O_{land}$ records expressed as a 3 point running average of $\Delta\delta^{18}O_{sea\text{-}land}$ values; Dark lines - $\Delta\delta^{18}O_{9501\text{-}cave}$. Light lines - $\Delta\delta^{18}O_{9509\text{-}cave}$. A - $\Delta\delta^{18}O_{sea(9501\ \&\ 9509)\text{-}Soreq}$. B - $\Delta\delta^{18}O_{sea\text{-}Ma'ale\ Efrayim}$. C - $\Delta\delta^{18}O_{sea\text{-}Peqi'in}$. D - $\Delta\delta^{18}O_{sea\text{-}Zalmon}$. E – Deposition periods in Mizpe Shelagim Cave attributed to short warming periods within the last glacial period (Ayalon et al., 2013). F - Lake Lisan Curve modified after Torfstein et al. (2013). Further detail in Section 7.4

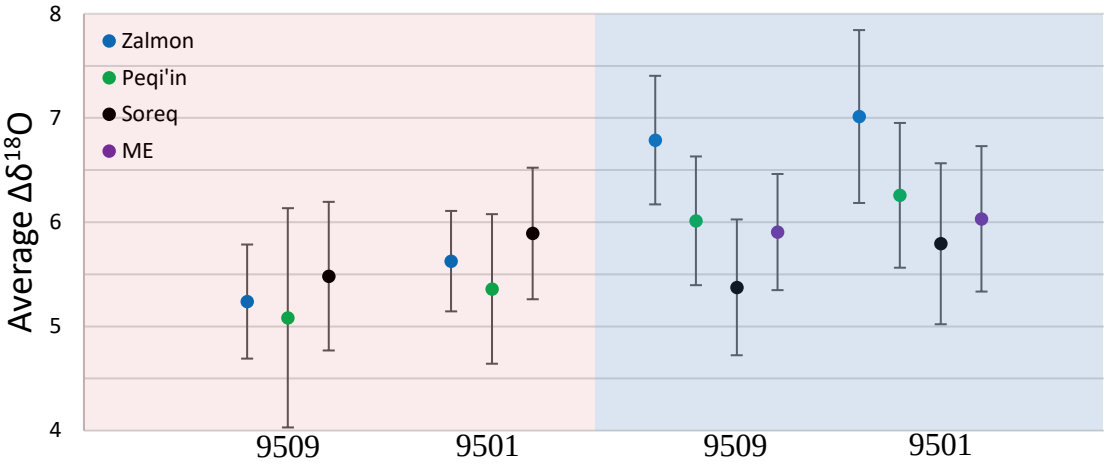

Figure 32: Average $\Delta\delta^{18}O_{sea\text{-}cave}$ values for MIS1 (light red) and the last glacial period (light blue). Standard deviation as black error bars. Values presented in Table 10 in the appendix.
Average $\Delta\delta^{18}O_{sea\text{-}Soreq}$ are similar for both MIS1 and the last glacial. Average glacial $\Delta\delta^{18}O_{sea\text{-}Peqi'in}$ is ~1 higher than during MIS1. Average glacial $\Delta\delta^{18}O_{sea\text{-}Zalmon\ is}$ ~1.5 higher than during MIS1.
$\Delta\delta^{18}O_{9509\text{-}land}$ are consistently lower than $\Delta\delta^{18}O_{9501\text{-}cave}$ for all 4 caves and both time periods.

5.5 High $\delta^{13}C$/low $\delta^{18}O$ events

Speleothems from caves in the Eastern Mediterranean have, on two occasions, shown behavior of exceptionally high $\delta^{13}C$ values (>-4‰) coinciding with very low $\delta^{18}O$ values (~-9‰). These events coincide with the timing of sapropel events (increased freshwater supply to the Eastern Mediterranean Sea and deposition of organic rich layers). This unique composition has been observed from ~128 to 121 ka in Soreq Cave (Bar-Matthews et al., 2000), Peqi'in Cave (Bar-Matthews et al., 2003) and Jerusalem Cave (Frumkin et al., 2000). It has also been observed for a shorter period in Soreq Cave from ~9.5 to 7.5 ka. Here we explore the behavior of Zalmon Cave speleothems during these time intervals.

This feature is absent in a Zalmon Cave speleothem from 9.5 to 7.5ka. ZAL6 is the most accurately dated sample in this study with continuous deposition from 13 to 6.7 ka. $\delta^{13}C$ values remain low (reaching a maximum value of -10.74‰, Figure 21) and no change in growth rate (Figure 15). Neither does the $\delta^{18}O$ record show a sharp drop during the period in question and even rises by ~0.5‰ simultaneously with the drop by ~1‰ of the record from Soreq Cave. This feature is also absent from Jerusalem Cave possibly due to low sampling resolution.

There may be a hint of the combined high $\delta^{13}C$ and low $\delta^{18}O$ in Zalmon Cave during MIS5. ZAL5 was deposited during part of the time interval between 128 and 121 ka. To accurately estimate the depositional period, the exceptionally high $\delta^{13}C$ values were used

to constrain the age (Figure 26). Immediately after the sharp increase in $\delta^{13}C$ at 128 ka deposition appears to have ceased, therefore it is not clear whether the depositional hiatus is associated with the event. A stalagmite sample from Kanaan Cave in Lebanon conclusively shows that $\delta^{13}C$ of speleothems remains below -10‰ (Nehme et al., 2015). This indicates that the response to this extreme hydrological change associated with sapropel events did not extend to this region in Lebanon.

Frumkin et al. (2000) suggested these very high $\delta^{13}C$ values are the result of a rapid decrease in the total amount of biogenic activity. In the absence of vegetation, speleothems' $\delta^{13}C$ is dictated by mixing of local atmospheric CO_2 (~-7‰) and bedrock (~0-2‰). Exceptionally high $\delta^{13}C$ values can be accounted for by carbonate rock almost entirely stripped of vegetation and soil cover. In this scenario, infiltrating water would have very little interaction with soil CO_2 and would equilibrate with the atmosphere and CO_2 from lichens and cyanobacteria with possible enrichment from aeolian dust (Danin et al., 1983). Speleothems may be deposited without biogenic CO_2 if the temperature inside the cave is warmer than above the ground (Dreybrodt, 1982). This is the case during the colder winter months which is also the wet season today (Bar-Matthews et al., 1996). This setting would lead to slow growth rates caused by slower dissolution rates of the host rock calcite. A possible explanation could be rapid warming and drying causing destruction of vegetation, possibly aided by forest fires (Frumkin et al., 2000). An alternative explanation, provided by Bar-Matthews et al. (2003), is enhanced rainfall which stripped the soil cover caused by deluge events associated with sapropel events.

Kaufman et al. (1998), Ayalon et al. (1999) and Bar-Matthews et al. (2000) suggested that the sharp drop in the concentrations of Sr, Ba, and U, and in the ratios of $(^{234}U/^{238}U)_0$ and $^{87}Sr/^{86}Sr$ of Soreq Cave provide further evidence for enhanced weathering of the host rock due to increasing rainfall.

While changes in growth rate were not conclusively identified for Zalmon Cave speleothems, low $(^{234}U/^{238}U)_0$ calculated according to Kaufman et al. (1998) are observed during sapropel events S1 and S5 for sample ZAL6 and ZAL5 respectively (Figure 33). A decrease in $(^{234}U/^{238}U)_0$ is also observed at ~55 to 50 ka during the timing of the missing sapropel S2. Similar evidence exists as well in Kanaan Cave for samples dated between 133 to 126 ka (Nehme et al., 2015). These findings possibly indicate that enhanced

weathering of the host rock had occurred although, it is not evident from the coupling of high $\delta^{13}C$ and low $\delta^{18}O$ values.

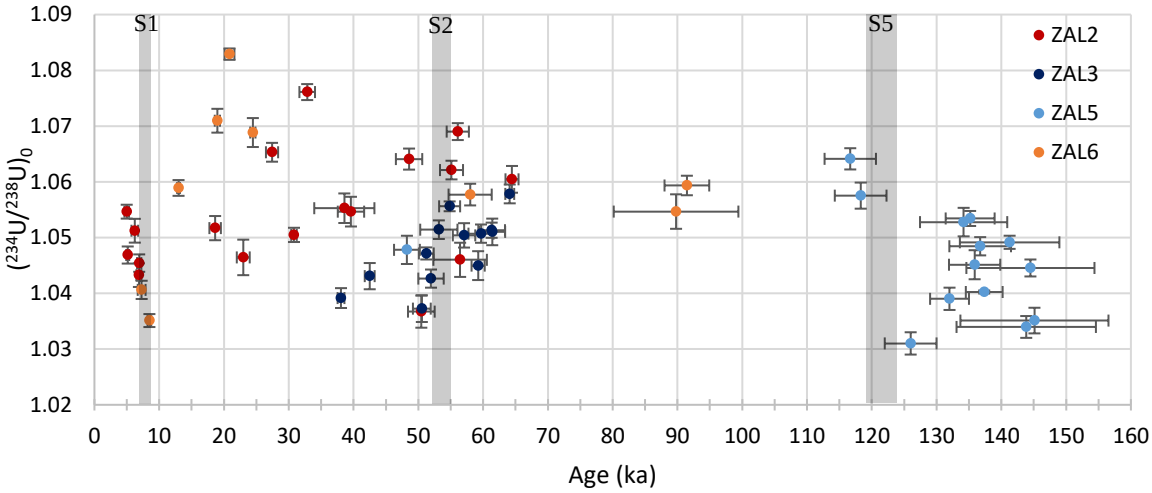

Figure 33: $(^{234}U/^{238}U)_0$ ratios of dated samples from ZAL2, ZAL3, ZAL5 and ZAL6 calculated according to Kaufman et al. (1998). Sapropel events S1, S2 and S5 as grey rectangles (Bar-Matthews et al., 2000). Horizontal error bars with 2σ certainty. Vertical error bars with 1σ certainty. Some of the horizontal error bars are within the symbol. Lowest $(^{234}U/^{238}U)_0$ values are observed during sapropel events S1, S5 and a decrease in $(^{234}U/^{238}U)_0$ is observed during S2.

5.6 Conditions for hominin dispersal and settlement

The isotopic profiles of Zalmon Cave indicate that throughout the late Quaternary, the Eastern Galilee has always been a reasonably habitable region. Continuous growth periods along with low $\delta^{18}O$ values indicate adequate amounts of rainfall. The low $\delta^{13}C$ indicates a high C3/C4 vegetation ratio signifying conditions for potentially flourishing sources of nourishment.

The Levant is bounded in the north by the Taurus Mountains, in the west by the Mediterranean Sea, and on the south and east by deserts. In the Sahara-Negev, moister conditions occurred during MIS6 to 5 transition (Vaks et al., 2010), when anatomically modern humans apparently migrated into the Sahara and out of Africa. Archaeological data from northern Israel indicates that one of the major waves of early modern human expansion out of the African continent occurred between 130 and 100 ka (Schwarcz et al., 1988; Valladas et al., 1988; Mercier et al., 1993). In the Negev, the transition from MIS5 to the last glacial period was characterized by a drop in annual rainfall (Vaks et al., 2010). Hominins extended their home range during the Pleistocene from Africa to Eurasia or vice versa and had to move through the Levant, a relatively narrow terrestrial "corridor," rendering it the main 'Out of Africa' corridor (Vaks et al., 2007). Ancient

hominins would have probably found the conditions in the Levant habitable and welcoming.

During the transition from MIS5 to MIS4, rapid cooling of Europe had possibly driven hominins south toward a more temperate climate. Neanderthal skeletal remains from Amud Cave dated to the beginning of the last glacial, (~71 to 44 ka) confirm the presence of Neanderthals in the region (Valladas et al., 1999). A skull of a modern human of African origin in Manot Cave dated to ~55 ka (Hershkovitz et al., 2015) suggests additional dispersal out of Africa during MIS3. The findings from Zalmon Cave suggest that climatic conditions in northern Israel could act as an incentive to these migrations.

5.7 Conclusions

- Speleothems were deposited in Zalmon Cave both during glacial and interglacial periods.
- Climatic conditions in the eastern Lower Galilee and central Israel during interglacial periods were similar.
- Lower glacial $\delta^{13}C$ and $\delta^{18}O$ imply more humid and warmer climate in the north compared to central Israel.
- Three lines of evidence support the southern shift of storm tracks during the last glacial, resulting in more precipitation in Eastern Galilee region with respect to central Israel:

  1) Lower $\delta^{18}O$ values of Zalmon Cave compared to Soreq Cave.

  2) Lower glacial $\Delta\delta^{18}O_{9509\text{-}cave}$ values compared to $\Delta\delta^{18}O_{9501\text{-}cave}$ values.

  3) High $\Delta\delta^{18}O_{sea\text{-}Zalmon}$ values coinciding with high levels of Lake Lisan.
- $\Delta\delta^{18}O_{sea\text{-}land}$ relationships mostly indicate a change in precipitation.
- Lower $(^{234}U/^{238}U)_0$ values are observed during the timing of sapropel events S1, S5 and the missing sapropel S2, plausibly indicating enhanced weathering of the host rock.
- Paleoclimate conditions in Eastern Galilee region can explain why hominins that dispersed out of Africa and south of Europe could survive in the region.

6 References

Affek, H.P., Bar-Matthews, M., Ayalon, A., Matthews, A., and Eiler, J.M., 2008, Glacial/interglacial temperature variations in Soreq cave speleothems as recorded by "clumped isotope" thermometry: Geochimica et Cosmochimica Acta, v. 72, no. 22, p. 5351–5360, doi: 10.1016/j.gca.2008.06.031.

Agnon, A., 2014, Pre-Instrumental Earthquakes Along the Dead Sea Rift, *in* Dead Sea Transform Fault System : Reviews, p. 207–261.

Almogi-Labin, A., Bar-Matthews, M., Shriki, D., Kolosovsky, E., Paterne, M., Schilman, B., Ayalon, A., Aizenshtat, Z., and Matthews, A., 2009, Climatic variability during the last ~90ka of the southern and northern Levantine Basin as evident from marine records and speleothems: Quaternary Science Reviews, v. 28, no. 25–26, p. 2882–2896, doi: 10.1016/j.quascirev.2009.07.017.

Arkin, Y., Braun, M., Starinsky, A., Hamaoui, M., and Raab, M., 1965, Type sections of Cretaceous formations in the Jerusalem Bet Semesh area: Geological Survey of Israel.

Ayalon, A., Bar-Matthews, M., Frumkin, A., and Matthews, A., 2013, Last Glacial warm events on Mount Hermon: the southern extension of the Alpine karst range of the east Mediterranean: Quaternary Science Reviews, v. 59, p. 43–56, doi: 10.1016/j.quascirev.2012.10.047.

Ayalon, A., Bar-Matthews, M., and Kaufman, A., 2002, Climatic conditions during marine oxygen isotope stage 6 in the eastern Mediterranean region from the isotopic composition of speleothems of Soreq Cave, Israel: Geology, v. 30, no. 4, p. 303–306, doi: 10.1130/0091-7613(2002)030<0303:CCDMOI>2.0.CO.

Ayalon, A., Bar-Matthews, M., and Kaufman, A., 1999, Petrography, strontium, barium and uranium concentrations, and strontium and uranium isotope ratios in speleothems as palaeoclimatic proxies: Soreq Cave, Israel: The Holocene, v. 9, no. 6, p. 715–722.

Ayalon, A., Bar-Matthews, M., and Sass, E., 1998, Rainfall-recharge relationships within a karstic terrain in the Eastern Mediterranean semi-arid region, Israel: δ 18O and δD characteristics: Journal of Hydrology, v. 207, no. 1–2, p. 18–31, doi: 10.1016/S0022-1694(98)00119-X.

Ayalon, A., Bar-Matthews, M., and Schilman, B., 2004, Rainfall isotopic characteristics in various vites in Israel and the relationships with the unsaturated zone water.:

Bar-Matthews, M., 2014, History of Water in the Middle East and North Africa, *in* Treatise on Geochemistry, Elsevier, p. 109–128.

Bar-Matthews, M., and Ayalon, A., 2011, Mid-Holocene climate variations revealed by high-resolution speleothem records from Soreq Cave, Israel and their correlation with cultural changes: The Holocene, v. 21, no. 1, p. 163–171, doi:

10.1177/0959683610384165.

Bar-Matthews, M., Ayalon, A., Gilmour, M., Matthews, A., and Hawkesworth, C.J., 2003, Sea–land oxygen isotopic relationships from planktonic foraminifera and speleothems in the Eastern Mediterranean region and their implication for paleorainfall during interglacial intervals: Geochimica et Cosmochimica Acta, v. 67, no. 17, p. 3181–3199, doi: 10.1016/S0016-7037(02)01031-1.

Bar-Matthews, M., Ayalon, A., and Kaufman, A., 1997, Late Quaternary Paleoclimate in the Eastern Mediterranean Region from Stable Isotope Analysis of Speleothems at Soreq Cave, Israel: Quaternary Research, v. 47, no. 2, p. 155–168, doi: 10.1006/qres.1997.1883.

Bar-Matthews, M., Ayalon, A., and Kaufman, A., 2000, Timing and hydrological conditions of Sapropel events in the Eastern Mediterranean, as evident from speleothems, Soreq cave, Israel: Chemical Geology, v. 169, no. 1–2, p. 145–156, doi: 10.1016/S0009-2541(99)00232-6.

Bar-Matthews, M., Ayalon, A., Matthews, A., Sass, E., and Halicz, L., 1996, Carbon and oxygen isotope study of the active water-carbonate system in a karstic Mediterranean cave: Implications for paleoclimate research in semiarid regions: Geochimica et Cosmochimica Acta, v. 60, no. 2, p. 337–347, doi: 10.1016/0016-7037(95)00395-9.

Bartov, Y., Stein, M., Enzel, Y., Agnon, A., and Reches, Z., 2002, Lake Levels and Sequence Stratigraphy of Lake Lisan, the Late Pleistocene Precursor of the Dead Sea: Quaternary Research, v. 57, no. 1, p. 9–21, doi: 10.1006/qres.2001.2284.

Le Beon, M., Klinger, Y., Amrat, A.Q., Agnon, A., Dorbath, L., Baer, G., Ruegg, J.C., Charade, O., and Mayyas, O., 2008, Slip rate and locking depth from GPS profiles across the southern Dead Sea Transform: Journal of Geophysical Research: Solid Earth, v. 113, no. 11, p. 1–19, doi: 10.1029/2007JB005280.

Boch, R., Spötl, C., and Frisia, S., 2011, Origin and palaeoenvironmental significance of lamination in stalagmites from Katerloch Cave, Austria: Sedimentology, v. 58, no. 2, p. 508–531, doi: 10.1111/j.1365-3091.2010.01173.x.

Bogoch, R., and Sneh, A., 2008, Geological map of Israel, 1:50000 Israel Geological Survey (Sheet 4-1).

Braun, Y., Kagan, E., Bar-Matthews, M., Ayalon, A., and Agnon, A., 2009, Dating speleoseismites near the Dead Sea Transform and the Carmel Fault: Clues to coupling of a plate boundary and its branch: Israel Journal of Earth Sciences, v. 58, no. 3, p. 257–273, doi: 10.1560/IJES.58.3-4.257.

Chorowicz, J., Collet, B., Bonavia, F.F., and Korme, T., 1994, Northwest to north-northwest extension direction in the Ethiopian rift deduced from the orientation of extension structures and fault-slip analysis: Geological Society of America Bulletin, v. 106, no. 12, p. 1560–1570, doi: 10.1130/0016-

7606(1994)105<1560:NTNNED>2.3.CO;2.

Danin, A., Gerson, R., and Garty, J., 1983, Weathering patterns on hard limestone and dolomite by endolithic lichens and cyanobacteria: supporting evidence for eolian contribution to Terra Rossa soil.: Soil Science, v. 136, no. 4, p. 213–217, doi: 10.1097/00010694-198310000-00003.

Dansgaard, W., 1964, Stable isotopes in precipitation: Tellus, v. 16, no. 4, p. 436–468, doi: 10.3402/tellusa.v16i4.8993.

Dorale, J. a., 1998, Climate and Vegetation History of the Midcontinent from 75 to 25 ka: A Speleothem Record from Crevice Cave, Missouri, USA: Science, v. 282, no. 1998, p. 1871–1874, doi: 10.1126/science.282.5395.1871.

Dorale, J.A., and Liu, Z., 2009, Limitations of hendy test criteria in judging the paleoclimatic suitability of speleothems and the need for replication: Journal of Cave and Karst Studies, v. 71, no. 1, p. 73–80, doi: PNR61.

Dreybrodt, W., 1982, A possible mechanism for growth of calcite speleothems without participation of biogenic carbon dioxide: Earth and Planetary Science Letters, v. 58, no. 2, p. 293–299, doi: 10.1016/0012-821X(82)90202-3.

Dreybrodt, W., 1999, Chemical kinetics, speleothem growth and climate: Boreas, v. 28, no. 3, p. 347–356.

Enzel, Y., Amit, R., Dayan, U., Crouvi, O., Kahana, R., Ziv, B., and Sharon, D., 2008, The climatic and physiographic controls of the eastern Mediterranean over the late Pleistocene climates in the southern Levant and its neighboring deserts: Global and Planetary Change, v. 60, no. 3–4, p. 165–192, doi: 10.1016/j.gloplacha.2007.02.003.

Enzel, Y., Bookman (Ken Tor), R., Sharon, D., Gvirtzman, H., Dayan, U., Ziv, B., and Stein, M., 2003, Late Holocene climates of the Near East deduced from Dead Sea level variations and modern regional winter rainfall: Quaternary Research, v. 60, no. 3, p. 263–273, doi: 10.1016/j.yqres.2003.07.011.

Flexer, A., Freund, R., Reiss, Z., and Buchbinder, B., 1970, Santonian paleostructure of the Galilee: Israel Journal of Earth Sciences, v. 19, p. 141–146.

Freund, R., 1970, Geometry of faulting in Galilee: Israel Journal of Earth Sciences, v. 19, no. 3–4, p. 117.

Freund, R., Zak, I., and Garfunkel, Z., 1968, Age and Rate of the Sinistral Movement along the Dead Sea Rift: Nature, v. 220, no. 5164, p. 253–255, doi: 10.1038/220253a0.

Friedman, I., and O'Neil, J.R., 1977, Data of geochemistry: Compilation of stable isotope fractionation factors of geochemical interest:

Frisia, S., 2015, Microstratigraphic logging of calcite fabrics in speleothems as tool for palaeoclimate studies: International Journal of Speleology, v. 44, no. 1, p. 1–16, doi:

10.5038/1827-806X.44.1.1.

Frisia, S., and Borsato, A., 2010, Chapter 6 Karst, *in* Carbonates in continental settings: facies, environments, and processes, p. 269–318.

Frisia, S., Borsato, A., Fairchild, I.J., and McDermott, F., 2000, Calcite Fabrics, Growth Mechanisms, and Environments of Formation in Speleothems from the Italian Alps and Southwestern Ireland: Journal of Sedimentary Research, v. 70, no. 5, p. 1183–1196, doi: 10.1306/022900701183.

Frumkin, A., Bar-Yosef, O., and Schwarcz, H.P., 2011, Possible paleohydrologic and paleoclimatic effects on hominin migration and occupation of the Levantine Middle Paleolithic☆: Journal of Human Evolution, v. 60, no. 4, p. 437–451, doi: 10.1016/j.jhevol.2010.03.010.

Frumkin, A., and Fischhendler, I., 2005, Morphometry and distribution of isolated caves as a guide for phreatic and confined paleohydrological conditions: Geomorphology, v. 67, no. 3–4, p. 457–471, doi: 10.1016/j.geomorph.2004.11.009.

Frumkin, A., Ford, D.C., and Schwarcz, H.P., 1999, Continental Oxygen Isotopic Record of the Last 170,000 Years in Jerusalem: Quaternary Research, v. 51, no. 3, p. 317–327, doi: 10.1006/qres.1998.2031.

Frumkin, A., Ford, D.C., and Schwarcz, H.P., 2000, Paleoclimate and vegetation of the Last Glacial Cycles in Jerusalem from a Speleothem Record: Global Biogeochemical Cycles, v. 14, no. 3, p. 863–870, doi: 10.1029/1999GB001245.

Frumkin, A., Lisker, S., and Vaks, A., 2007, Glacial Quaternary of the Levant from speleothems , lakes and loess: v. 5, p. 30–31.

Garfunkel, Z., 1981, Internal structure of the Dead Sea leaky transform (rift) in relation to plate kinematics: Tectonophysics, v. 80, no. 1–4, p. 81–108, doi: 10.1016/0040-1951(81)90143-8.

Garfunkel, Z., Zak, I., and Freund, R., 1981, Active faulting in the dead sea rift: Tectonophysics, v. 80, no. 1–4, p. 1–26, doi: 10.1016/0040-1951(81)90139-6.

Ginat, H., Enzel, Y., and Avni, Y., 1998, Translocated Plio-Pleistocene drainage systems along the Arava fault of the Dead Sea transform: Tectonophysics, v. 284, no. 1–2, p. 151–160, doi: 10.1016/S0040-1951(97)00165-0.

Goldsmith, Y., Polissar, P.J., Ayalon, A., Bar-Matthews, M., DeMenocal, P.B., and Broecker, W.S., 2016, The modern and Last Glacial Maximum hydrological cycles of the Eastern Mediterranean and the Levant from a water isotope perspective: Earth and Planetary Science Letters, doi: 10.1016/j.epsl.2016.10.017.

Goring-Morris, A.N., and Belfer-Cohen, A., 2011, Neolithization Processes in the Levant: Current Anthropology, v. 52, no. S4, p. S195–S208, doi: 10.1086/658860.

Grant, K.M., Rohling, E.J., Bar-Matthews, M., Ayalon, A., Medina-Elizalde, M.,

Ramsey, C.B., Satow, C., and Roberts, A.P., 2012, Rapid coupling between ice volume and polar temperature over the past 150,000 years: Nature, v. 491, no. 7426, p. 744–747, doi: 10.1038/nature11593.

Hall, J.K., Udintsev, G.B., and Odinikov, Y.Y., 1994, The bottom relief of the Levantine Sea: Geologic Structure of the Northeastern Mediterranean: Jerusalem (Historical Productions-Hall Ltd.), p. 5–32.

Hellstrom, J., 2006, U–Th dating of speleothems with high initial 230Th using stratigraphical constraint: Quaternary Geochronology, v. 1, no. 4, p. 289–295, doi: 10.1016/j.quageo.2007.01.004.

Hendy, C.., 1971, The isotopic geochemistry of speleothems—I. The calculation of the effects of different modes of formation on the isotopic composition of speleothems and their applicability as palaeoclimatic indicators: Geochimica et Cosmochimica Acta, v. 35, no. 8, p. 801–824, doi: 10.1016/0016-7037(71)90127-X.

Hershkovitz, I., Marder, O., Ayalon, A., Bar-matthews, M., Yasur, G., Boaretto, E., Caracuta, V., Alex, B., Frumkin, A., Goder-goldberger, M., Gunz, P., Holloway, R.L., Latimer, B., Lavi, R., et al., 2015, Levantine cranium from Manot Cave (Israel) foreshadows the first European modern humans: Nature, doi: 10.1038/nature14134.

Hovers, E., Rak, Y., Lavi, R., and Kimbel, W.H., 1995, Hominid Remains from Amud Cave in the context of the Levantine Middle Paleolithic: Paléorient, v. 21, no. 2, p. 47–61.

IMS - Israel Meteorological Service, 2011, Average annual precipitation map 1981-2010: , p. 1.

Jaffey, A.H., Flynn, K.F., Glendenin, L.E., Bentley, W.C., and Essling, A.M., 1971, Precision measurement of half-lives and specific activities of U235 and U238: Physical Review C, v. 4, no. 5, p. 1889–1906, doi: 10.1103/PhysRevC.4.1889.

Kagan, E.J., Agnon, A., Bar-Matthews, M., and Ayalon, A., 2005, Dating large infrequent earthquakes by damaged cave deposits: Geology, v. 33, no. 4, p. 261–264, doi: 10.1130/G21193.1.

Kaufman, A., 1971, U-Series dating of Dead Sea Basin carbonates: Geochimica et Cosmochimica Acta, v. 35, no. 12, p. 1269–1281, doi: 10.1016/0016-7037(71)90115-3.

Kaufman, A., Wasserburg, G.J., Porcelli, D., Bar-Matthews, M., Ayalon, A., and Halicz, L., 1998, U-Th isotope systematics from the Soreq cave, Israel and climatic correlations: Earth and Planetary Science Letters, v. 156, no. 3–4, p. 141–155, doi: 10.1016/S0012-821X(98)00002-8.

Kim, S.-T., and O'Neil, J.R., 1997, Equilibrium and nonequilibrium oxygen isotope effects in synthetic carbonates: Geochimica et Cosmochimica Acta, v. 61, no. 16, p. 3461–3475, doi: 10.1016/S0016-7037(97)00169-5.

Klinger, Y., Avouac, J.P., Dorbath, L., Karaki, N.A., and Tisnerat, N., 2000, Seismic behaviour of the Dead Sea fault along Araba valley, Jordan: Geophysical Journal International, v. 142, no. 3, p. 769–782, doi: 10.1046/j.1365-246x.2000.00166.x.

Kolodny, Y., Stein, M., and Machlus, M., 2005, Sea-rain-lake relation in the Last Glacial East Mediterranean revealed by $\delta^{18}O$-$\delta^{13}C$ in Lake Lisan aragonites: Geochimica et Cosmochimica Acta, v. 69, no. 16, p. 4045–4060, doi: 10.1016/j.gca.2004.11.022.

Li, W.-X., Lundberg, J., Dickin, A.P., Ford, D.C., Schwarcz, H.P., McNutt, R., and Williams, D., 1989, High-precision mass-spectrometric uranium-series dating of cave deposits and implications for palaeoclimate studies: Nature, v. 339, no. 6225, p. 534–536, doi: 10.1038/339534a0.

Lisiecki, L.E., and Raymo, M.E., 2005, A Pliocene-Pleistocene stack of 57 globally distributed benthic $\delta^{18}O$ records: Paleoceanography, v. 20, no. 1, p. n/a-n/a, doi: 10.1029/2004PA001071.

Lisker, S., Vaks, A., Bar-Matthews, M., Porat, R., and Frumkin, A., 2009, Stromatolites in caves of the Dead Sea Fault Escarpment: implications to latest Pleistocene lake levels and tectonic subsidence: Quaternary Science Reviews, v. 28, no. 1–2, p. 80–92, doi: 10.1016/j.quascirev.2008.10.015.

Lisker, S., Vaks, A., Bar Matthews, M., Porat, R., and Frumkin, A., 2010, Late Pleistocene palaeoclimatic and palaeoenvironmental reconstruction of the Dead Sea area (Israel), based on speleothems and cave stromatolites: Quaternary Science Reviews, v. 29, no. 9–10, p. 1201–1211, doi: 10.1016/j.quascirev.2010.01.018.

Machlus, M., Enzel, Y., Goldstein, S.L., Marco, S., and Stein, M., 2000, Reconstructing low levels of Lake Lisan by correlating fan-delta and lacustrine deposits: Quaternary International, v. 73–74, p. 137–144, doi: 10.1016/S1040-6182(00)00070-7.

Mahmoud, Y., Masson, F., Meghraoui, M., Cakir, Z., Alchalbi, A., Yavasoglu, H., Yönlü, O., Daoud, M., Ergintav, S., and Inan, S., 2013, Kinematic study at the junction of the East Anatolian fault and the Dead Sea fault from GPS measurements: Journal of Geodynamics, v. 67, p. 30–39, doi: 10.1016/j.jog.2012.05.006.

Marco, S., Rockwell, T., Heimann, A., Frieslander, U., and Agnon, A., 2005, Late Holocene activity of the Dead Sea Transform revealed in 3D palaeoseismic trenches on the Jordan Gorge segment: Earth and Planetary Science Letters, v. 234, no. 1–2, p. 189–205, doi: 10.1016/j.epsl.2005.01.017.

Masson, F., Hamiel, Y., Agnon, A., Klinger, Y., and Deprez, A., 2015, Variable behavior of the Dead Sea Fault along the southern Arava segment from GPS measurements: Comptes Rendus Geoscience, v. 347, no. 4, p. 161–169, doi: 10.1016/j.crte.2014.11.001.

Matmon, A., Enzel, Y., Zilberman, E., and Heimann, A., 1999, Late Pliocene and Pleistocene reversal of drainage systems in northern Israel: tectonic implications: Geomorphology, v. 28, no. 1–2, p. 43–59, doi: 10.1016/S0169-555X(98)00097-X.

Mcbrearty, S., and Brooks, A.S., 2000, The revolution that wasn't: a new interpretation of the origin of modern human behavior.: Journal of human evolution, v. 39, no. 5, p. 453–563, doi: 10.1006/jhev.2000.0435.

McDermott, F., 2004, Palaeo-climate reconstruction from stable isotope variations in speleothems: a review: Quaternary Science Reviews, v. 23, no. 7–8, p. 901–918, doi: 10.1016/j.quascirev.2003.06.021.

McGarry, S., Bar-Matthews, M., Matthews, A., Vaks, A., Schilman, B., and Ayalon, A., 2004, Constraints on hydrological and paleotemperature variations in the Eastern Mediterranean region in the last 140ka given by the δD values of speleothem fluid inclusions: Quaternary Science Reviews, v. 23, no. 7–8, p. 919–934, doi: 10.1016/j.quascirev.2003.06.020.

Mercier, N., Valladas, H., Bar-Yosef, O., Vandermeersch, B., Stringer, C., and Joron, J.-L., 1993, Thermoluminescence date for the Mousterian burial site of Es-Skhul, Mt. Carmel: J. Archaeol. Sci., v. 20, no. 2, p. 169–174, doi: 10.1006/jasc.1993.1012.

Mickler, P.J., Banner, J.L., Stern, L., Asmerom, Y., Edwards, R.L., and Ito, E., 2004, Stable isotope variations in modern tropical speleothems: Evaluating equilibrium vs. kinetic isotope effects: Geochimica et Cosmochimica Acta, v. 68, no. 21, p. 4381–4393, doi: 10.1016/j.gca.2004.02.012.

Mickler, P.J., Stern, L.A., and Banner, J.L., 2006, Large kinetic isotope effects in modern speleothems: Geological Society of America Bulletin, v. 118, no. 1–2, p. 65–81, doi: 10.1130/B25698.1.

Migowski, C., Stein, M., Prasad, S., Negendank, J.F.W., and Agnon, A., 2006, Holocene climate variability and cultural evolution in the Near East from the Dead Sea sedimentary record: Quaternary Research, v. 66, no. 3, p. 421–431, doi: 10.1016/j.yqres.2006.06.010.

Mitchell, S.G., Matmon, A., Bierman, P.R., Enzel, Y., Caffee, M., and Rizzo, D., 2001, Displacement history of a limestone normal fault scarp, northern Israel, from cosmogenic ^{36}Cl: Journal of Geophysical Research: Solid Earth, v. 106, no. B3, p. 4247–4264.

Nehme, C., Verheyden, S., Noble, S.R., Farrant, A.R., Sahy, D., Hellstrom, J., Delannoy, J.J., and Claeys, P., 2015, Reconstruction of MIS 5 climate in the central Levant using a stalagmite from Kanaan Cave, Lebanon: Climate of the Past, v. 11, no. 12, p. 1785–1799, doi: 10.5194/cp-11-1785-2015.

Neugebauer, I., Schwab, M.J., Waldmann, N.D., Tjallingii, R., Frank, U., Hadzhiivanova, E., Naumann, R., Taha, N., Agnon, A., Enzel, Y., and Brauer, A., 2016, Hydroclimatic variability in the Levant during the early last glacial (~ 117–75 ka) derived from micro-facies analyses of deep Dead Sea sediments: Climate of the Past, v. 12, no. 1, p. 75–90, doi: 10.5194/cp-12-75-2016.

Niemi, T.M., Zhang, H.W., Atallah, M., and Harrison, J.B.J., 2001, Late Pleistocene and

Holocene slip rate of the Northern Wadi Araba fault, Dead Sea Transform, Jordan: Journal of Seismology, v. 5, no. 3, p. 449–474, doi: 10.1023/A:1011487912054.

NOAA – National Oceanic and Atmospheric Administartion. https://maps.ngdc.noaa.gov

Orland, I.J., Burstyn, Y., Bar-Matthews, M., Kozdon, R., Ayalon, A., Matthews, A., and Valley, J.W., 2014, Seasonal climate signals (1990–2008) in a modern Soreq Cave stalagmite as revealed by high-resolution geochemical analysis: Chemical Geology, v. 363, p. 322–333, doi: 10.1016/j.chemgeo.2013.11.011.

Picard, L., 1943, Structure and evolution of Palestine: with comparative notes on neighboring countries.:

Prasad, S., Vos, H., Negendank, J.F.W., Waldmann, N., Goldstein, S.L., and Stein, M., 2004, Evidence from Lake Lisan of solar influence on decadal- To centennial-scale climate variability during marine oxygen isotope stage 2: Geology, v. 32, no. 7, p. 581–584, doi: 10.1130/G20553.1.

Richards, D. a, and Dorale, J. a, 2003, Uranium-series Chronology and Environmental Applications of Speleothems: Reviews in Mineralogy and Geochemistry, v. 52, no. 1, p. 407–460, doi: 10.2113/0520407.

Ron, H., Freund, R., and Garfunkel, Z., 1984, Block rotation by strike-slip faulting: structural and paleomagnetic evidence: Journal of Geophysical Research, v. 89, no. B7, p. 6256–6270, doi: 10.1029/JB089iB07p06256.

Saaroni, H., Halfon, N., Ziv, B., Alpert, P., and Kutiel, H., 2010, Links between the rainfall regime in Israel and location and intensity of Cyprus lows: International Journal of Climatology, v. 30, no. 7, p. 1014–1025, doi: 10.1002/joc.1912.

Schwarcz, H.P., 1986, Geochronology and isotopic geochemistry of speleathems: Handbook of environmental isotope geochemistry, v. 2, p. 271–303.

Schwarcz, H.P., Grün, R., Vandermeersch, B., Bar-Yosef, O., Valladas, H., and Tchernov, E., 1988, ESR dates for the hominid burial site of Qafzeh in Israel: Journal of Human Evolution, v. 17, no. 8, p. 733–737, doi: 10.1016/0047-2484(88)90063-2.

Stein, M., 2001, The sedimentary and geochemical record of neogene-quaternary water bodies in the Dead Sea basin - Inferences for the regional paleoclimatic history: Journal of Paleolimnology, v. 26, no. 3, p. 271–282, doi: 10.1023/A:1017529228186.

Stein, M., Starinsky, A., Katz, A., Goldstein, S.L., Machlus, M., and Schramm, A., 1997, Strontium isotopic, chemical, and sedimentological evidence for the evolution of Lake Lisan and the Dead Sea: Geochimica et Cosmochimica Acta, v. 61, no. 18, p. 3975–3992, doi: 10.1016/S0016-7037(97)00191-9.

Torfstein, A., Goldstein, S.L., Kushnir, Y., Enzel, Y., Haug, G., and Stein, M., 2015, Dead Sea drawdown and monsoonal impacts in the Levant during the last interglacial: Earth and Planetary Science Letters, v. 412, p. 235–244, doi:

10.1016/j.epsl.2014.12.013.

Torfstein, A., Goldstein, S.L., Stein, M., and Enzel, Y., 2013, Impacts of abrupt climate changes in the Levant from Last Glacial Dead Sea levels: Quaternary Science Reviews, v. 69, p. 1–7, doi: 10.1016/j.quascirev.2013.02.015.

Torfstein, A., Haase-Schramm, A., Waldmann, N., Kolodny, Y., and Stein, M., 2009, U-series and oxygen isotope chronology of the mid-Pleistocene Lake Amora (Dead Sea basin): Geochimica et Cosmochimica Acta, v. 73, no. 9, p. 2603–2630, doi: 10.1016/j.gca.2009.02.010.

Vaks, A., Bar-Matthews, M., Ayalon, A., Matthews, A., Frumkin, A., Dayan, U., Halicz, L., Almogi-Labin, A., and Schilman, B., 2006, Paleoclimate and location of the border between Mediterranean climate region and the Saharo-Arabian Desert as revealed by speleothems from the northern Negev Desert, Israel: Earth and Planetary Science Letters, v. 249, no. 3–4, p. 384–399, doi: 10.1016/j.epsl.2006.07.009.

Vaks, A., Bar-Matthews, M., Ayalon, A., Matthews, A., Halicz, L., and Frumkin, A., 2007, Desert speleothems reveal climatic window for African exodus of early modern humans: Geology, v. 35, no. 9, p. 831–834, doi: 10.1130/G23794A.1.

Vaks, A., Bar-Matthews, M., Ayalon, A., Schilman, B., Gilmour, M., Hawkesworth, C.J., Frumkin, A., Kaufman, A., and Matthews, A., 2003, Paleoclimate reconstruction based on the timing of speleothem growth and oxygen and carbon isotope composition in a cave located in the rain shadow in Israel: Quaternary Research, v. 59, no. 2, p. 182–193, doi: 10.1016/S0033-5894(03)00013-9.

Vaks, A., Bar-Matthews, M., Matthews, A., Ayalon, A., and Frumkin, A., 2010, Middle-Late Quaternary paleoclimate of northern margins of the Saharan-Arabian Desert: reconstruction from speleothems of Negev Desert, Israel: Quaternary Science Reviews, v. 29, no. 19–20, p. 2647–2662, doi: 10.1016/j.quascirev.2010.06.014.

Vaks, A., Woodhead, J., Bar-Matthews, M., Ayalon, A., Cliff, R.A., Zilberman, T., Matthews, A., and Frumkin, A., 2013, Pliocene–Pleistocene climate of the northern margin of Saharan–Arabian Desert recorded in speleothems from the Negev Desert, Israel: Earth and Planetary Science Letters, v. 368, p. 88–100, doi: 10.1016/j.epsl.2013.02.027.

Valladas, H., Mercier, N., Froget, L., Hovers, E., Joron, J.-L., Kimbel, W.H., and Rak, Y., 1999, TL Dates for the Neanderthal Site of the Amud Cave, Israel: Journal of Archaeological Science, v. 26, no. 3, p. 259–268, doi: 10.1006/jasc.1998.0334.

Valladas, H., Reyss, J.L., Joron, J.L., Valladas, G., Bar-Yosef, O., and Vandermeersch, B., 1988, Thermoluminescence dating of Mousterian Troto-Cro-Magnon' remains from Israel and the origin of modern man: Nature, v. 331, p. 614–616, doi: 10.1038/331614a0.

Waldmann, N., Starinsky, A., and Stein, M., 2007, Primary carbonates and Ca-chloride brines as monitors of a paleo-hydrological regime in the Dead Sea basin: Quaternary

Science Reviews, v. 26, no. 17–18, p. 2219–2228, doi: 10.1016/j.quascirev.2007.04.019.

Waldmann, N., Stein, M., Ariztegui, D., and Starinsky, A., 2009, Stratigraphy, depositional environments and level reconstruction of the last interglacial Lake Samra in the Dead Sea basin: Quaternary Research, v. 72, no. 1, p. 1–15, doi: 10.1016/j.yqres.2009.03.005.

Wedepohl, K.H., 1995, The composition of the continental crust: Geochimica et Cosmochimica Acta, v. 59, no. 7, p. 1217–1232, doi: 10.1016/0016-7037(95)00038-2.

Zak, I., 1967, The Geology of Mt. Sedom: Unpublished PhD thesis, The Hebrew University, Jerusalem (in Hebrew with English abstract).

Ziv, B., Saaroni, H., Pargament, R., Harpaz, T., and Alpert, P., 2014, Trends in rainfall regime over Israel, 1975–2010, and their relationship to large-scale variability: Regional Environmental Change, v. 14, no. 5, p. 1751–1764, doi: 10.1007/s10113-013-0414-x.

7 Appendix

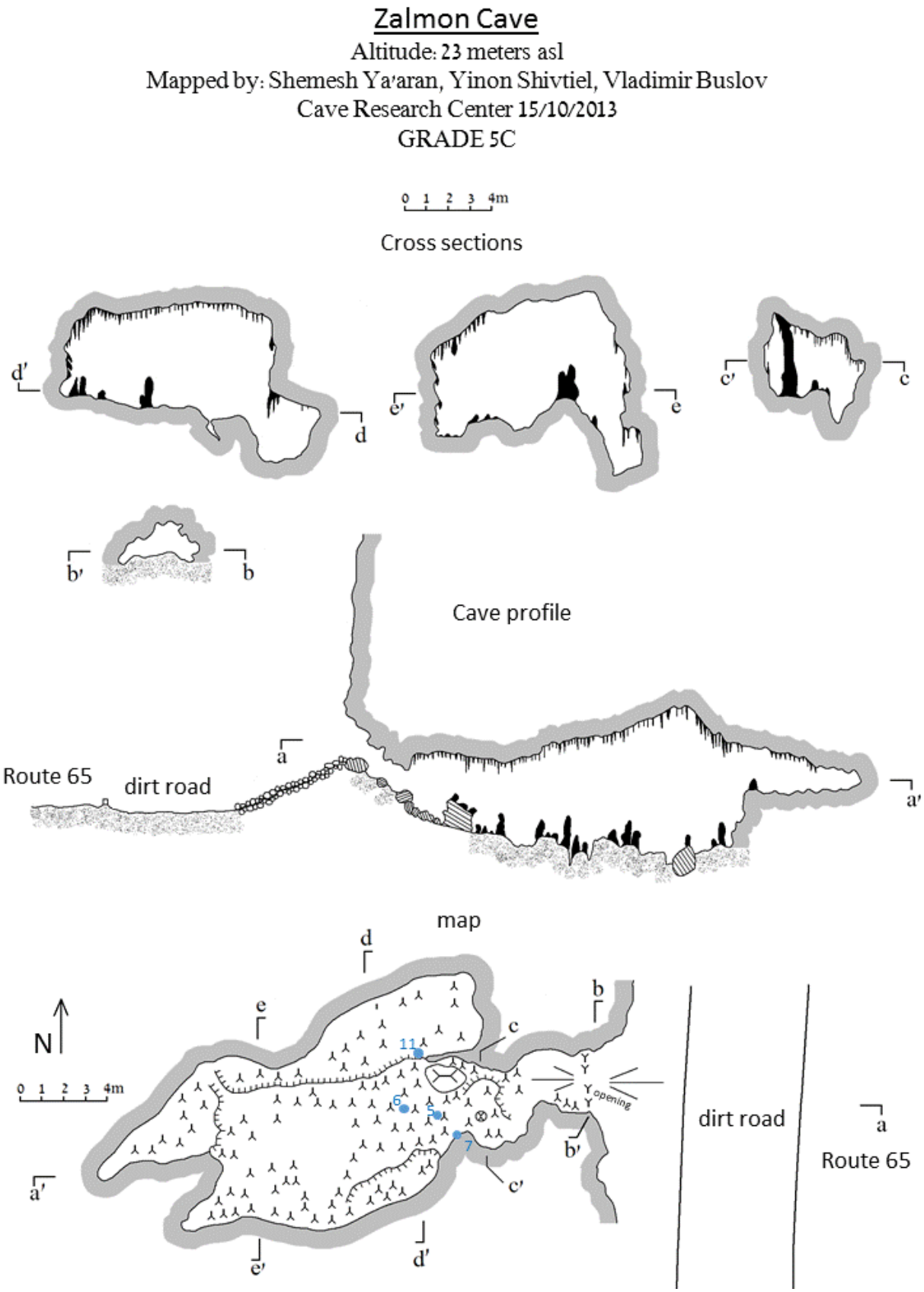

Figure 34: Zalmon cave map and cross sections. Stalagmites sampled in-situ marked as blue circles.

7.1 Dating Results

Table 1: Dating results of stalagmite ZAL1. From left to right: The stratigraphic order of the sample from top to bottom, the sample name, concentration of ^{238}U in ppm and error, measured $^{234}U/^{238}U$ ratio and error, measured $^{230}Th/^{234}U$ ratio and error, calculated (uncorrected) age in ka with 2σ error, $^{230}Th/^{232}Th$ ratio and error, corrected $^{234}U/^{238}U$ ratio and error based on a correction factor of 1.8, corrected $^{230}Th/^{234}U$ ratio and error based on a correction factor of 1.8 and the corrected age in ka with 2σ error. Ages out of stratigraphic order are in red. Most of the dates are in stratigraphic order. Three dates are anomalously out of stratigraphic order (ZAL1-B, ZAL1-Q and ZAL1-F).

Strat. order	Sample name	238U (ppm)	Error (1σ)	Measured $^{234}U/^{238}U$	Error (1σ)	Measured $^{230}Th/^{234}U$	Error (1σ)	Age (ka)	Error (2σ)	$^{230}Th/^{232}Th$	Error (1σ)	Corrected $^{234}U/^{238}U$	Error (1σ)	Corrected $^{230}Th/^{234}U$	Error (1σ)	Corrected age (ka)	Error (2σ)
1	ZAL1 C	0.3595	0.0003	1.058	0.001	0.426	0.002	60.0	0.6	294	1	1.058	0.001	0.425	0.002	59.8	0.6
2	ZAL1 M	0.2001	0.0001	1.042	0.003	0.383	0.011	52.3	3.8	185	8	1.042	0.003	0.381	0.011	51.9	3.8
3	ZAL1 L	0.2173	0.0002	1.051	0.002	0.383	0.007	52.3	2.6	188	4	1.051	0.002	0.381	0.007	51.9	2.6
4	ZAL1 K	0.2947	0.0002	1.056	0.001	0.399	0.004	55.1	1.6	147	2	1.056	0.001	0.396	0.004	54.6	1.6
5	ZAL1 T	0.3711	0.0003	1.057	0.001	0.460	0.004	66.6	1.4	26.8	0.2	1.059	0.001	0.443	0.003	63.3	1.4
6	ZAL1 S	0.1789	0.0002	1.056	0.002	0.542	0.005	84.2	2.5	39.5	0.4	1.058	0.002	0.531	0.005	81.6	2.5
7	ZAL1 J	0.1745	0.0001	1.045	0.002	0.518	0.004	78.9	2.0	111	1	1.046	0.002	0.514	0.004	78.0	2.0
8	ZAL1 I	0.1420	0.0002	1.049	0.003	0.512	0.004	77.4	1.9	78	1	1.049	0.003	0.506	0.004	76.2	1.9
9	ZAL1 R	0.1423	0.0000	1.048	0.002	0.489	0.009	72.7	3.8	111	2	1.049	0.002	0.485	0.009	71.8	3.8
10	ZAL1 H	0.1505	0.0001	1.037	0.002	0.492	0.004	73.3	1.8	99	1	1.038	0.002	0.487	0.004	72.3	1.8
11	ZAL1 G	0.2666	0.0002	1.052	0.003	0.477	0.002	69.9	1.0	33.1	0.2	1.054	0.003	0.463	0.002	67.2	1.0
12	ZAL1 B	0.3600	0.0003	1.038	0.001	0.744	0.002	146.0	2.2	173	1	1.038	0.001	0.742	0.002	145.2	2.2
13	ZAL1 Q	0.1476	0.0001	1.040	0.002	0.698	0.010	128.8	7.6	64	1	1.040	0.002	0.693	0.010	126.7	7.6
14	ZAL1 F	0.1769	0.0002	1.033	0.003	0.664	0.005	117.6	3.4	146	1	1.033	0.003	0.661	0.005	116.7	3.4
15	ZAL1 P	0.1623	0.0001	1.043	0.002	0.542	0.007	84.3	3.5	45	1	1.044	0.002	0.532	0.007	81.9	3.5
16	ZAL1 E	0.1677	0.0001	1.042	0.003	0.505	0.003	76.1	1.2	33.2	0.2	1.043	0.003	0.492	0.003	73.2	1.2
17	ZAL1 O	0.1560	0.0001	1.045	0.003	0.539	0.012	83.7	5.8	31.1	0.7	1.046	0.003	0.524	0.012	80.2	5.8
18	ZAL1 D	0.1402	0.0001	1.034	0.002	0.689	0.005	125.7	3.9	168	1	1.035	0.002	0.686	0.005	124.9	3.9
19	ZAL1 N	0.1343	0.0001	1.038	0.002	0.742	0.007	145.4	5.5	80	1	1.039	0.002	0.738	0.006	143.7	5.5
20	ZAL1 A	0.1148	0.0001	1.037	0.002	0.778	0.005	161.0	4.6	64.1	0.4	1.038	0.002	0.773	0.005	158.7	4.6

Table 2: Dating results of stalagmite ZAL2. Column descriptions are as in Table 1. The majority of this stalagmite was deposited in the last glacial period (MIS 2-4). Aside from a single sample (ZAL2 R) ages are in stratigraphic order The top 5 samples have a high ratio of detrital component indicated by a $^{230}Th/^{232}Th$ ratio of less than 30 resulting in a change of more than 10% to the corrected age.

Strat. order	Sample name	238U (ppm)	Error (1σ)	Measured $^{234}U/^{238}U$	Error (1σ)	Measured $^{230}Th/^{234}U$	Error (1σ)	Age (ka)	Error (2σ)	$^{230}Th/^{232}Th$	Error (1σ)	Corrected $^{234}U/^{238}U$	Error (1σ)	Corrected $^{230}Th/^{234}U$	Error (1σ)	Corrected age (ka)	Error (2σ)
1	**ZAL2 C**	0.1263	0.0001	1.047	0.002	0.053	0.001	**6.0**	0.2	13.8	0.3	1.047	0.002	0.046	0.001	**5.1**	0.3
2	**ZAL2 L**	0.1580	0.0001	1.054	0.001	0.052	0.002	**5.8**	0.4	13.6	0.4	1.055	0.001	0.045	0.001	**5.0**	0.4
3	**ZAL2 K**	0.1251	0.0001	1.051	0.002	0.062	0.002	**7.0**	0.5	19.9	0.7	1.051	0.002	0.056	0.002	**6.2**	0.5
4	**ZAL2 J**	0.1428	0.0001	1.043	0.002	0.068	0.002	**7.6**	0.4	19.4	0.5	1.043	0.002	0.061	0.001	**6.9**	0.4
5	**ZAL2 I**	0.1781	0.0002	1.045	0.002	0.066	0.001	**7.4**	0.3	29.0	0.6	1.045	0.002	0.062	0.001	**6.9**	0.3
6	**ZAL2 R**	0.1901	0.0002	1.045	0.003	0.413	0.011	**57.7**	4.1	65	2	1.046	0.003	0.406	0.011	**56.5**	4.1
7	**ZAL2 Q**	0.3368	0.0003	1.046	0.003	0.194	0.004	**23.4**	1.0	86	2	1.046	0.003	0.191	0.004	**23.0**	1.0
8	**ZAL2 P**	0.3598	0.0003	1.052	0.002	0.161	0.003	**19.0**	0.9	88	2	1.052	0.002	0.158	0.003	**18.6**	0.9
9	**ZAL2 H**	0.2728	0.0002	1.065	0.002	0.223	0.003	**27.4**	0.9	165	3	1.065	0.002	0.221	0.003	**27.2**	0.9
10	**ZAL2 B**	0.3078	0.0002	1.050	0.001	0.247	0.001	**30.8**	0.4	352	2	1.051	0.001	0.246	0.001	**30.7**	0.4
11	**ZAL2 G**	0.3987	0.0004	1.076	0.001	0.262	0.004	**32.8**	1.2	274	5	1.076	0.001	0.260	0.004	**32.8**	1.2
12	**ZAL2 O**	0.2199	0.0003	1.055	0.003	0.306	0.007	**39.6**	2.0	185	4	1.055	0.003	0.304	0.007	**39.3**	2.0
13	**ZAL2 N**	0.3606	0.0004	1.055	0.003	0.299	0.015	**38.6**	4.6	140	7	1.055	0.003	0.297	0.015	**38.6**	4.6
14	**ZAL2 M**	0.1672	0.0002	1.037	0.003	0.372	0.006	**50.5**	2.1	120	2	1.037	0.003	0.369	0.006	**49.8**	2.1
15	**ZAL2 F**	0.2716	0.0002	1.064	0.002	0.362	0.006	**48.6**	2.0	167	3	1.064	0.002	0.359	0.006	**48.2**	2.0
16	**ZAL2 E**	0.2678	0.0001	1.062	0.002	0.399	0.005	**55.1**	1.8	391	5	1.062	0.002	0.398	0.005	**54.9**	1.8
17	**ZAL2 D**	0.3839	0.0003	1.069	0.002	0.405	0.005	**56.1**	1.7	384	5	1.069	0.002	0.404	0.005	**55.9**	1.7
18	**ZAL2 A**	0.2768	0.0001	1.060	0.002	0.449	0.003	**64.5**	1.0	443	2	1.061	0.002	0.448	0.003	**64.3**	1.0

Table 3: Dating results of stalagmite ZAL3. Column descriptions are as in Table 1.

Strat. order	Sample name	238U (ppm)	Error (1σ)	Measured $^{234}U/^{238}U$	Error (1σ)	Measured $^{230}Th/^{234}U$	Error (1σ)	Age (ka)	Error (2σ)	$^{230}Th/^{232}Th$	Error (1σ)	Corrected $^{234}U/^{238}U$	Error (1σ)	Corrected $^{230}Th/^{234}U$	Error (1σ)	Corrected age (ka)	Error (2σ)
1	**ZAL3 D**	0.1830	0.0001	1.039	0.002	0.302	0.002	**39.1**	0.5	57.3	0.3	1.040	0.002	0.2959	0.0016	**38**	0.5
2	**ZAL3 C**	0.2557	0.0002	1.043	0.002	0.333	0.002	**43.9**	0.8	46.7	0.3	1.044	0.002	0.3242	0.0023	**42**	0.8
3	**ZAL3 M**	0.1834	0.0001	1.037	0.002	0.373	0.004	**50.5**	1.4	133	1	1.037	0.002	0.3695	0.0039	**50**	1.4
4	**ZAL3 L**	0.1893	0.0001	1.043	0.002	0.381	0.006	**52.0**	2.0	219	3	1.043	0.002	0.3790	0.0056	**52**	2.0
5	**ZAL3 K**	0.4320	0.0002	1.047	0.001	0.377	0.003	**51.2**	1.1	501	5	1.047	0.001	0.3762	0.0031	**51**	1.1
6	**ZAL3 J**	0.2167	0.0001	1.056	0.001	0.398	0.005	**54.8**	1.6	235	3	1.056	0.001	0.3957	0.0045	**54.5**	1.6
7	**ZAL3 B**	0.2077	0.0002	1.045	0.003	0.421	0.003	**59.2**	1.0	267	2	1.045	0.003	0.4198	0.0026	**59**	1.0
8	**ZAL3 I**	0.3707	0.0004	1.050	0.002	0.410	0.005	**57.1**	1.7	512	6	1.050	0.002	0.4089	0.0047	**57**	1.7
9	**ZAL3 H**	0.1860	0.0002	1.051	0.002	0.424	0.005	**59.7**	1.9	144	2	1.051	0.002	0.4209	0.0051	**59.1**	1.9
10	**ZAL3 G**	0.2431	0.0002	1.051	0.002	0.388	0.008	**53.2**	2.9	242	5	1.052	0.002	0.3863	0.0080	**53**	2.9
11	**ZAL3 F**	0.2562	0.0002	1.051	0.002	0.433	0.005	**61.4**	2.0	231	3	1.051	0.002	0.4313	0.0051	**61**	2.0
12	**ZAL3 E**	0.2971	0.0002	1.051	0.001	0.433	0.005	**61.3**	2.1	153	2	1.052	0.001	0.4299	0.0053	**61**	2.1
13	**ZAL3 A**	0.7555	0.0005	1.058	0.002	0.448	0.002	**64.1**	0.7	672	3	1.058	0.002	0.4469	0.0017	**64**	0.7

Table 4: Dating results of stalagmite ZAL4. Column descriptions are as in Table 1.

Strat. order	Sample name	238U (ppm)	Error (1σ)	Measured $^{234}U/^{238}U$	Error (1σ)	Measured $^{230}Th/^{234}U$	Error (1σ)	Age (ka)	Error (2σ)	$^{230}Th/^{232}Th$	Error (1σ)	Corrected $^{234}U/^{238}U$	Error (1σ)	Corrected $^{230}Th/^{234}U$	Error (1σ)	Corrected age (ka)	Error (2σ)
1	**ZAL4 H**	0.1340	0.0001	1.059	0.002	0.597	0.006	**97.6**	1.0	82.5	0.8	1.060	0.002	0.591	0.006	**96.2**	1.0
2	**ZAL4 L**	0.2177	0.0002	1.056	0.002	0.590	0.004	97.0	2.0	161	1	1.057	0.002	0.587	0.004	**95.8**	2.0
3	**ZAL4 G**	0.1765	0.0001	1.057	0.002	0.662	0.006	**116.3**	4.1	140	1	1.057	0.002	0.659	0.006	**116.3**	4.1
4	**ZAL4 K**	0.2100	0.0002	1.045	0.002	0.891	0.013	**231.6**	25.2	241	4	1.045	0.002	0.891	0.013	**230.9**	25.2
5	**ZAL4 J**	0.1573	0.0001	1.059	0.002	0.726	0.009	**138.2**	7.2	73	1	1.060	0.002	0.722	0.009	**136.3**	7.2
6	**ZAL4 F**	0.1517	0.0002	1.053	0.004	0.646	0.006	**111.4**	3.9	226.3	2.2	1.053	0.004	0.644	0.006	**111.4**	3.9
7	**ZAL4 E**	0.1894	0.0013	1.058	0.002	0.636	0.006	**108.4**	3.4	224.1	2.0	1.058	0.002	0.634	0.006	**108.4**	3.4
8	**ZAL4 D**	0.1799	0.0002	1.044	0.002	0.664	0.004	**117.2**	2.4	161.7	0.9	1.044	0.002	0.661	0.004	**117.2**	2.4
9	**ZAL4 C**	0.2382	0.0003	1.063	0.003	0.632	0.004	**107.1**	2.7	278	2	1.064	0.003	0.630	0.004	**107.1**	2.7
10	**ZAL4 I**	0.4813	0.0004	1.077	0.002	0.290	0.004	**37.2**	1.3	107.8	1.2	1.078	0.002	0.286	0.004	**36.5**	1.3
11	**ZAL4 B**	0.2532	0.0002	1.065	0.003	0.675	0.004	**120.1**	2.7	474.2	3.0	1.065	0.003	0.674	0.004	**120.1**	2.7
12	**ZAL4 A**	0.2861	0.0003	1.064	0.002	0.677	0.005	**120.9**	3.3	264.8	2.0	1.065	0.002	0.676	0.005	**120.9**	3.3

Table 5: Dating results of stalagmite ZAL5. Column descriptions are as in Table 1.

Strat. order	Sample name	238U (ppm)	Error (1σ)	Measured $^{234}U/^{238}U$	Error (1σ)	Measured $^{230}Th/^{234}U$	Error (1σ)	Age (ka)	Error (2σ)	$^{230}Th/^{232}Th$	Error (1σ)	Corrected $^{234}U/^{238}U$	Error (1σ)	Corrected $^{230}Th/^{234}U$	Error (1σ)	Corrected age (ka)	Error (2σ)
1	**ZAL5 B**	0.2036	0.0003	1.048	0.003	0.359	0.006	**48.2**	2.0	87.4	1.5	1.048	0.003	0.354	0.006	**47.4**	2.0
2	**ZAL5 J**	0.2162	0.0002	1.058	0.002	0.668	0.006	**118**	4	124	1	1.058	0.002	0.665	0.006	**117**	4
3	**ZAL5 N**	0.3217	0.0003	1.064	0.002	0.664	0.006	**117**	4	634	7	1.064	0.002	0.663	0.006	**116**	4
4	**ZAL5 I**	0.3201	0.0004	1.031	0.002	0.690	0.004	**126**	4	568	4	1.031	0.002	0.689	0.004	**126**	4
5	**ZAL5 H**	0.2549	0.0003	1.0390	0.002	0.708	0.005	**132**	3	531	4	1.039	1.002	0.707	0.005	**132**	3
6	**ZAL5 G**	0.3284	0.0002	1.053	0.003	0.715	0.009	**134**	7	1405	20	1.053	0.003	0.715	0.009	**134**	7
7	**ZAL5 F**	0.2575	0.0002	1.049	0.001	0.733	0.010	**141**	8	782	13	1.049	0.001	0.733	0.010	**141**	8
8	**ZAL5 E**	0.4265	0.0004	1.053	0.001	0.718	0.005	**135**	4	657	5	1.054	0.001	0.717	0.005	**135**	4
9	**ZAL5 D**	0.4581	0.0004	1.040	0.000	0.722	0.004	**137**	3	1444	9	1.040	0.000	0.722	0.004	**137**	3
10	**ZAL5 M**	0.7325	0.0007	1.048	0.002	0.721	0.006	**137**	5	2442	24	1.048	0.002	0.721	0.006	**136**	5
11	**ZAL5 C**	0.3852	0.0008	1.045	0.003	0.719	0.005	**136**	4	838	6	1.045	0.003	0.718	0.005	**135**	4
12	**ZAL5 L**	0.1549	0.0002	1.035	0.002	0.741	0.013	**145**	11	635	12	1.035	0.002	0.741	0.013	**145**	11
13	**ZAL5 K**	0.2202	0.0002	1.034	0.002	0.738	0.013	**144**	11	936	25	1.034	0.002	0.738	0.013	**143**	11
14	**ZAL5 O**	0.2652	0.0002	1.045	0.002	0.741	0.012	**145**	10	415	7	1.045	0.002	0.740	0.012	**144**	10
15	**ZAL5 A**	0.2397	0.0003	1.030	0.003	0.836	0.008	**193**	11	682	7	1.030	0.003	0.836	0.008	**193**	11

Table 6: Dating results of stalagmite ZAL6. Column descriptions are as in Table 1.

Strat. order	Sample name	238U (ppm)	Error (1σ)	Measured $^{234}U/^{238}U$	Error (1σ)	Measured $^{230}Th/^{234}U$	Error (1σ)	Age (ka)	Error (2σ)	$^{230}Th/^{232}Th$	Error (1σ)	Corrected $^{234}U/^{238}U$	Error (1σ)	Corrected $^{230}Th/^{234}U$	Error (1σ)	Corrected age (ka)	Error (2σ)
1	**ZAL6 F**	0.3032	0.0002	1.041	0.002	0.065	0.003	**7.3**	0.6	36.0	1.5	1.041	0.002	0.062	0.002	**6.9**	0.6
2	**ZAL6 A**	0.3937	0.0001	1.035	0.001	0.075	0.001	**8.5**	0.3	131	2	1.035	0.001	0.074	0.001	**8.4**	0.3
3	**ZAL6 D**	0.5628	0.0010	1.059	0.001	0.113	0.001	**13.0**	0.2	98.2	0.8	1.059	0.001	0.111	0.001	**12.8**	0.2
4	**ZAL6 E**	0.5929	0.0016	1.071	0.002	0.160	0.002	**19.0**	0.4	275	3	1.071	0.002	0.160	0.002	**18.9**	0.4
5	**ZAL6 G**	0.7172	0.0010	1.083	0.001	0.175	0.003	**20.9**	0.8	108	2	1.083	0.001	0.172	0.003	**20.5**	0.8
6	**ZAL6 B**	0.6503	0.0007	1.069	0.003	0.202	0.001	**24.5**	0.4	363	3	1.069	0.003	0.201	0.001	**24.5**	0.4
7	**ZAL6 H**	0.3493	0.0002	1.058	0.002	0.415	0.009	**58.0**	3.3	122	3	1.058	0.002	0.412	0.009	**57.4**	3.3
8	**ZAL6 I**	0.1372	0.0002	1.055	0.003	0.565	0.020	**89.8**	9.6	43.9	1.7	1.056	0.003	0.555	0.019	**87.3**	9.6
9	**ZAL6 C**	0.2261	0.0001	1.059	0.002	0.573	0.007	**91.5**	3.5	541	7	1.059	0.002	0.572	0.007	**91.3**	3.5

Table 7: Dating results of stalagmite ZAL7. Column descriptions are as in Table 1.

Strat. order	Sample name	238U (ppm)	Error (1σ)	Measured $^{234}U/^{238}U$	Error (1σ)	Measured $^{230}Th/^{234}U$	Error (1σ)	Age (ka)	Error (2σ)	$^{230}Th/^{232}Th$	Error (1σ)	Corrected $^{234}U/^{238}U$	Error (1σ)	Corrected $^{230}Th/^{234}U$	Error (1σ)	Corrected age (ka)	Error (2σ)
1	**ZAL7 C**	0.2099	0.0002	1.027	0.003	0.698	0.006	**129**	1	130	1	1.027	0.003	0.695	0.006	**128**	1
2	**ZAL7 G**	0.4583	0.0008	1.053	0.003	0.899	0.004	**237**	9	857	4	1.053	0.003	0.899	0.004	**237**	9
3	**ZAL7 F**	0.4965	0.0004	1.036	0.002	0.909	0.006	**250**	14	1414	10	1.036	0.002	0.909	0.006	**250**	14
4	**ZAL7 B**	0.1345	0.0002	1.033	0.003	0.873	0.007	**219**	12	310	3	1.033	0.003	0.873	0.007	**219**	12
5	**ZAL7 E**	0.1887	0.0003	1.030	0.003	0.908	0.009	**251**	21	457	4	1.030	0.003	0.907	0.009	**250**	21
6	**ZAL7 D**	0.4338	0.0010	1.053	0.002	0.941	0.006	**284**	20	1750	13	1.053	0.002	0.941	0.006	**284**	20
7	**ZAL7 A**	0.7340	0.0005	1.045	0.001	0.951	0.004	**302**	14	1190	5	1.045	0.001	0.951	0.004	**302**	14

Table 8: Dating results of stalagmite ZAL11. Column descriptions are as in Table 1.

Strat. order	Sample name	238U (ppm)	Error (1σ)	Measured $^{234}U/^{238}U$	Error (1σ)	Measured $^{230}Th/^{234}U$	Error (1σ)	Age (ka)	Error (2σ)	$^{230}Th/^{232}Th$	Error (1σ)	Corrected $^{234}U/^{238}U$	Error (1σ)	Corrected $^{230}Th/^{234}U$	Error (1σ)	Corrected age (ka)	Error (2σ)
1	**ZAL11 H**	0.4516	0.0009	1.040	0.003	0.597	0.003	**98.0**	1.7	8.10	0.04	1.046	0.003	0.537	0.003	**83.2**	1.7
2	**ZAL11 G**	0.1784	0.0002	1.036	0.003	0.533	0.005	**82.3**	2.5	89.8	0.9	1.036	0.003	0.528	0.005	**81.1**	2.5
3	**ZAL11 F**	0.1850	0.0005	1.042	0.004	0.593	0.005	**96.9**	3.0	97.9	0.9	1.043	0.004	0.588	0.005	**96.4**	3.0
4	**ZAL11 E**	0.1599	0.0002	1.047	0.002	0.703	0.005	**130**	4	291	3	1.047	0.002	0.702	0.005	**130**	4
5	**ZAL11 D**	0.2389	0.0002	1.049	0.002	0.733	0.005	**141**	4	333	2	1.049	0.002	0.732	0.005	**141**	4
6	**ZAL11 C**	0.1819	0.0001	1.033	0.002	0.683	0.007	**124**	5	463	5	1.033	0.002	0.682	0.007	**123**	5
7	**ZAL11 B**	0.2240	0.0003	1.026	0.002	0.668	0.007	**119**	4	306	3	1.026	0.002	0.667	0.007	**119**	4
8	**ZAL11 A**	0.1402	0.0007	0.892	0.016	1.16	0.02	**>550**	-	504	4	0.891	0.016	1.17	0.02	**>550**	-

7.2 *Isotopic measurements*

Table 9: Isotopic Measurement data. From left to right: Sample ID, measured $\delta^{13}C$, measured $\delta^{18}O$, measured age (corrected age for samples with $^{230}Th/^{232}Th<100$), 2σ dating error and the age used according to the age model and wiggle matching.

Sample ID	$\delta^{13}C$	$\delta^{18}O$	measured age	Error (2σ)	Wiggle matched age
ZAL1-1	-10.71	-3.77			161.73
ZAL1-2	-10.86	-4.01			161.05
ZAL1-3	-11.07				160.36
ZAL1-4	-10.57	-3.95			159.68
ZAL1-5	-10.56	-3.72	158.7	4.6	159.00
ZAL1-6	-10.46	-3.43			158.32
ZAL1-7	-10.38	-3.87			157.64
ZAL1-8	-10.64	-4.03			156.95
ZAL1-9	-11.02	-4.13			156.27
ZAL1-10	-10.42	-4.29			155.59
ZAL1-11	-10.24	-3.74			154.91
ZAL1-12	-10.04	-3.73			154.23
ZAL1-13	-9.69	-3.65			153.55
ZAL1-14	-9.88	-3.56			152.86
ZAL1-15	-10.30				152.18
ZAL1-16	-9.90	-3.52			151.50
ZAL1-17	-10.06	-3.59			150.82
ZAL1-18	-11.07	-3.96			150.14
ZAL1-19	-10.68	-3.81			149.45
ZAL1-20	-10.44	-4.09			148.77
ZAL1-21	-10.31	-4.05			148.09
ZAL1-22	-10.59	-3.99			147.41
ZAL1-23	-10.44	-3.90			146.73
ZAL1-24	-10.35	-3.93			146.05
ZAL1-25	-10.70	-3.94			145.36
ZAL1-26	-10.97	-3.93			144.68
ZAL1-27	-10.92	-3.84	143.7	5.5	144.00
ZAL1-28	-11.10	-4.21			143.00
ZAL1-29	-11.21	-4.29			142.00
ZAL1-30	-10.66	-4.34			141.00
ZAL1-31	-10.86	-3.88			140.00
ZAL1-32	-11.18	-3.91			139.00
ZAL1-33	-11.14	-4.29			138.00
ZAL1-34	-11.26	-4.46			137.00
ZAL1-35	-11.37	-4.44			136.00
ZAL1-36	-10.92	-3.90			135.00
ZAL1-37	-10.75	-3.81			134.00
ZAL1-38	-10.20	-3.98			133.00
ZAL1-39	-10.49	-3.62			132.00
ZAL1-40					131.00
ZAL1-41	-10.65	-3.99			130.00
ZAL1-42	-10.70	-3.60	125.7	3.9	129.00
					hiatus
ZAL1-43	-9.98	-3.40			80.30
ZAL1-44	-10.11	-4.03			80.10
ZAL1-45	-10.20	-4.32			79.91
ZAL1-46	-10.23	-4.35			79.71
ZAL1-47	-10.32	-4.14	80.2	5.8	79.51

ZAL1-48	-10.10	-4.26			79.32
ZAL1-49	-10.21	-4.23			79.12
ZAL1-50	-10.40	-4.00			78.93
ZAL1-51	-10.36	-4.12			78.73
ZAL1-52	-9.56	-4.49			78.53
ZAL1-53	-10.20	-4.55			78.34
ZAL1-54	-10.07	-4.38			78.14
ZAL1-55	-10.08	-4.11	73.2	1.2	77.94
ZAL1-56	-10.26	-4.20			77.75
ZAL1-57	-10.28	-4.04			77.55
ZAL1-58	-10.33	-3.98			77.36
ZAL1-59	-9.79	-4.09			77.16
ZAL1-60	-9.83	-4.50			76.96
ZAL1-61	-10.45	-3.96			76.77
ZAL1-62	-10.30	-3.86			76.57
ZAL1-63	-10.17	-4.91			76.37
ZAL1-64	-10.01	-3.89			76.18
ZAL1-65	-10.15	-4.13			75.98
ZAL1-66	-10.09	-4.28			75.78
ZAL1-67	-10.32	-4.14	81.9	3.5	75.59
ZAL1-68	-10.60	-4.06			75.39
ZAL1-69	-10.78	-4.04			75.20
ZAL1-70	-10.17	-3.83			75.00
ZAL1-71	-9.76	-3.73			74.80
ZAL1-72	-10.01	-4.25			74.61
ZAL1-73	-9.83	-4.28			74.41
ZAL1-74	-10.48	-4.24			74.21
ZAL1-75	-10.22	-4.39			74.02
ZAL1-76	-10.12	-4.27			73.82
ZAL1-77	-10.01	-4.03			73.63
ZAL1-78	-9.53	-3.85			73.43
ZAL1-79	-9.92	-3.48			73.23
ZAL1-80	-9.49	-3.38			73.04
ZAL1-81	-9.45	-3.67			72.84
ZAL1-82	-9.00	-2.75			72.64
ZAL1-83	-8.90	-2.71			72.45
ZAL1-84	-9.35	-3.28			72.25
ZAL1-85	-9.34	-3.15			72.05
ZAL1-86	-9.36	-3.38			71.86
ZAL1-87	-9.37	-3.37	117	3	71.66
ZAL1-88	-8.56	-3.52			71.47
ZAL1-89	-8.59	-3.48			71.27
ZAL1-90	-9.26	-3.23	127	8	71.07
ZAL1-91	-9.31	-3.42			70.88
ZAL1-92	-10.46	-4.20			70.68
ZAL1-93	-10.76	-4.32			70.48
ZAL1-94	-10.43	-4.59			70.29
ZAL1-95	-10.51	-4.59			70.09
ZAL1-96	-10.74	-4.39			69.90
ZAL1-97	-10.54	-4.94	146	2	69.70
ZAL1-98	-10.57	-5.06			69.50
ZAL1-99	-10.91	-5.49			69.31
ZAL1-100	-9.91	-5.07			69.11
ZAL1-101	-1.10	-5.36			68.91
ZAL1-102	0.64	-5.35			68.72
ZAL1-103	-1.44	-5.23			68.52
ZAL1-104	-7.6	-4.89			68.32
ZAL1-105	-10.85	-5.59	67.2	1	68.13

ZAL1-106	-11.22	-5.58			67.93
ZAL1-107	-9.54	-4.43			67.74
ZAL1-108	-9.40	-3.53			67.54
ZAL1-109	-8.83	-3.88			67.34
ZAL1-110	-10.97	-5.23			67.15
ZAL1-111	-11.25	-5.09	73.3	1.8	66.95
ZAL1-112	-11.76	-5.54			66.75
ZAL1-113	-10.75	-5.31			66.56
ZAL1-114	-10.72	-5.56			66.36
ZAL1-115	-10.69	-5.78	72.7	3.8	66.17
ZAL1-116	-11.40	-6.02			65.97
ZAL1-117	-10.74	-5.54			65.77
ZAL1-118	-9.58	-4.79			65.58
ZAL1-119	-9.68	-4.60			65.38
ZAL1-120	-8.76	-4.08			65.18
ZAL1-121	-8.81	-4.35			64.99
ZAL1-122	-9.82	-5.11			64.79
ZAL1-123	-10.08	-5.05			64.60
ZAL1-124	-10.19	-4.97			64.40
ZAL1-125	-10.64	-4.09			64.20
ZAL1-126	-10.87	-4.93			64.01
ZAL1-127	-10.52	-5.33			63.81
ZAL1-128	-10.51	-4.89	76.2	1.9	63.61
ZAL1-129	-9.84	-4.48			63.42
ZAL1-130	-9.93	-4.12			63.22
ZAL1-131	-9.22	-3.98			63.02
ZAL1-132	-8.82	-4.61			62.83
ZAL1-133	-9.48	-5.31			62.63
ZAL1-134	-8.23	-4.43			62.44
ZAL1-135	-8.51	-4.39	78.9	2	62.24
ZAL1-136	-8.36	-4.13			62.04
ZAL1-137	-8.98	-4.07			61.85
ZAL1-138	-9.14	-3.96			61.65
ZAL1-139	-10.31	-5.84			61.45
ZAL1-140	-10.19	-5.80			61.26
ZAL1-141	-10.10	-5.58			61.06
ZAL1-142	-10.34	-5.89			60.87
ZAL1-143	-10.46	-5.44			60.67
ZAL1-144	-10.36	-5.08			60.47
ZAL1-145	-10.02	-5.05			60.28
ZAL1-146	-10.17	-5.57			60.08
ZAL1-147	-9.80	-5.62			59.88
ZAL1-148	-9.82	-5.44			59.69
ZAL1-149	-10.06	-5.94			59.49
ZAL1-150	-10.46	-5.97			59.29
ZAL1-151	-7.99	-5.45			59.10
ZAL1-152	-8.64	-6.13			58.90
ZAL1-153	-8.37	-4.67			58.71
ZAL1-154	-7.96	-4.45			58.51
ZAL1-155	-6.76	-3.54	81.6	2.5	58.31
ZAL1-156	-6.92	-3.54			58.12
ZAL1-157	-9.76	-4.59			57.92
ZAL1-158	-10.65	-4.81			57.72
ZAL1-159	-9.72	-4.63			57.53
ZAL1-160	-9.66	-4.59			57.33
ZAL1-161	-8.56	-4.02			57.14
ZAL1-162	-8.38	-3.86			56.94
ZAL1-163	-9.16	-4.20			56.74

ZAL1-164	-7.73	-4.05			56.55
ZAL1-165	-7.10	-3.75	63.3	1.4	56.35
ZAL1-166	-7.41	-4.00			56.16
ZAL1-167	-7.43	-3.91			55.96
ZAL1-168	-7.45	-3.51			55.77
ZAL1-169	-7.88	-4.83			55.58
ZAL1-170	-7.96	-4.25			55.39
ZAL1-171	-7.74	-4.14			55.19
ZAL1-172	-7.78	-4.28	55.1	1.6	55.00
ZAL1-173	-8.12	-4.48			54.82
ZAL1-174	-8.07	-3.99			54.64
ZAL1-175	-7.76	-3.92			54.45
ZAL1-176	-7.99	-3.79			54.27
ZAL1-177	-9.40	-4.03			54.09
ZAL1-178	-9.70	-4.23			53.91
ZAL1-179	-10.03	-4.43			53.73
ZAL1-180	-10.23	-4.83	52.3	2.4	53.55
ZAL1-181	-9.91	-4.55			53.36
ZAL1-182	-8.41	-3.92			53.18
ZAL1-183	-8.10	-3.84			53.00
ZAL1-184	-7.87	-3.83			52.82
ZAL1-185	-8.86	-3.94			52.64
ZAL1-186	-8.82	-4.14			52.45
ZAL1-187	-8.69	-3.88			52.27
ZAL1-188	-9.85	-4.47			52.09
ZAL1-189	-10.31	-4.90			51.91
ZAL1-190	-9.86	-4.91			51.73
ZAL1-191	-9.57	-4.47			51.55
ZAL1-192	-9.70	-4.12	52.3	3.8	51.36
ZAL1-193	-10.13	-4.59			51.18
ZAL1-194	-8.98	-4.36			51.00
ZAL1-195	-8.39	-4.24			50.82
ZAL1-196	-7.53	-3.95			50.64
ZAL1-197	-7.86	-3.69			50.45
ZAL1-198	-8.86	-4.53			50.27
ZAL1-199	-9.13	-4.66			50.09
ZAL1-200	-9.13	-4.57			49.91
ZAL1-201	-9.03	-3.83			49.73
ZAL1-202	-7.51	-3.90			49.55
ZAL1-203	-8.23	-3.75	60	0.6	49.36
ZAL1-204	-6.74	-3.61			49.18
ZAL1-205	-6.23	-3.49			49.00

Sample ID	$\delta^{13}C$	$\delta^{18}O$	measured age	Error (2σ)	Wiggle matched age
ZAL2-1	-9.14	-4.00			64.69
ZAL2-2	-8.50	-3.96			64.55
ZAL2-3	-8.25	-4.91			64.42
ZAL2-4	-8.23	-4.96			64.28
ZAL2-5	-8.56	-5.10			64.14
ZAL2-6	-9.74	-5.04	64.5	1	64.00
ZAL2-7	-9.72	-5.15			63.86
ZAL2-8	-9.57	-4.93			63.72
ZAL2-9	-9.65	-4.96			63.58
ZAL2-10	-9.72	-4.96			63.45
ZAL2-11	-9.56	-4.84			63.31
ZAL2-12	-9.54	-4.96			63.17
ZAL2-13	-9.61	-5.16			63.03
ZAL2-14	-9.76	-5.25			62.89
ZAL2-15	-9.25	-4.62			62.75
ZAL2-16	-9.00	-4.63			62.62
ZAL2-17	-9.18	-4.14			62.48
ZAL2-18	-7.53	-3.82			62.34
ZAL2-19	-6.87	-3.93			62.20
					hiatus
ZAL2-20	-10.00	-5.02			59.74
ZAL2-21	-10.30	-5.39			59.60
ZAL2-22	-10.48	-5.15			59.45
ZAL2-23	-9.73	-4.68			59.31
ZAL2-24	-10.67	-5.35			59.16
ZAL2-25	-10.72	-5.08			59.02
ZAL2-26	-10.26	-5.06			58.88
ZAL2-27	-10.23	-5.25			58.73
ZAL2-28	-10.18	-4.94			58.59
ZAL2-29	-10.23	-4.92			58.44
ZAL2-30	-10.26	-4.81			58.30
ZAL2-31	-9.94	-5.13			58.16
ZAL2-32	-10.23	-5.05			58.01
ZAL2-33	-10.04	-5.04			57.87
ZAL2-34	-10.28	-4.88			57.72
ZAL2-35	-10.06	-5.05			57.58
ZAL2-36	-10.54	-5.12			57.44
ZAL2-37	-10.40	-5.36			57.29
ZAL2-38	-10.31	-5.78			57.15
ZAL2-39	-10.20	-4.98			57.00
ZAL2-40	-10.10	-4.80			56.86
ZAL2-41	-9.81	-4.53			56.72
ZAL2-42	-9.78	-4.59			56.57
ZAL2-43	-9.65	-4.61			56.43
ZAL2-44	-8.87	-4.33			56.28
ZAL2-45	-9.31	-4.34	56.3	2	56.20
ZAL2-46	-9.59	-5.26			56.12
ZAL2-47	-10.05	-5.30			56.03
ZAL2-48	-9.66	-5.20			55.95
ZAL2-49	-9.74	-4.55			55.86
ZAL2-50	-9.99	-4.72			55.78
ZAL2-51	-9.74	-4.41			55.69
ZAL2-52	-10.23	-3.84			55.61
ZAL2-53	-8.58	-3.22			55.52
ZAL2-54	-9.32	-3.58			55.44

ZAL2-55	-9.24	-4.11			55.35
ZAL2-56	-9.19	-4.60			55.27
ZAL2-57	-10.09	-4.27			55.18
ZAL2-58	-10.37	-4.94			55.10
ZAL2-59	-9.59	-4.20			55.01
ZAL2-60	-9.47	-4.31			54.93
ZAL2-61	-9.07	-4.66			54.84
ZAL2-62	-8.18	-4.47			54.76
ZAL2-63	-8.16	-4.11			54.67
ZAL2-64	-8.52	-4.62			54.59
ZAL2-65	-8.48	-4.53			54.50
ZAL2-66	-8.08	-4.51			54.42
ZAL2-67	-8.02	-4.47			54.33
ZAL2-68	-7.60	-4.23			54.25
ZAL2-69	-7.29	-3.95			54.16
ZAL2-70	-7.59	-4.08			54.08
ZAL2-71	-8.10	-4.34			53.99
ZAL2-72	-8.92	-4.62			53.91
ZAL2-73	-10.07	-4.56			53.82
ZAL2-74	-10.77	-5.00			53.74
ZAL2-75	-10.57	-5.15			53.65
ZAL2-76	-11.20	-5.23			53.57
ZAL2-77	-10.24	-5.00			53.48
ZAL2-78	-10.38	-4.89	55.1	1.8	53.40
ZAL2-79	-10.43	-4.83			53.29
ZAL2-80	-11.15	-5.06			53.18
ZAL2-81	-10.96	-5.14			53.07
ZAL2-82	-10.42	-5.08			52.97
ZAL2-83	-10.62	-5.20			52.86
ZAL2-84	-10.14	-4.76			52.75
ZAL2-85	-10.24	-4.94			52.64
ZAL2-86	-11.12	-5.14			52.53
ZAL2-87	-10.69	-5.35			52.42
ZAL2-88	-10.81	-5.30			52.31
ZAL2-89	-11.03	-5.28			52.21
ZAL2-90	-10.33	-4.83			52.10
ZAL2-91	-10.57	-5.05			51.99
ZAL2-92	-10.42	-5.04			51.88
ZAL2-93	-11.23	-6.05			51.77
ZAL2-94	-10.14	-5.08			51.66
ZAL2-95	-10.87	-4.84			51.55
ZAL2-96	-11.17	-5.36			51.45
ZAL2-97	-11.18	-5.02			51.34
ZAL2-98	-11.29	-5.05			51.23
ZAL2-99	-10.95	-5.05			51.12
ZAL2-100	-11.20	-5.09			51.01
ZAL2-101	-10.99	-5.06			50.90
ZAL2-102	-11.22	-5.21			50.79
ZAL2-103	-10.83	-5.09			50.69
ZAL2-104	-10.96	-4.96			50.58
ZAL2-105	-11.15	-5.02			50.47
ZAL2-106	-11.53	-5.59			50.36
ZAL2-107	-11.32	-5.52			50.25
ZAL2-108	-11.48	-5.31			50.14
ZAL2-109	-10.99	-5.42			50.03
ZAL2-110	-10.92	-5.04			49.93
ZAL2-111	-10.77	-5.16	48.6	2	49.82
ZAL2-112	-10.65	-5.06			49.71

ZAL2-113	-11.02	-4.88	50.5	2	49.60
ZAL2-114	-11.87	-5.25			49.49
ZAL2-115	-12.50	-4.95			49.38
					hiatus
ZAL2-116	-9.93	-4.61	38.6	4.6	42.00
ZAL2-117	-9.48	-4.28			41.57
ZAL2-118	-11.93	-5.01			41.14
ZAL2-119	-10.89	-5.14			40.71
ZAL2-120	-11.05	-4.87			40.29
ZAL2-121	-11.15	-4.86			39.86
ZAL2-122	-11.27	-4.82			39.43
ZAL2-123	-11.44	-4.83	39.6	2	39.00
ZAL2-124	-11.10	-4.38			38.57
ZAL2-125	-11.20	-4.72			38.01
ZAL2-126	-10.99	-4.52			37.44
ZAL2-127	-10.90	-4.58			36.88
ZAL2-128	-10.17	-4.64			36.32
ZAL2-129	-11.36	-5.09			35.75
ZAL2-130	-10.18	-4.57			35.19
ZAL2-131	-10.73	-4.69			34.63
ZAL2-132	-10.98	-5.04			34.06
ZAL2-133	-10.82	-5.18			33.50
ZAL2-134	-10.85	-4.93	32.8	1.2	32.80
ZAL2-135	-11.20	-4.37			32.54
ZAL2-136	-11.12	-4.93			32.28
ZAL2-137	-11.49	-4.77			32.01
ZAL2-138	-11.60	-4.58			31.75
ZAL2-139	-11.59	-5.37			31.49
ZAL2-140	-11.26	-4.26			31.23
ZAL2-141	-10.85	-4.57			30.96
ZAL2-142	-10.94	-4.64	30.7	0.4	30.80
ZAL2-143	-10.85	-4.33			30.22
ZAL2-144	-10.93	-4.20			29.63
ZAL2-145	-10.96	-4.26			29.05
ZAL2-146	-11.26	-4.21			28.47
ZAL2-147	-11.33	-4.40			27.88
ZAL2-148	-11.04	-4.25	27.2	0.9	27.20
ZAL2-149	-11.10	-4.50			26.56
ZAL2-150	-11.07	-4.21			25.92
ZAL2-151	-10.99	-4.33			25.28
ZAL2-152	-10.83	-4.74			24.63
ZAL2-153	-10.98	-5.51			23.99
ZAL2-154	-10.28	-4.09			23.35
ZAL2-155	-9.75	-3.69	18.6	0.9	22.71
ZAL2-156	-9.57	-3.79			22.07
ZAL2-157	-10.19	-4.12			21.43
ZAL2-158	-9.68	-4.29			20.78
ZAL2-159	-10.31	-4.23			20.14
ZAL2-160	-10.97	-4.16	23	1	19.50
ZAL2-161	-10.68	-4.25	56.5	4.1	18.86
ZAL2-162	-10.65	-4.81			18.22
					hiatus
ZAL2-163	-11.19	-6.18			6.90
ZAL2-164	-11.34	-5.91			6.89
ZAL2-165	-11.48	-5.76			6.88
ZAL2-166	-11.30	-5.79	6.9	0.32	6.88
ZAL2-167	-10.44	-5.76			6.87
ZAL2-168	-10.59	-5.61			6.86

ZAL2-169	-8.38	-5.09			6.85
ZAL2-170	-9.53	-5.69			6.84
ZAL2-171	-10.26	-5.96			6.84
ZAL2-172	-10.86	-5.64	6.9	0.4	6.83
ZAL2-173	-10.92	-5.99			6.82
ZAL2-174	-10.03	-5.99			6.81
ZAL2-175	-11.01	-5.77			6.80
ZAL2-176	-10.06	-5.58			6.79
ZAL2-177	-10.48	-5.90			6.79
ZAL2-178	-9.74	-6.17			6.78
ZAL2-179	-10.19	-6.04			6.77
ZAL2-180	-9.58	-5.70			6.76
ZAL2-181	-10.12	-5.77			6.75
ZAL2-182	-9.41	-5.70			6.75
ZAL2-183	-9.86	-5.56			6.74
ZAL2-184	-9.37	-5.64			6.73
ZAL2-185	-9.68	-6.08			6.72
ZAL2-186	-9.46	-6.06			6.71
ZAL2-187	-9.02	-5.84			6.71
ZAL2-188	-9.72	-5.88			6.70
ZAL2-189	-9.47	-5.64			6.69
ZAL2-190	-9.40	-5.45			6.68
ZAL2-191	-9.39	-5.37			6.67
ZAL2-192	-9.09	-5.49			6.66
ZAL2-193	-9.02	-5.52			6.66
ZAL2-194	-9.30	-5.39			6.65
ZAL2-195	-9.34	-5.45			6.64
ZAL2-196	-9.13	-5.15			6.63
ZAL2-197	-9.00	-5.52			6.62
ZAL2-198	-9.28	-5.75			6.62
ZAL2-199	-8.92	-5.57			6.61
ZAL2-200	-9.08	-5.46	6.2	0.5	6.60
ZAL2-201	-9.04	-5.52			6.53
ZAL2-202	-9.20	-5.79			6.46
ZAL2-203	-9.19	-5.56			6.40
ZAL2-204	-9.05	-5.52			6.33
ZAL2-205	-8.94	-5.35			6.26
ZAL2-206	-8.89	-5.50			6.19
ZAL2-207	-9.13	-6.28			6.12
ZAL2-208	-9.21	-5.79			6.06
ZAL2-209	-9.17	-5.68			5.99
ZAL2-210	-9.50	-6.27			5.92
ZAL2-211	-9.37	-6.41			5.85
ZAL2-212	-10.53	-5.71			5.78
ZAL2-213	-10.47	-5.65			5.72
ZAL2-214	-10.75	-6.14			5.65
ZAL2-215	-10.76	-5.77			5.58
ZAL2-216	-9.96	-5.43			5.51
ZAL2-217	-9.98	-5.42			5.44
ZAL2-218	-9.77	-5.30			5.38
ZAL2-219	-9.83	-5.35	5	0.4	5.31
ZAL2-220	-10.45	-5.23			5.24
ZAL2-221	-10.63	-5.26			5.17
ZAL2-223	-10.76	-5.47			5.10
ZAL2-224	-10.69	-5.61	5.1	0.3	5.04
ZAL2-224	-10.76	-5.47			4.97
ZAL2-225	-10.73	-5.56			4.90

Sample ID	$\delta^{13}C$	$\delta^{18}O$	measured age	Error (2σ)	Wiggle matched age
ZAL3-1	-9.58	-4.19	64.1	0.7	64.40
ZAL3-2	-8.29	-3.91			64.23
ZAL3-3	-9.15	-4.35			64.05
ZAL3-4	-9.69	-4.54			63.88
ZAL3-5	-9.79	-4.74			63.71
ZAL3-6	-9.57	-4.35			63.54
ZAL3-7	-10.31	-5.50			63.36
ZAL3-8	-10.18	-5.19			63.19
ZAL3-9	-10.07	-5.03			63.02
ZAL3-10	-10.03	-5.05			62.85
ZAL3-11	-9.88	-5.02			62.67
ZAL3-12	-9.73	-5.40	61.3	2	62.50
ZAL3-13	-9.44	-5.18			62.44
ZAL3-14	-6.93	-4.17			62.39
ZAL3-15	-7.75	-4.30			62.33
ZAL3-16	-10.92	-5.48			62.28
ZAL3-17	-10.45	-4.66			62.22
ZAL3-18	-9.64	-4.77			62.17
ZAL3-19	-9.29	-4.33			62.11
ZAL3-20	-9.80	-4.33			62.06
ZAL3-21	-10.39	-3.93			62.00
ZAL3-22	-10.76	-4.95			61.94
ZAL3-23	-11.00	-5.43			61.89
ZAL3-24	-11.28	-5.33	61.4	2	61.83
ZAL3-25	-11.70	-5.31			61.78
ZAL3-26	-11.61	-5.29			61.72
ZAL3-27	-9.67	-4.06			61.67
ZAL3-28	-9.83	-4.08			61.61
ZAL3-29	-9.25	-4.31			61.56
ZAL3-30	-9.23	-4.11			61.50
ZAL3-31	-9.18	-3.90			61.44
ZAL3-32	-9.49	-4.33			61.39
ZAL3-33	-9.55	-4.61			61.33
ZAL3-34	-10.11	-5.13			61.28
ZAL3-35	-9.91	-4.63			61.22
ZAL3-36	-10.47	-4.77			61.17
ZAL3-37	-10.66	-4.95			61.11
ZAL3-38	-10.79	-5.30			61.06
ZAL3-39	-10.46	-5.08			61.00
ZAL3-40	-10.22	-5.79			60.94
ZAL3-41	-9.55	-5.44			60.89
ZAL3-42	-10.47	-4.91			60.83
ZAL3-43	-10.30	-5.12			60.78
ZAL3-44	-10.41	-4.68	53.2	2.8	60.72
ZAL3-45	-11.17	-5.07			60.67
ZAL3-46	-11.30	-4.85			60.61
ZAL3-47	-11.21	-4.99			60.56
ZAL3-48	-11.51	-6.11			60.50
ZAL3-49	-11.62	-6.40			60.44
ZAL3-50	-10.80	-6.01			60.39
ZAL3-51	-10.43	-5.60			60.33
ZAL3-52	-9.97	-5.02			60.28
ZAL3-53	-9.78	-4.93			60.22
ZAL3-54	-10.53	-5.87			60.17
ZAL3-55	-10.36	-5.60			60.11

ZAL3-56	-10.18	-5.30			60.06
ZAL3-57	-10.37	-4.66	59.7	2	60.00
ZAL3-58	-10.35	-4.52			59.96
ZAL3-59	-11.19	-5.89			59.93
ZAL3-60	-11.33	-5.81			59.89
ZAL3-61	-11.86	-5.69			59.86
ZAL3-62	-11.51	-5.79			59.82
ZAL3-63	-11.14	-5.69			59.79
ZAL3-64	-10.96	-5.60			59.75
ZAL3-65	-11.38	-5.41			59.72
ZAL3-66	-11.37	-5.45			59.68
ZAL3-67	-10.36	-5.03			59.65
ZAL3-68	-10.20	-5.29			59.61
ZAL3-69	-9.83	-5.01			59.58
ZAL3-70	-9.66	-4.80			59.54
ZAL3-71	-9.91	-4.96			59.51
ZAL3-72	-9.65	-5.32			59.47
ZAL3-73	-9.69	-5.04			59.44
ZAL3-74	-9.39	-4.67			59.40
ZAL3-75	-9.66	-4.90			59.36
ZAL3-76	-9.28	-4.70			59.33
ZAL3-77	-8.61	-4.37			59.29
ZAL3-78	-9.53	-4.96			59.26
ZAL3-79	-9.37	-4.72			59.22
ZAL3-80	-10.99	-5.42			59.19
ZAL3-81	-11.30	-5.39			59.15
ZAL3-82	-11.05	-5.44			59.12
ZAL3-84	-11.11	-5.32			59.08
ZAL3-85	-11.10	-4.89			59.05
ZAL3-86	-11.16	-5.13			59.01
ZAL3-87	-12.20	-5.67			58.94
ZAL3-88	-11.06	-5.56			58.91
ZAL3-89	-11.14	-4.99			58.87
ZAL3-90	-11.45	-5.04			58.84
ZAL3-91	-11.23	-5.19	57.1	1.8	58.80
ZAL3-92	-11.60	-5.50			58.78
ZAL3-93	-11.39	-5.58			58.75
ZAL3-94	-11.79	-5.42			58.73
ZAL3-95	-11.14	-5.07			58.70
ZAL3-96	-11.31	-5.30			58.68
ZAL3-97	-11.23	-5.13			58.65
ZAL3-98	-11.25	-5.26			58.63
ZAL3-99	-11.46	-4.97			58.60
ZAL3-100	-11.07	-4.71			58.58
ZAL3-101	-11.02	-5.44			58.55
ZAL3-102	-10.69	-4.78			58.53
ZAL3-103	-10.47	-5.25	59.2	1	58.50
ZAL3-104	-10.80	-5.04			58.40
ZAL3-105	-9.72	-4.35			58.29
ZAL3-106	-10.12	-4.63			58.19
ZAL3-107	-9.00	-4.33			58.08
ZAL3-108	-9.65	-4.44			57.98
ZAL3-109	-9.89	-4.99			57.87
ZAL3-110	-8.76	-4.53			57.77
ZAL3-111	-10.40	-4.96			57.66
ZAL3-112	-10.42	-5.27			57.56
ZAL3-113	-10.28	-5.10			57.45
ZAL3-114	-10.58	-5.22			57.35

ZAL3-115	-10.45	-5.02			57.25
ZAL3-116	-9.88	-4.82			57.14
ZAL3-117	-10.52	-5.46			57.04
ZAL3-118	-10.36	-5.57			56.93
ZAL3-119	-9.94	-4.72			56.83
ZAL3-120	-9.71	-4.78			56.72
ZAL3-121	-9.89	-5.05			56.62
ZAL3-122	-9.83	-4.80			56.51
ZAL3-123	-9.44	-4.39			56.41
ZAL3-124	-9.45	-4.73			56.30
ZAL3-125	-9.20	-4.57	54.8	1.6	56.20
ZAL3-126	-10.06	-4.89			56.08
ZAL3-127	-11.06	-5.08			55.96
ZAL3-128	-10.57	-4.44			55.85
ZAL3-129	-11.08	-5.28			55.73
ZAL3-130	-11.14	-5.39			55.61
ZAL3-131	-10.76	-5.07			55.49
ZAL3-132	-10.44	-4.63			55.38
ZAL3-133	-10.41	-4.44			55.26
ZAL3-134	-10.16	-4.32			55.14
ZAL3-135	-9.82	-4.12			55.02
ZAL3-136	-10.15	-4.29			54.91
ZAL3-137	-9.85	-4.21			54.79
ZAL3-138	-9.49	-4.54			54.67
ZAL3-139	-9.38	-4.61			54.55
ZAL3-140	-9.75	-4.85			54.44
ZAL3-141	-8.92	-4.09			54.32
ZAL3-142	-8.59	-4.07			54.20
ZAL3-143	-8.44	-4.18			54.08
ZAL3-144	-8.53	-4.23			53.96
ZAL3-145	-10.50	-5.28			53.85
ZAL3-146	-11.29	-5.42			53.73
ZAL3-147	-11.36	-5.45			53.61
ZAL3-148	-11.43	-6.05			53.49
ZAL3-149	-11.31	-5.19			53.38
ZAL3-150	-11.18	-5.24			53.26
ZAL3-151	-11.39	-5.47			53.14
ZAL3-152	-11.74	-5.97			53.02
ZAL3-153	-11.06	-5.77			52.91
ZAL3-154	-8.70	-5.00			52.79
ZAL3-155	-7.90	-4.68			52.67
ZAL3-156	-9.55	-4.83			52.55
ZAL3-157	-10.98	-5.05			52.44
ZAL3-158	-11.44	-5.10			52.32
ZAL3-159	-11.18	-5.80	51.2	1.2	52.20
ZAL3-160	-11.21	-5.65			52.15
ZAL3-161	-11.30	-5.22			52.11
ZAL3-162	-11.16	-5.36			52.06
ZAL3-163	-9.19	-4.35			52.02
ZAL3-164	-9.04	-4.40			51.97
ZAL3-165	-7.73	-4.52			51.92
ZAL3-166	-8.74	-4.50			51.88
ZAL3-167	-8.63	-4.41			51.83
ZAL3-168	-9.35	-6.45			51.78
ZAL3-169	-11.22	-5.24			51.74
ZAL3-170	-11.23	-5.71			51.69
ZAL3-171	-10.53	-5.36			51.65
ZAL3-172	-11.32	-5.52			51.60

ZAL3-173	-11.15	-5.69			51.55
ZAL3-174	-10.54	-5.15			51.51
ZAL3-175	-8.21	-4.83			51.46
ZAL3-176	-7.66	-4.75			51.42
ZAL3-177	-7.93	-5.25			51.37
ZAL3-178	-8.71	-5.03			51.32
ZAL3-179	-11.34	-5.95			51.28
ZAL3-180	-11.22	-6.60			51.23
ZAL3-181	-10.96	-5.64			51.18
ZAL3-182	-10.81	-6.05			51.14
ZAL3-183	-9.96	-5.89			51.09
ZAL3-184	-10.25	-5.46			51.05
ZAL3-185	-10.13	-5.39	52	2	51.00
ZAL3-186	-10.23	-5.49			50.98
ZAL3-187	-10.19	-5.14			50.95
ZAL3-188	-10.65	-4.88			50.93
ZAL3-189	-10.82	-5.46			50.90
ZAL3-190	-9.45	-5.00			50.88
ZAL3-191	-9.01	-4.85			50.85
ZAL3-192	-9.08	-4.54			50.83
ZAL3-193	-9.62	-5.10			50.80
ZAL3-194	-10.18	-3.88			50.78
ZAL3-195	-10.58	-4.30			50.75
ZAL3-196	-10.10	-4.40			50.73
ZAL3-197	-9.23	-4.41			50.70
ZAL3-198	-9.54	-4.61			50.68
ZAL3-199	-10.03	-4.63			50.65
ZAL3-200	-10.21	-4.55			50.63
ZAL3-201	-10.27	-4.74			50.60
ZAL3-202	-10.86	-5.00			50.58
ZAL3-203	-10.80	-5.21			50.55
ZAL3-204	-10.87	-5.20			50.53
ZAL3-205	-10.91	-5.18			50.50
ZAL3-206	-11.09	-6.31			50.48
ZAL3-207	-11.22	-7.19			50.45
ZAL3-208	-10.93	-7.46			50.43
ZAL3-209	-10.51	-5.25			50.40
ZAL3-210	-10.76	-4.97			50.38
ZAL3-211	-11.40	-6.64			50.35
ZAL3-212	-11.44	-5.94			50.33
ZAL3-213	-11.49	-5.68			50.30
ZAL3-214	-11.37	-5.58			50.28
ZAL3-215	-11.07	-5.48			50.25
ZAL3-216	-10.85	-5.40			50.23
ZAL3-217	-10.74	-5.40			50.20
ZAL3-218	-10.84	-4.72			50.18
ZAL3-219	-10.83	-4.87			50.15
ZAL3-220	-10.69	-4.98			50.13
ZAL3-221	-11.05	-5.34			50.10
ZAL3-222	-10.77	-5.23			50.08
ZAL3-223	-10.86	-5.05			50.05
ZAL3-224	-10.52	-5.16			50.03
ZAL3-225	-10.78	-5.15	50.5	1.4	50.00
ZAL3-226	-10.29	-4.93			49.94
ZAL3-227	-10.61	-5.25			49.88
ZAL3-228	-10.66	-4.94			49.81
ZAL3-229	-10.79	-5.10			49.75
ZAL3-230	-11.29	-5.15			49.69

ZAL3-231	-11.22	-4.89			49.63
ZAL3-232	-11.32	-4.14			49.56
ZAL3-233	-11.14	-4.33	42	0.8	49.50
ZAL3-234	-11.67	-5.47			49.44

Sample ID	$\delta^{13}C$	$\delta^{18}O$	measured age	Error (2σ)	Wiggle matched age
ZAL4-1	-11.16	-5.02			120.78
ZAL4-2	-11.11	-4.69			120.69
ZAL4-3	-11.03	-4.50	120.9	3.3	120.60
ZAL4-4	-10.82	-4.24			120.51
ZAL4-5	-10.99	-4.52			120.42
ZAL4-6	-11.01	-5.48			120.33
ZAL4-7	-11.09	-5.43			120.23
ZAL4-8	-11.36	-4.90			120.14
ZAL4-9	-11.25	-5.14			120.05
ZAL4-10	-10.93	-5.27			119.96
ZAL4-11	-11.01	-5.49			119.87
ZAL4-12	-10.71	-5.37			119.78
ZAL4-13	-10.59	-5.23			119.69
ZAL4-14	-10.67	-4.15			119.60
ZAL4-15	-10.97	-4.23			119.50
ZAL4-16	-11.39	-5.67			119.41
ZAL4-17	-11.38	-5.28			119.32
ZAL4-18	-11.62	-5.23			119.23
ZAL4-19	-11.41	-4.95			119.14
ZAL4-20	-11.22	-5.01			119.05
ZAL4-21	-11.17	-4.99			118.96
ZAL4-22	-11.21	-4.84			118.86
ZAL4-23	-11.18	-4.78			118.77
ZAL4-24	-11.02	-5.40			118.68
ZAL4-25	-10.73	-5.34			118.59
ZAL4-26	-11.13	-5.00			118.50
ZAL4-27	-11.41	-5.18			118.41
ZAL4-28	-11.38	-5.74			118.32
ZAL4-29	-10.92	-5.32			118.23
ZAL4-30	-10.89	-5.15	120.1	2.7	118.13
ZAL4-31	-11.10	-5.24			118.04
ZAL4-32	-10.90	-5.23			117.95
ZAL4-33	-11.08	-5.15			117.86
ZAL4-34	-11.22	-5.38			117.77
ZAL4-35	-10.77	-5.07			117.68
ZAL4-36	-10.44	-4.65			117.59
ZAL4-37	-10.64	-4.81			117.49
ZAL4-38	-10.74	-4.73			117.40
ZAL4-39	-10.99	-4.75			117.31
ZAL4-40	-11.43	-5.05			117.22
ZAL4-41	-11.54	-5.09			117.13
ZAL4-42	-11.55	-4.88			117.04
ZAL4-43	-10.89	-4.70			116.95
ZAL4-44	-11.08	-4.82			116.86
ZAL4-45	-11.48	-4.90			116.76
ZAL4-46	-11.12	-4.90			116.67
ZAL4-47	-10.88	-4.81			116.58
ZAL4-48	-11.01	-4.82			116.49
ZAL4-49	-10.58	-4.53			116.40
ZAL4-50	-10.92	-4.72			116.31
ZAL4-51	-10.70	-4.92			116.22
ZAL4-52	-10.62	-4.75			116.12
ZAL4-53	-11.11	-4.70			116.03
ZAL4-54	-11.09	-5.39			115.94
ZAL4-55	-10.89	-5.12			115.85

ZAL4-56	-10.95	-4.72			115.76
ZAL4-57	-10.29	-4.89			115.67
ZAL4-58	-10.28	-4.47			115.58
ZAL4-59	-10.83	-4.71			115.49
ZAL4-60	-10.64	-4.61			115.39
ZAL4-61	-10.89	-4.86			115.30
ZAL4-62	-10.39	-4.46			115.21
ZAL4-63	-10.65	-4.33			115.12
ZAL4-64	-10.61	-4.83			115.03
ZAL4-65	-10.80	-4.76			114.94
ZAL4-66	-10.30	-5.25			114.85
ZAL4-67	-10.09	-5.78			114.75
ZAL4-68	-10.59	-4.72	36.5	1.3	114.66
ZAL4-69	-10.62	-4.80			114.57
ZAL4-70	-10.36	-4.44			114.48
ZAL4-71	-10.52	-5.53			114.39
ZAL4-72	-10.88	-5.93			114.30
ZAL4-73	-10.64	-4.63			114.21
ZAL4-74	-10.86	-4.35			114.11
ZAL4-75	-10.94	-4.62			114.02
ZAL4-76	-10.81	-4.86			113.93
ZAL4-77	-11.27	-4.99			113.84
ZAL4-78	-11.25	-5.15			113.75
ZAL4-79	-10.34	-4.24			113.66
ZAL4-80	-10.43	-4.19			113.57
ZAL4-81	-10.34	-4.31			113.48
ZAL4-82	-10.63	-4.18			113.38
ZAL4-83	-10.79	-4.15			113.29
ZAL4-84	-10.31	-4.09			113.20
ZAL4-85	-9.98	-4.21			113.11
ZAL4-86	-11.14	-4.54			113.02
ZAL4-87	-10.66	-4.42			112.93
ZAL4-88	-10.70	-4.67			112.84
ZAL4-89	-10.92	-4.49			112.74
ZAL4-90	-10.64	-4.55			112.65
ZAL4-91	-10.47	-4.30			112.56
ZAL4-92	-10.66	-4.47			112.47
ZAL4-93	-10.78	-4.43			112.38
ZAL4-94	-10.51	-4.23			112.29
ZAL4-95	-10.94	-4.74			112.20
ZAL4-96	-10.71	-4.53			112.11
ZAL4-97	-10.92	-4.95			112.01
ZAL4-98	-11.30	-5.14			111.92
ZAL4-99	-11.12	-4.99			111.83
ZAL4-100	-11.01	-4.82			111.74
ZAL4-101	-10.94	-4.86			111.65
ZAL4-102	-11.46	-5.11			111.56
ZAL4-103	-11.18	-5.42			111.47
ZAL4-104	-11.59	-5.27			111.37
ZAL4-105	-11.21	-5.10			111.28
ZAL4-106	-11.48	-5.18			111.19
ZAL4-107	-11.20	-5.10			111.10
ZAL4-108	-11.18	-4.89			111.01
ZAL4-109	-10.98	-4.89			110.92
ZAL4-110	-11.16	-4.82			110.83
ZAL4-111	-11.38	-5.02			110.74
ZAL4-112	-11.41	-5.02			110.64
ZAL4-113	-11.48	-5.05			110.55

ZAL4-114	-11.36	-4.73			110.46
ZAL4-115	-11.51	-4.68			110.37
ZAL4-116	-11.29	-4.62			110.28
ZAL4-117	-11.60	-4.67			110.19
ZAL4-118	-12.03				110.10
ZAL4-119	-12.13	-4.85			110.00
ZAL4-120	-11.67	-4.94			109.91
ZAL4-121	-12.21	-4.99			109.82
ZAL4-122	-11.83	-5.30			109.73
ZAL4-123	-11.75	-5.50			109.64
ZAL4-124	-11.63	-4.93			109.55
ZAL4-125	-11.77	-4.83			109.46
ZAL4-126	-11.98	-5.09			109.37
ZAL4-127	-11.77	-5.28			109.27
ZAL4-128	-12.09	-5.47			109.18
ZAL4-129	-11.11	-5.32			109.09
ZAL4-130	-10.62	-5.17	107.1	2.7	109.00
ZAL4-131	-10.72	-5.35			108.91
ZAL4-132	-10.68	-5.55			108.82
ZAL4-133	-9.92	-5.29			108.73
ZAL4-134	-9.99	-5.34			108.63
ZAL4-135	-9.97	-5.46			108.54

Sample ID	$\delta^{13}C$	$\delta^{18}O$	measured age	Error (2σ)	Wiggle matched age
ZAL5-1	-11.07	-4.33	193	10	146.00
ZAL5-2	-10.83	-3.85			145.93
ZAL5-3	-11.86	-4.88			145.85
ZAL5-4	-11.56	-4.32			145.78
ZAL5-5	-11.54	-4.12			145.70
ZAL5-6	-10.71	-4.51			145.63
ZAL5-7	-11.31	-4.69			145.56
ZAL5-8	-10.67	-4.24			145.48
ZAL5-9	-11.13	-4.27			145.41
ZAL5-10	-11.38	-4.72			145.33
ZAL5-11	-11.84	-4.63			145.26
ZAL5-12	-11.65	-4.59			145.19
ZAL5-13	-11.84	-4.82			145.11
ZAL5-14	-11.16	-4.62			145.04
ZAL5-15	-11.58	-4.78			144.96
ZAL5-16	-11.21	-4.81			144.89
ZAL5-17	-10.88	-4.62			144.81
ZAL5-18	-11.01	-4.45			144.74
ZAL5-19	-10.98	-4.54			144.67
ZAL5-20	-11.21	-4.47			144.59
ZAL5-21	-11.05	-4.45			144.52
ZAL5-22	-11.21	-4.50			144.44
ZAL5-23	-11.24	-4.55			144.37
ZAL5-24	-10.82	-3.79			144.30
ZAL5-25	-10.62	-4.11			144.22
ZAL5-26	-10.70	-4.49			144.15
ZAL5-27	-10.67	-5.02			144.07
ZAL5-28	-10.57	-4.36			144.00
ZAL5-29	-10.40	-4.08			143.93
ZAL5-30	-10.71	-3.74			143.85
ZAL5-31	-10.73	-4.40			143.78
ZAL5-32	-11.08	-5.35			143.70
ZAL5-33	-10.78	-5.25			143.63
ZAL5-34	-10.46	-4.47	145	10	143.56
ZAL5-35	-10.59	-4.64			143.48
ZAL5-36	-10.92	-4.02			143.41
ZAL5-37	-10.96	-4.82			143.33
ZAL5-38	-11.54	-5.39			143.26
ZAL5-39	-11.58	-4.57			143.19
ZAL5-40	-11.83	-4.51			143.11
ZAL5-41	-11.76	-4.49			143.04
ZAL5-42	-11.77	-4.44			142.96
ZAL5-43	-11.86	-4.74			142.89
ZAL5-44	-10.93	-3.89			142.81
ZAL5-45	-11.25	-4.24			142.74
ZAL5-46	-11.17	-4.02			142.67
ZAL5-47	-12.19				142.59
ZAL5-48	-11.70	-4.97			142.52
ZAL5-49	-11.58	-4.92			142.44
ZAL5-50	-11.68	-4.58			142.37
ZAL5-51	-11.76	-4.52			142.30
ZAL5-52	-11.67	-4.89			142.22
ZAL5-53	-11.08	-4.81			142.15
ZAL5-54	-11.52	-4.60			142.07
ZAL5-55	-10.98	-4.28			142.00

ZAL5-56	-11.16	-4.82	144	11	141.93
ZAL5-57	-11.34	-5.08			141.85
ZAL5-58	-11.38	-4.85			141.78
ZAL5-59	-11.38	-4.79			141.70
ZAL5-60	-11.60	-5.28			141.63
ZAL5-61	-11.35	-4.31			141.56
ZAL5-62	-11.30	-4.92			141.48
ZAL5-63	-11.28	-4.33			141.41
ZAL5-64	-11.12	-4.45			141.33
ZAL5-65	-11.99	-4.78			141.26
ZAL5-66					141.19
ZAL5-67	-11.50	-4.74			141.11
ZAL5-68	-11.98	-4.87			141.04
ZAL5-69	-11.63	-4.82			140.96
ZAL5-70	-11.63	-4.89			140.89
ZAL5-71	-11.31	-4.53			140.81
ZAL5-72	-11.66	-4.55			140.74
ZAL5-73	-11.92	-4.72			140.67
ZAL5-74	-11.92	-4.91			140.59
ZAL5 - 75	-11.36	-4.44			140.52
ZAL5 - 76	-12.05	-5.40			140.44
ZAL5 - 77	-10.76	-4.23			140.37
ZAL5 - 78	-10.07	-3.75			140.30
ZAL5 - 79	-10.09	-3.58			140.22
ZAL5 - 80	-10.44	-4.17			140.15
ZAL5 - 81	-10.46	-4.07			140.07
ZAL5 - 82	-10.54	-4.39	145	10	140.00
ZAL5 - 83	-10.47	-4.33			139.93
ZAL5 - 84	-10.39	-4.26			139.85
ZAL5 - 85	-11.17	-4.22			139.78
ZAL5 - 86	-10.68	-4.17			139.70
ZAL5 - 87	-10.24	-3.80			139.63
ZAL5 - 88	-10.74	-4.31			139.56
ZAL5 - 89	-10.78	-4.22			139.48
ZAL5 - 90	-11.03	-4.69			139.41
ZAL5 - 91	-10.79	-4.62			139.33
ZAL5 - 92	-10.28	-4.28			139.26
ZAL5 - 93	-10.34	-4.20			139.19
ZAL5 - 94	-10.03	-3.91			139.11
ZAL5 - 95	-10.09	-4.06			139.04
ZAL5 - 96	-10.21	-4.05			138.96
ZAL5-97	-9.61	-3.70			138.89
ZAL5-98	-10.58	-4.24			138.81
ZAL5-99	-10.14	-3.95			138.74
ZAL5-100	-10.44	-3.88			138.67
ZAL5-101	-10.54	-4.42			138.59
ZAL5-102	-10.93	-4.75			138.52
ZAL5-103	-10.83	-4.95			138.44
ZAL5-104					138.37
ZAL5-105	-11.16	-4.57			138.30
ZAL5-106	-11.36	-4.54			138.22
ZAL5-107	-11.23	-4.42			138.15
ZAL5-108	-11.63	-4.24			138.07
ZAL5-109	-11.47	-3.78	136	4	138.00
ZAL5-110	-11.30	-3.90			137.97
ZAL5-111	-11.63	-4.20			137.93
ZAL5-112	-11.84	-4.07			137.90
ZAL5-113	-10.84	-3.84			137.87

ZAL5-114	-11.66	-3.98			137.84
ZAL5-115	-11.53	-3.88			137.80
ZAL5-116	-11.43	-4.07			137.77
ZAL5-117	-11.38	-3.97			137.74
ZAL5-118	-11.50	-4.40			137.70
ZAL5-119	-11.57	-4.52			137.67
ZAL5-120					137.64
ZAL5-121	-11.33	-4.25			137.60
ZAL5-122	-11.23	-4.14			137.57
ZAL5-123	-11.72	-4.69			137.54
ZAL5-124	-11.38	-4.39			137.51
ZAL5-125	-11.07	-4.43			137.47
ZAL5-126	-11.12	-4.62			137.44
ZAL5-127	-10.97	-4.65			137.41
ZAL5-128	-10.68	-4.48			137.37
ZAL5-129	-10.62	-4.60			137.34
ZAL5-130	-10.73	-4.16			137.31
ZAL5-131	-10.31	-3.77			137.27
ZAL5-132	-10.91	-3.87			137.24
ZAL5-133	-10.62	-3.88			137.21
ZAL5-134	-10.91	-4.42			137.18
ZAL5-135	-11.14	-4.40			137.14
ZAL5-136					137.11
ZAL5-137	-11.36	-4.09			137.08
ZAL5-138	-11.46	-4.28			137.04
ZAL5-139	-11.18	-4.36			137.01
ZAL5-140	-11.20	-4.58			136.98
ZAL5-141	-11.19	-4.33			136.95
ZAL5-142	-11.40	-4.48			136.91
ZAL5-143	-10.99	-4.29			136.88
ZAL5-144	-11.16	-4.21			136.85
ZAL5-145	-10.77	-3.76			136.81
ZAL5-146	-11.00	-3.83			136.78
ZAL5-147	-11.32	-4.03			136.75
ZAL5-148	-11.49	-4.20			136.71
ZAL5-149	-11.88	-4.49			136.68
ZAL5-150	-12.16	-4.75			136.65
ZAL5-151	-11.72	-4.42			136.62
ZAL5-152	-11.68	-4.39			136.58
ZAL5-153	-11.62	-4.18			136.55
ZAL5-154	-11.20	-4.34			136.52
ZAL5-155	-11.46	-4.46			136.48
ZAL5-156	-11.26	-4.33			136.45
ZAL5-157	-11.28	-4.42			136.42
ZAL5-158	-11.81	-4.65	137	5	136.38
ZAL5-159	-11.99	-4.30			136.35
ZAL5-160	-12.52	-4.79			136.32
ZAL5-161	-11.65	-4.17			136.29
ZAL5-162	-11.81	-3.93			136.25
ZAL5-163	-11.67	-3.81			136.22
ZAL5-164	-11.98	-4.21			136.19
ZAL5-165	-12.00	-4.49			136.15
ZAL5-166	-11.94	-3.70			136.12
ZAL5-167	-11.97	-4.07			136.09
ZAL5-168	-11.38	-3.68			136.05
ZAL5-169	-11.56	-3.58			136.02
ZAL5-170	-11.51	-4.44			135.99
ZAL5-171	-11.14	-3.81			135.96

ZAL5-172	-11.27	-4.04			135.92
ZAL5-173	-11.11	-3.94			135.89
ZAL5-174	-11.48	-4.13			135.86
ZAL5-175	-11.60	-3.97			135.82
ZAL5-176	-11.75	-4.50			135.79
ZAL5-177	-12.07	-4.71			135.76
ZAL5-178	-12.20	-5.10			135.73
ZAL5-179	-11.90	-4.70			135.69
ZAL5-180	-11.95	-4.39			135.66
ZAL5-181	-11.76	-4.50			135.63
ZAL5-182	-12.11	-4.45			135.59
ZAL5-183	-11.75	-4.26			135.56
ZAL5-184	-11.70	-4.36			135.53
ZAL5-185	-11.36	-4.14			135.49
ZAL5-186	-11.30	-3.88			135.46
ZAL5-187	-11.84	-4.43			135.43
ZAL5-188	-11.19	-4.04			135.40
ZAL5-189	-11.14	-4.22			135.36
ZAL5-190	-11.22	-3.83			135.33
ZAL5-191	-11.05	-3.58			135.30
ZAL5-192					135.26
ZAL5-193	-11.25	-3.98			135.23
ZAL5-194	-11.28	-3.99			135.20
ZAL5-195					135.16
ZAL5-196	-10.99	-3.89			135.13
ZAL5-198	-10.96	-3.85			135.10
ZAL5-198	-10.63				135.07
ZAL5-199	-10.52	-3.62			135.03
ZAL5-200	-10.97	-4.14			135.00
ZAL5-201	-10.95	-4.04			134.97
ZAL5-202	-10.77	-3.96			134.93
ZAL5-203	-10.56	-4.32			134.90
ZAL5-204	-10.61	-4.44			134.87
ZAL5-205	-10.63	-4.13			134.84
ZAL5-206	-11.15	-4.32			134.80
ZAL5-207	-11.35	-4.58			134.77
ZAL5-208	-11.64	-4.53			134.74
ZAL5-209	-11.50	-4.22			134.70
ZAL5-210	-11.41	-4.42			134.67
ZAL5-211	-11.16	-4.50			134.64
ZAL5-212	-11.40	-4.45	137	3	134.60
ZAL5-213	-11.01	-4.49			134.57
ZAL5-214	-11.21	-4.76			134.54
ZAL5-215	-11.16	-4.90			134.51
ZAL5-216	-11.45	-4.62			134.47
ZAL5-217	-11.25	-4.51			134.44
ZAL5-218	-11.21	-4.48			134.41
ZAL5-219	-10.91	-4.40			134.37
ZAL5-220	-11.03	-4.38			134.34
ZAL5-221	-11.13	-4.67			134.31
ZAL5-222	-11.15	-4.60			134.27
ZAL5-223	-11.02	-5.59	135	4	134.24
ZAL5-224	-11.00	-4.98			134.21
ZAL5-225	-11.72	-5.10			134.18
ZAL5-226	-12.26	-5.86			134.14
ZAL5-227	-11.94	-6.03			134.11
ZAL5-228	-11.86	-5.64	141	8	134.08
ZAL5-229					134.04

ZAL5-230	-11.78	-5.61			134.01
ZAL5-231					133.98
ZAL5-232	-11.90	-5.85			133.95
ZAL5-233	-11.84	-6.05			133.91
ZAL5-234	-11.62	-5.80			133.88
ZAL5-235	-11.53	-5.76			133.85
ZAL5-236	-12.00	-5.91			133.81
ZAL5-237	-12.05	-5.68			133.78
ZAL5-238	-11.95	-5.55			133.75
ZAL5-239	-12.07	-5.41			133.71
ZAL5-240	-11.72	-5.06			133.68
ZAL5-241	-11.54	-5.30			133.65
ZAL5-242	-11.41	-5.28			133.62
ZAL5-243	-11.51	-5.25			133.58
ZAL5-244	-11.88	-5.73			133.55
ZAL5-245	-11.90	-6.09			133.52
ZAL5-246	-11.38	-5.25			133.48
ZAL5-247	-11.62	-5.21			133.45
ZAL5-248	-11.62	-5.56			133.42
ZAL5-249	-11.97	-5.74			133.38
ZAL5-250	-11.73	-4.95			133.35
ZAL5-251	-12.05	-4.93			133.32
ZAL5-252	-11.07	-4.88			133.29
ZAL5-253	-11.20	-4.79			133.25
ZAL5-254	-10.86	-4.70			133.22
ZAL5-255	-10.86	-4.65			133.19
ZAL5-256	-10.53	-4.13			133.15
ZAL5-257	-10.94	-4.23			133.12
ZAL5-258	-10.86	-4.50			133.09
ZAL5-259	-11.10	-4.48			133.05
ZAL5-260	-11.65	-5.30			133.02
ZAL5-261	-11.04	-5.03			132.99
ZAL5-262	-10.72	-5.42			132.96
ZAL5-263	-11.17				132.92
ZAL5-264	-11.73	-5.24			132.89
ZAL5-265	-11.69	-5.28	134	7	132.86
ZAL5-266	-11.92	-5.26			132.82
ZAL5-267	-11.86	-5.47			132.79
ZAL5-268	-11.52	-4.81			132.76
ZAL5-269	-11.66	-5.32			132.73
ZAL5-270	-11.96	-4.47			132.69
ZAL5-271	-12.10	-4.65			132.66
ZAL5-272	-11.33	-4.49			132.63
ZAL5-273	-11.28	-4.42			132.59
ZAL5-274	-10.98	-4.59			132.56
ZAL5-275	-11.00	-4.82			132.53
ZAL5-276	-11.08	-4.93			132.49
ZAL5-277	-10.94	-4.77			132.46
ZAL5-278	-10.77	-4.52			132.43
ZAL5-279	-10.59	-4.55			132.40
ZAL5-280	-10.78	-4.74			132.36
ZAL5-281	-10.71	-4.76			132.33
ZAL5-282	-10.49	-4.68			132.30
ZAL5- 283	-10.47	-5.03			132.26
ZAL5- 284	-10.59	-5.35			132.23
ZAL5- 285	-10.13	-4.67			132.20
ZAL5- 286	-10.36	-4.75			132.16
ZAL5- 287					132.13

ZAL5- 288	-10.99	-5.36			132.10
ZAL5- 289	-11.24	-4.95			132.07
ZAL5- 290	-11.05	-5.05			132.03
ZAL5- 291	-11.09	-5.05	132	4	132.00
ZAL5-292	-11.48	-5.30			131.92
ZAL5-293					131.84
ZAL5-294	-11.87	-5.56			131.75
ZAL5-295	-12.22	-6.23			131.67
ZAL5-296	-12.26	-5.99			131.59
ZAL5-297	-12.07	-5.55			131.51
ZAL5-298	-12.24	-5.72			131.42
ZAL5-299	-11.85	-5.46			131.34
ZAL5-300	-12.42	-5.72			131.26
ZAL5-301	-11.73	-5.03			131.18
ZAL5-302	-12.13	-5.49			131.09
ZAL5-303	-11.71	-4.77			131.01
ZAL5-304					130.93
ZAL5-305	-11.84	-5.51			130.85
ZAL5-306	-12.01	-4.91			130.76
ZAL5-307					130.68
ZAL5-308					130.60
ZAL5-309	-11.75	-5.02			130.52
ZAL5-310	-11.89	-5.29			130.44
ZAL5-311					130.35
ZAL5-312					130.27
ZAL5-313	-11.43	-5.95			130.19
ZAL5-314	-11.94	-5.72			130.11
ZAL5-315	-11.63	-5.47			130.02
ZAL5-316	-11.65	-5.29			129.94
ZAL5-317	-11.29	-5.10			129.86
ZAL5-318		-6.02			129.78
ZAL5-319	-12.94	-6.05			129.69
ZAL5-320	-11.55	-5.44			129.61
ZAL5-321					129.53
ZAL5-322					129.45
ZAL5-323	-12.67	-6.21			129.36
ZAL5-324	-12.61	-5.79			129.28
ZAL5-325	-12.23	-6.61	126	4	129.20
ZAL5-326	-12.69	-6.11			129.12
ZAL5-327	-12.50	-5.91			129.04
ZAL5-328	-12.91	-6.04			128.95
ZAL5-329	-12.49	-6.33			128.87
ZAL5-330	-12.62	-6.65			128.79
ZAL5-331	-12.96	-6.66			128.71
ZAL5-332					128.62
ZAL5-333	-13.33	-7.06			128.54
ZAL5-334					128.46
ZAL5-335	-12.94	-6.55			128.38
ZAL5-336	-12.78	-6.81			128.29
ZAL5-337	-12.62	-7.11			128.21
ZAL5-338	-12.40	-6.40			128.13
ZAL5-339	-12.10	-6.76			128.05
ZAL5-340	-12.23	-6.55			127.96
ZAL5-341	-11.41	-7.27			127.88
ZAL5-342	-11.34	-7.38			127.80
ZAL5-343	-9.58	-6.19			127.72
ZAL5-344	-10.00				127.64
ZAL5-345	-0.33	-6.28			127.55

ZAL5-346	-0.09	-6.35			127.47
					hiatus
ZAL5-347	-7.99	-5.39			121.01
ZAL5-348	-4.92	-4.31			120.93
ZAL5-349	-5.48	-4.08			120.85
ZAL5-350	-5.46	-3.61			120.76
ZAL5-351	-7.37	-4.31	116.7	4	120.68
ZAL5-352	-9.45	-4.52			120.60
ZAL5-353	-8.78	-4.52			120.52
ZAL5-354	-8.57	-4.39			120.44
ZAL5-355	-8.56	-4.41	118	4	120.35
ZAL5-356	-10.06	-5.82			120.27
ZAL5-357	-10.51	-5.16			120.19
ZAL5-358	-8.52	-4.86			120.11
					hiatus
ZAL5-359	-6.03	-4.04			47.60
ZAL5-360	-7.98	-3.84			47.50
ZAL5-361	-9.19	-3.89			47.40
ZAL5-362	-9.10	-3.94			47.30
ZAL5-363	-7.92	-3.42	47.2	2	47.20
ZAL5-364	-6.80	-3.93			47.10
ZAL5-365	-8.62				47.00

Sample ID	$\delta^{13}C$	$\delta^{18}O$	measured age	Error (2σ)	Wiggle matched age
ZAL6-1	-8.70	-4.38			
ZAL6-2	-8.31	-4.08			
ZAL6-3	-10.90	-4.81			
ZAL6-4	-10.98	-4.87			
ZAL6-5	-10.93	-4.64			
ZAL6-6	-11.23	-4.00			
ZAL6-7	-11.30	-3.86			
ZAL6-8	-11.50	-4.05	24.5	0.4	24.50
ZAL6-9	-10.80	-3.75			23.99
ZAL6-10	-11.24	-4.02			23.47
ZAL6-11	-11.25	-4.18			22.96
ZAL6-12	-11.24	-4.10			22.44
ZAL6-13	-11.16	-4.22			21.93
ZAL6-14	-11.08	-4.15			21.41
ZAL6-15	-11.04	-4.20	20.9	0.76	20.90
ZAL6-16	-10.48	-4.07			20.74
ZAL6-17	-10.38	-3.86			20.58
ZAL6-18	-10.60	-4.39			20.43
ZAL6-19	-10.43	-4.38			20.27
ZAL6-20	-10.62	-4.33			20.11
ZAL6-21	-10.58	-4.28			19.95
ZAL6-22	-11.31	-4.24			19.79
ZAL6-23	-11.27	-4.32			19.63
ZAL6-24	-10.78	-4.23			19.48
ZAL6-25	-10.78	-4.13			19.32
ZAL6-26	-10.84	-4.39			19.16
ZAL6-27	-10.76	-4.19	19	0.4	19.00
ZAL6-28	-10.98	-4.26			18.20
ZAL6-29	-10.99	-4.36			17.40
ZAL6-30	-11.10	-4.17			16.60
ZAL6-31	-11.39	-4.57			15.80
ZAL6-32	-11.54	-4.73			15.00
					hiatus
ZAL6-33	-11.34	-4.09			13.18
ZAL6-34	-11.72	-4.03	12.8	0.22	12.75
ZAL6-35	-12.28	-3.94			12.33
ZAL6-36	-12.76	-4.59			11.90
ZAL6-37	-12.86	-4.88			11.28
ZAL6-38	-13.19	-4.99			10.85
ZAL6-39	-13.15	-5.33			10.43
ZAL6-40	-12.59	-5.62			10.00
ZAL6-41	-12.22	-5.42			9.58
ZAL6-42	-12.69	-6.07			9.15
ZAL6-43	-13.19	-6.05			8.73
ZAL6-44	-11.96	-5.98	8.5	0.3	8.50
ZAL6-45	-11.61	-6.05			8.27
ZAL6-46	-10.91	-5.33			8.04
ZAL6-47	-10.74	-5.34			7.81
ZAL6-48	-11.20	-5.40			7.59
ZAL6-49	-11.63	-5.74			7.36
ZAL6-50	-11.48	-5.66			7.13
ZAL6-51	-11.10	-5.45	6.9	0.6	6.90
ZAL6-52	-11.20	-5.63			6.67

7.3 Isotopic profiles

The combined data from six samples was used to create Figure 29. ZAL2, ZAL3, ZAL4 and ZAL5 are presented as an 8 point running mean. ZAL6 and the bottom portion of ZAL1 are samples with slow very growth rate and are presented unmodified. Where two speleothems cover the same interval (e.g. ZAL2 and ZAL3 from 65 to 49 ka) the sample with higher resolution was chosen. The top segment of ZAL1 is presented as a broken line due to its age reversals and problematic age model.

7.4 Sea-land ($\Delta\delta^{18}O$) graphs

Figure 31 was created using "interp1" command in MATLAB 2013b which returns interpolated values of a 1-D function at specific query points using linear interpolation:

```
vq = interp1(x,v,xq)
Vector x contains the sample points, and v contains the corresponding values, v(x). Vector xq contains the coordinates of the query points.
```

The command line used:

```
ZAL_interp_O9501=interp1(ZAL_age,ZALO18,age9501);
```

`ZAL_age` is the vector of age values, `ZALO18` is the vector of corresponding $\delta^{18}O$ values and `age9501` is vector of the core's age values. The result, "`ZAL_interp_O9501`", is a vector of interpolated $\delta^{18}O$ values at the dates sampled from the core. This vector is then reduced from `9501_O18` (the corresponding $\delta^{18}O$ values of the core). The result is plotted against `age9501` and displayed as a 3 point running average.

The same method is applied to both marine cores and four cave records.

Table 10: Average $\Delta\delta^{18}O_{sea\text{-}land}$ values and standard deviation for MIS1 (light red) and the last glacial period (light blue) presented in Figure 32.

Core \ Cave	Zalmon	Peqi'in	Soreq	Ma'ale Efrayim
9509	5.24±0.55‰	5.08±0.48‰	5.63±0.48‰	-
9501	5.63±0.48‰	5.36±0.72‰	5.89±0.63‰	-
9509	6.79±0.62‰	6.01±0.62‰	5.37±0.65‰	5.91±0.56‰
9501	7.01±0.83‰	6.26±0.69‰	5.79±0.77‰	6.03±0.70‰

תקציר

משקעי מערות משמשים לשחזור אקלים העבר. עשרות מערות נחקרו במזרח התיכון עד כה, אבל עד מחקר זה לא נמצאו מערות נטיפים נגישות בגליל המזרחי. מערת צלמון, שהתגלתה לאחרונה, מקנה הזדמנות ללמוד על אקלים המזרח התיכון בחלקו הצפוני של בקע הירדן. המערה נפערת בשולי אגן ים המלח כ-8 ק"מ מערבית לכנרת. מחקר מערת צלמון, המתבסס על תיארוך מדויק ופרופילים איזוטופיים, מתווסף למחקרים קודמים ומוסיף תובנות על אקלים העבר של סוף הרביעון בלבנט. משקעי מערת צלמון גדלו בתקופות קרחוניות ובינקרחוניות, בניגוד למערות דרומיות יותר לאורך בקע ים המלח בהן ההשקעה העיקרית חלה בתקופות קרחוניות. השוואה בין הפרופיל האיזוטופי של פחמן ($\delta^{13}C$) וחמצן ($\delta^{18}O$) ממשקעי מערת צלמון לבין פרופילים איזוטופיים של ספלאותמים ממערות בצפון הגליל וממרכז הארץ מראה כי הרכבי $\delta^{13}C$ דומה בכולם לאורך רוב תקופות ההשקעה, דמיון המעיד על סוגי צמחייה דומים שמאפיינים גם את האקלים כיום. לעומת זאת ערכי $\delta^{18}O$ שונים בתקופה הקרחונית האחרונה. ערכי $\delta^{18}O$ של משקעי מערת צלמון בתקופת הקרח האחרונה נמוכים משל מערת פקיעין ומערת מעלה אפרים בכ-0.5-1‰ ובכ-1-2‰ ממערת שורק. השוני מצביע על טמפרטורות גבוהות יותר ו\או כמות משקעים גדולה באזור מערת צלמון בעיקר בהשוואה למרכז הארץ. בהתייחסות לסוגיית דלדול ^{18}O ממזרח ומצפון למרכז הארץ בתקופות קרחוניות, נחקרה השפעת פני הים הנמוכים והמערכת הסינופטית השונה בתקופה זו. השוואת ערכי $\delta^{18}O$ של ספלאותמים ממערות במזרח התיכון לערכי $\delta^{18}O$ בפורומיניפרים פלנקטונים מסוג *G. Ruber* מגלעינים ימיים שממול לחופי ישראל ($\Delta\delta^{18}O_{\text{ים-יבשה}}$) מראה בבירור שלוש תופעות המאפיינות את תקופת הקרח האחרונה: 1) ערכי $\Delta\delta^{18}O_{\text{ים-יבשה}}$ של משקעי מערת צלמון גבוהים יותר ביחס למשקעי מערת שורק במרכז ישראל. 2) הפרופילים היבשתיים דומים לגלעין מדרום מזרח הים התיכון ופחות לגלעין מצפון מזרח הים התיכון. 3) ערכי $\Delta\delta^{18}O_{\text{ים-צלמון}}$ הגבוהים ביותר מתרחשים בתקופה בה מפלס ימת הלשון גבוהים. שילוב ממצאים אלה מצביע על נדידה דרומה של מערכות הגשמים ועל כמות משקעים רבה יותר בצפון בקע הירדן במהלך תקופת הקרח האחרונה.

הסביבה הקדומה של צפון בקע הירדן על פי משקעי מערת צלמון, ישראל

עבודת גמר לתואר מוסמך במדעי הטבע

מוגשת על ידי:

יהונתן קינן

בהדרכת:

פרופ' אמוץ עגנון

פרופ' עמוס פרומקין

ד"ר מרים בר-מטיוס

דצמבר 2016

כסליו תשע"ז

החוג לגיאולוגיה

המכון למדעי כדור הארץ

הפקולטה למדעי הטבע

האוניברסיטה העברית בירושלים